NATIONAL TECHNICAL UNIVERSITY OF ATHENS

SCHOOL OF NAVAL ARCHITECTURE AND MARINE ENGINEERING

SHIPBUILDING TECHNOLOGY LABORATORY

DIPLOMA THESIS

Direct Laser Metal Deposition of Titanium Matrix Composites and Analysis of Microstructure and Mechanical Properties.

Damianidou Yvonni-Effrosyni

Thesis supervisor: Professor Dimitrios I. Pantelis

Athens,
March 2013

Abstract

This diploma thesis project presents the study of Ti-TiC composites after being processed by Direct Laser Metal Deposition. TiC-Ti6Al4V powder was used at a proportion of 10%-90% respectively. The experiments were conducted at the *Process and Engineering in Mechanics and Materials laboratory* (PIMM) of the École Nationale Supérieure d'Arts et Métiers (ENSAM) (member of the ParisTech), within the ERASMUS program under the supervision and guidance of Professor Olivier Castelneau, Head of the Research Group *CoMet : Behavior and Microstructure of Metals,* and Professor Patrice Peyre, Head of the Research Group *Laser: Laser Processes*.

Three parameters differentiated the manufactured samples which were afterwards examined with several methods. First, the beam's propagation was of Top Hat type in contrast to previous work realized at the PIMM laboratory, secondly two velocities were examined; 200 mm/min and 400 mm/min and finally and most importantly, of the eight samples that were produced half of them were remelted (laser pass without powder deposition).

To examine the impact of the aforementioned parameters, the following methods were realized; Surface roughness analysis, Optical Microcopy (OM), Scanning Electron Microsopy (SEM), X-ray diffraction (XRD) and Electron Backscattered Diffraction (EBSD) for the material and microstructure characterization. In addition, micro-hardness analysis for the eight samples and tensile tests on three new [DLMD] samples were also realized to examine the mechanical properties of the samples produced by the technique in survey.

In summary, the overall outcome of this research project is that the novel remelting factor is indeed advantageous as it improves the homogeneity along the microstructure of the fabricated samples. In addition, although the velocity did not greatly differentiate the results among the samples, samples manufactured with a velocity of 200 mm/min presented somewhat better results.

KEYWORDS:
Direct Laser Metal Deposition (DLMD); TiC reinforced titanium alloys-Ti6Al4V; Microstructures; Mechanical Properties; OM; SEM; EBSD; XRD; Hardness; Surface Roughness; Tensile Strength

Περίληψη

Αντικείμενο έρευνας της παρούσας Διπλωματικής Εργασίας αποτελεί η μελέτη του σύνθετου υλικού TiC-Ti6Al4V μετά από επεξεργασία με απευθείας εναπόθεση μετάλλου με λέιζερ (Direct Laser Metal Deposition Method). Για την εναπόθεση χρησιμοποιήθηκε πούδρα TiC-Ti6Al4V σε αναλογία 10%-90%, αντίστοιχα. Τα πειράματα διεξήχθησαν στο εργαστήριο Μηχανικών Υλικών και Μηχανικής (PIMM) της École Nationale Supérieure d'Arts et Métiers (ENSAM) (μέλος του ParisTech), στα πλαίσια του προγράμματος ERASMUS, υπό την εποπτεία και καθοδήγηση του Καθηγητή Olivier Castelneau , επικεφαλή της ερευνητικής ομάδας CoMet: Συμπεριφορά και Μικροδομής των Μετάλλων, και του Καθηγητή Patrice Peyre, επικεφαλή της ερευνητικής ομάδας Laser: Κατεργασίες με Laser.

Οι βασικές παράμετροι που εξετάζονται και διαφοροποιούν τα κατασκευασθέντα δείγματα είναι οι εξής: πρώτον, η ενεργειακή κατανομή της δέσμης είναι τύπου Top Hat σε αντίθεση με την τύπου Gaussian η οποία χρησιμοποιήθηκε στις προηγούμενες ερευνητικές εργασία που πραγματοποιήθηκαν στο εργαστήριο PIMM. Δεύτερον εξετάστηκαν δύο ταχύτητες: 200 mm/ min και 400 mm/min. Τέλος, η πιο σημαντική παράμετρος που εξετάστηκε ήταν ότι από τα οκτώ δείγματα που παρήχθησαν τα μισά υπέστησαν επανάτηξη (δηλαδή εναπόθεση λέιζερ χωρίς παράλληλη εναπόθεση σκόνης).

Για να εξετάστουν οι επιδράσεις των παραπάνω παραμέτρων, χρησιμοποιήθηκαν οι ακόλουθες μέθοδοι: Ανάλυση επιφανειακής τραχύτητας, Οπτικό μικροσκόπιο (OM), Ηλεκτρονικό Μικροσκόπιο Σαρώσεως (SEM), Μικροσκόπιο EBSD (EBSD), Περίθλαση ακτίνων-Χ (XRD), Μικροσκληρότητα και Δοκιμές Εφελκυσμού.

Από τα αποτελέσματα του ερευνητικού αυτού έργου προέκυψε ότι ο παράγοντας της ανάτηξης οδηγεί σε καλύτερα αποτελέσματα καθώς βελτιώνει την ομοιογένεια κατά μήκος της μικροδομής των κατασκευασμένων δειγμάτων. Επιπλέον, παρόλο που η ταχύτητα δε διαφοροποίησε σημαντικά τα αποτελέσματα μεταξύ των δειγμάτων, τα δείγματα που κατασκευάστηκαν με ταχύτητα 200 mm/min παρουσίασαν σχετικά καλύτερα αποτελέσματα.

ΛΕΞΕΙΣ ΚΛΕΙΔΙΑ:
Άμεση Εναπόθεση με Λέιζερ, (DLMD), Ti6Al4V ενισχυμένο κράμα τιτανίου με TiC, Μικροδομές, Μηχανικές ιδιότητες, Τραχύτητα επιφάνειας, Οπτικό μοκροσκόπιο (OM), Ηλεκτρονικό Μικροσκόπιο Σαρώσεως (SEM), Μικροσκόπιο (EBSD), Περίθλαση ακτίνων-Χ (XRD), Μικροσκληρότητα, Δοκιμές Εφελκυσμού.

Acknowledgements

First of all, I would like to thank **Professor Dimitrios I. Pantelis** for his teaching, support and guidance throughout my studies at the National Technical University of Athens. I am very grateful for the things he taught me, both scientific and moral, during the supervision of my Diploma Thesis and for giving me the opportunity to complete this project within the ERASMUS program at the Ecole Nationale Supérieure d'Arts et Métiers [ENSAM].

I would also like to thank **Professor Olivier Castelneau (**Senior Research Scientist at CNRS-PIMM Laboratory of the Ecole Nationale Supérieure d'Arts et Métiers [ENSAM]-France) and **Professor Patrice Peyre (**Senior Research Scientist at CNRS-PIMM Laboratory of the Ecole Nationale Supérieure d'Arts et Métiers [ENSAM]-France), for their continued guidance, mentoring and support throughout the realization of the experimental part of this project in France. Their patience and overall help were very significant and are greatly appreciated by the author. Also I would really like to thank **Cyril Gorny** for his help and for his willingness to always find solutions to any problem that would arise.

Furthermore, I would like to thank **Professor Thierry Baudin, Jocelyn Hoarau** and **Francois Brisset** from the ICMMO laboratory of the Paris-Sub University, for making it possible to have good results despite the difficulties and the distance that were involved.

Finally, I would like to thank my parents and my sister for their continuous support and love; things that value most and cannot be appreciated enough with words.

Contents

Introduction

A. Motivation

The extremely rapid technological developments and the constant need for new innovative solutions to complex problems, has reinforced the interest among the scientific society to better understand the use of composite materials in various applications and via various processes.

Metal Matrix Composites (MMCs) are widely used in today's most challenging industries such as biomedical engineering, the aircraft industry and the aerospace industry due to their advanced properties in comparison to the 'natural' materials. A MMC can be defined as *a material in which a continuous metallic phase (the matrix) is combined with another phase (the reinforcement) to strengthen the metal and increase high-temperature stability*.[1] Thus, MMCs have attracted a lot of attention over the last years. In particular, Titanium Matrix Composites (TMCs) are very often used as they present numerous advantages such as: high specific strength, elevated temperature resistance, low density, high elastic modulus and good corrosion resistance. Because of their high price though, it is very significant that new ways of processing them should be found to eliminate to the maximum the waste of the material that can occur during the process.

Rapid prototyping techniques and in particular Direct Laser Metal Deposition [DLMD], present this opportunity. Although the waste during the process is not negligible, the ability to recycle and reuse the material minimizes the overall waste at significant amounts. During [DLMD], by acquiring data from a CAD file of a component, powder is fed at a controlled rate into the focal point of the laser while they are both deposited simultaneously. Particles are melted and with the movement of the laser defined by the CAD file, a new layer is produced. This process presents numerous advantages such as the ability to form small quantities of functional prototypes, and to construct complex geometries. The aim of this current project is to investigate and advance the research concerning the relationship and the connection between the laser parameters and their effects on the microstructure obtained as well as on the mechanical properties of the manufactured samples. It is continuation of the work that was previously done by **Audrey Racle [28]** and **Ahmadou Mbaye [27]** in the context of the MAGIS-Paris Master's Program in the field of Materials Science and Engineering.

[1] "Metal Matrix Composite." *TheFreeDictionary.com*. N.p., n.d. Web. 29 June 2012. <http://encyclopedia2.thefreedictionary.com/metal matrix composite>.

B. Thesis Introduction

The aim of the current project, as previously mentioned, is to better understand the connection between the DLMD parameters and the effects they have on the microstructure and the mechanical properties of the fabricated samples. It is a very crucial and difficult subject as there are a lot of variables that contribute to the final products. With perseverance and methodical work, in every new study, scientists around the world try to implement new ideas on the ways those parameters could be linked together in order to present every time new results that could further clarify these connections.

For this reason, in the current study, apart from the slight changes of the principal parameters that were used, two novel parameters were introduced in comparison to the work that was previously done at the Process and Engineering in Mechanics and Materials laboratory (PIMM) of the École Nationale Supérieure d'Arts et Métiers [ENSAM]; first of all, the laser's transmission was of *Top hat* type (instead of *Gaussian type*) and secondly, half of the samples that were fabricated, in-between the simultaneous deposition of the powder and the laser, they underwent an only - laser pass in order to remelt the last layer that was formed.

The analysis that followed contained a lot of different methods in order to investigate the results that were received by these novelties from a multiple scope.

C. Thesis Outline

This introduction is followed by Part I, which consists of the Theoretical Part of the current thesis project. In Chapters I.1 and I.2, the basic theory of Rapid Prototyping Techniques and of Direct Laser Metal Deposition [DLMD] - which is the process addressed in this research – are presented. Chapter I.3 gives an in depth overview of Titanium and its properties which is the material used in the current research project. In Chapter I.4, the outcomes of previous scientific studies that have been conducted around the some topic are discussed. Following, in Part II the experimental procedures that were realized for the current diploma thesis are thoroughly presented. Part III consists of the results that were acquired after the completion of the experiments. The conclusions and suggestions for potential future work are presented in Part IV. Finally, Part V consists of all the references (articles, books, websites) used for the composition of this thesis project.

I. THEORETICAL PART

CHAPTER I.1

Rapid Prototyping Techniques

I.1 History of Rapid Prototyping Techniques

Rapid prototyping generally refers to techniques that produce shaped parts by gradual creation or addition of solid material. It is a revolutionary and powerful technology with wide range of applications. The process of prototyping comprises fast building up of a prototype or working model for the purpose of testing the various design features, ideas, concepts, functionality, output and performance. The user is able to give immediate feedback concerning the prototype and its performance. Rapid prototyping is an essential part of process of system designing and it is believed to be beneficial regarding the reduction of project cost and the risks that are to be concerned.

History of Rapid Prototyping **[2]**

Sixties-Seventies: The beginning

The first rapid prototyping techniques became accessible no sooner than in the late eighties, when they were used for production of prototype and model parts. The history though of rapid prototyping can be located at the late sixties, when University of Rochester engineering professor Herbert Voelcker developed the early mathematical theory and algorithms that form the basis for computer programs that design machine parts including how to specify the surfaces of parts in three-dimensions. In his attempt, Voelcker was particularly interested in automating a process that would take data from these computer programs to program the new computer-controlled machine tools. These theories shape the basis of modern computer programs which are used for designing almost all mechanical items i.e the development of Computer Aided Design (CAD) software programs as they are known today. They changed the designing methods in the seventies, without though totally replacing the old methods for designing, which were actually still very much in use. The old method elaborated either a machinist or machine tool controlled by a computer. The metal hunk was cut away and the needed part remained as per requirements. Most of Voelcker's work became an operational customary throughout the 1970s in terms of how mechanical parts were designed.

Eighties: The revolutionary idea

In 1987, Carl Deckard, a researcher form the University of Texas, introduced a new revolutionary idea. He pioneered the layer based manufacturing, as in building up the model layer by layer (single layer's width 0.1mm to 0.7mm). By printing 3D models he utilized laser light for fusing metal powder in solid prototypes, single layer at a time. These layers could be determined by breaking down the surface of the part into planar triangles that are comparable to "the facets of a jewel". The coordinates and orientation of these triangles comprise a mathematical representation that can then be translated programmatically. The results of this technique were extremely promising. Although the history of rapid prototyping is quite new, this technique of rapid prototyping has a very wide ranging scope and applications with remarkable results revolutionizing the designing and manufacturing processes.

The efforts of Voelcker and Deckard became the basis for Rapid Prototyping (often referred to as free form fabrication).

Despite the aforementioned, the industry also gives recognition as the father of rapid prototyping, to Charles Hull for the patent of Apparatus for Production of 3D Objects by

Stereolithography. Hull built up a patent portfolio covering many fundamental aspects of today's additive manufacturing technologies such as data preparation via triangulated models (STL file format) and slicing, and many exposure strategies such as alternating hatch directions.

Present-day Rapid Prototyping

Today, the computer engineer has to simply sketch the ideas on the computer screen with the help of a design program that is computer aided. Computer aided designing, most commonly known as CAD, allows to make modification as required and allowing the possibility of creating a physical prototype that is a precise and accurate 3D object.

Fig.1 displays a schematic representation of the evolution of rapid prototyping as a comparison of digital and analog manufacturing.

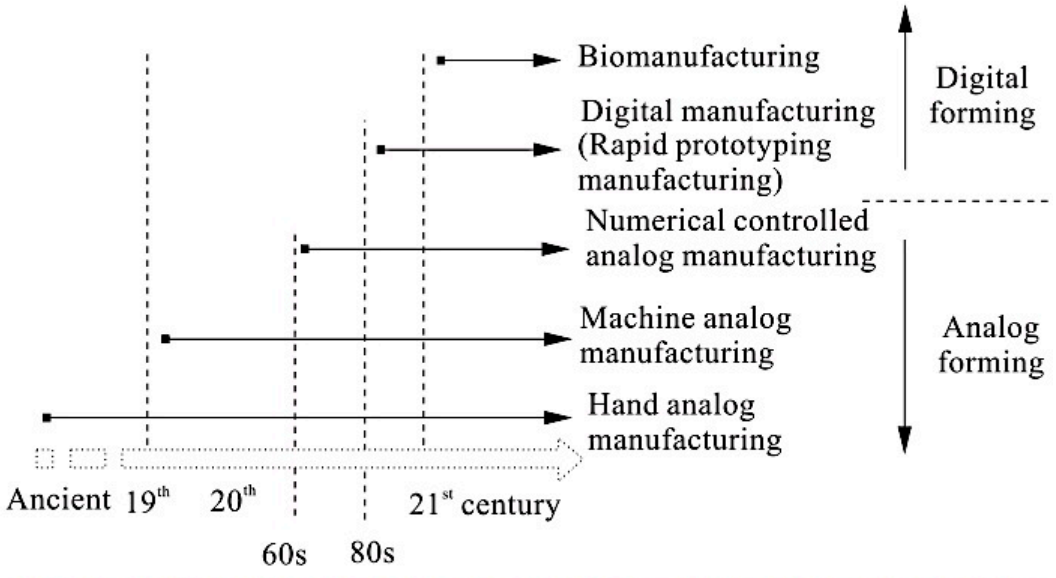

Figure 1: Illustration of digital and analog manufacturing [33].

I.2 Basic Principles of Rapid Prototyping Technologies

Although they are several rapid prototyping techniques, they all follow the same basic five-step principle. The steps are **[3], [4]**:

1. Creation of a CAD model of the design
2. Convert the CAD model to STL format
3. Slice the STL file into thin cross-sectional layers
4. Construct the model one layer above another
5. Clean and finish the model

CAD Model Creation: Initially, the object to be built is modeled using a Computer-Aided Design (CAD) software package. The designer can use a pre-existing CAD file or may wish to create one expressly for prototyping purposes. This process is identical for all of the RP build techniques.

***Conversion to STL Format*:** The various CAD packages use a number of different algorithms to represent solid objects. To establish consistency, the STL-format (stereolithography), which was the first Rapid Prototyping technique, has been adopted as the standard of the rapid prototyping industry. Conversion of the CAD file into STL format is therefore the next step. This format represents a three-dimensional surface as an assembly of planar triangles. The file contains the direction of the outward normal of each triangle and the coordinates of the vertices. Curved surfaces cannot be represented exactly because STL files use only planar elements. Increasing the number of triangles improves the approximation but it also increases the file size. Large, complicated files are more time-consuming to pre-process and build. In these cases, the designer must balance accuracy with manageability to produce a useful STL file. The **.stl** format is universal and thus this process is the same for all of the RP build techniques.

Slice the STL File: **'**Slicing the STL file' means that at this point of the procedure, a pre-processing program has to prepare the STL file to be built. There are several programs available and most of them allow the user to adjust the size, location and orientation of the model. Build orientation is critical for several reasons. First of all, properties of rapid prototypes vary from one coordinate direction to another. For example, prototypes are usually weaker and less accurate in the z (vertical) direction than in the x-y plane. Moreover, part orientation partially determines the amount of time required to build the model. By placing the shortest dimension in the z direction for instance, reduces the number of layers and thereby shortens the build time. The pre-processing software slices the STL model into a number of layers from 0.01 mm to 0.7 mm thick, depending on which technique is applied. The program can also generate an auxiliary structure to support the model during the build. Such supportive structures are useful for delicate features such as overhangs, internal cavities, and thin-walled sections.

Layer by Layer Construction: The fourth step is the actual construction of the part. Using one of the existing rapid prototyping technique machines, one layer at a time from polymers, paper, or powdered metal is built. Most machines are fairly autonomous, needing little human intervention.

Clean and Finish: The final step of this procedure is post-processing. This involves the removal of the prototype from the machine and the detachment of any supports. Prototypes may also require minor cleaning and surface treatment such as sanding, sealing, and/or painting which will improve its appearance and durability.

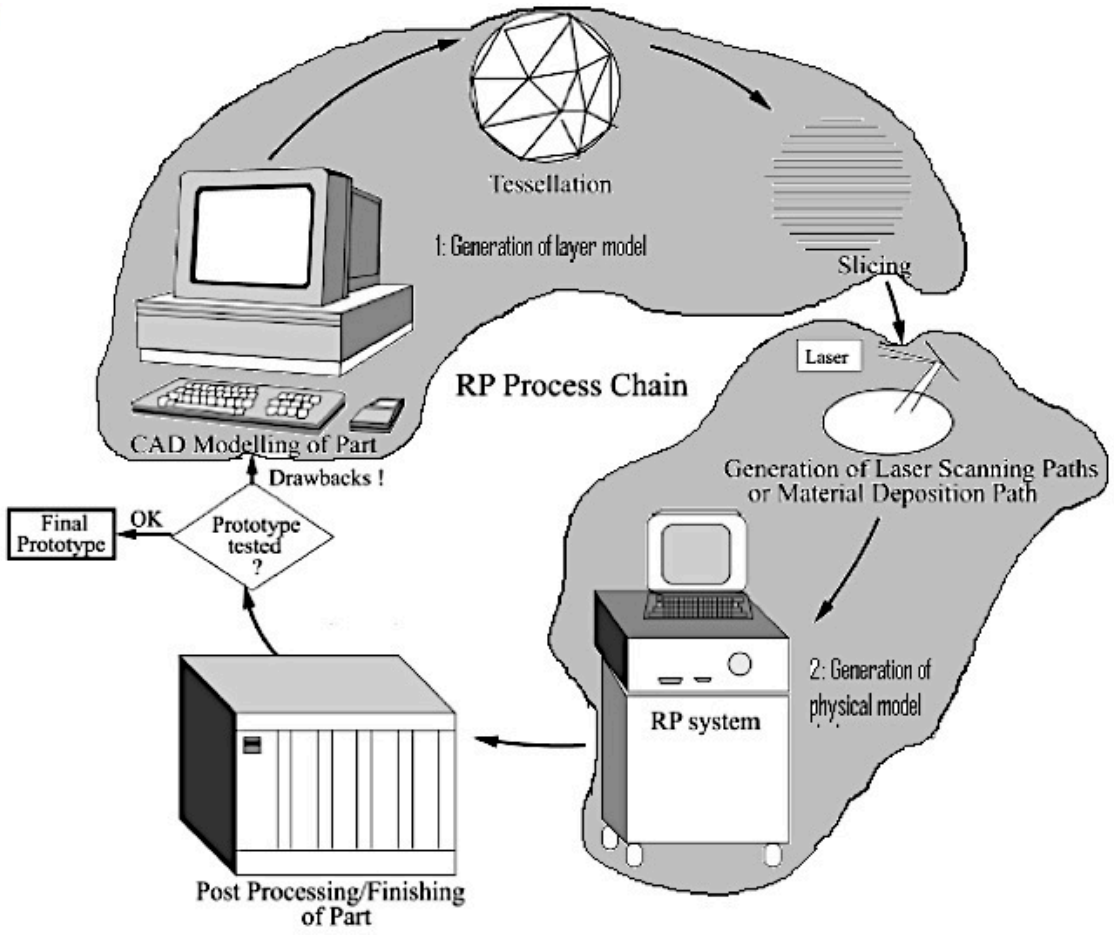

Figure 2: Process chain in Rapid Prototyping procedure steps [4].

I.3 Common Rapid Prototyping Technologies

Prototyping processes are classified in numerous ways. However, one representation based on German standard of production processes classifies RP processes according to state of aggregation of their original material as illustrated in Fig. 3 **[3],[4]**.

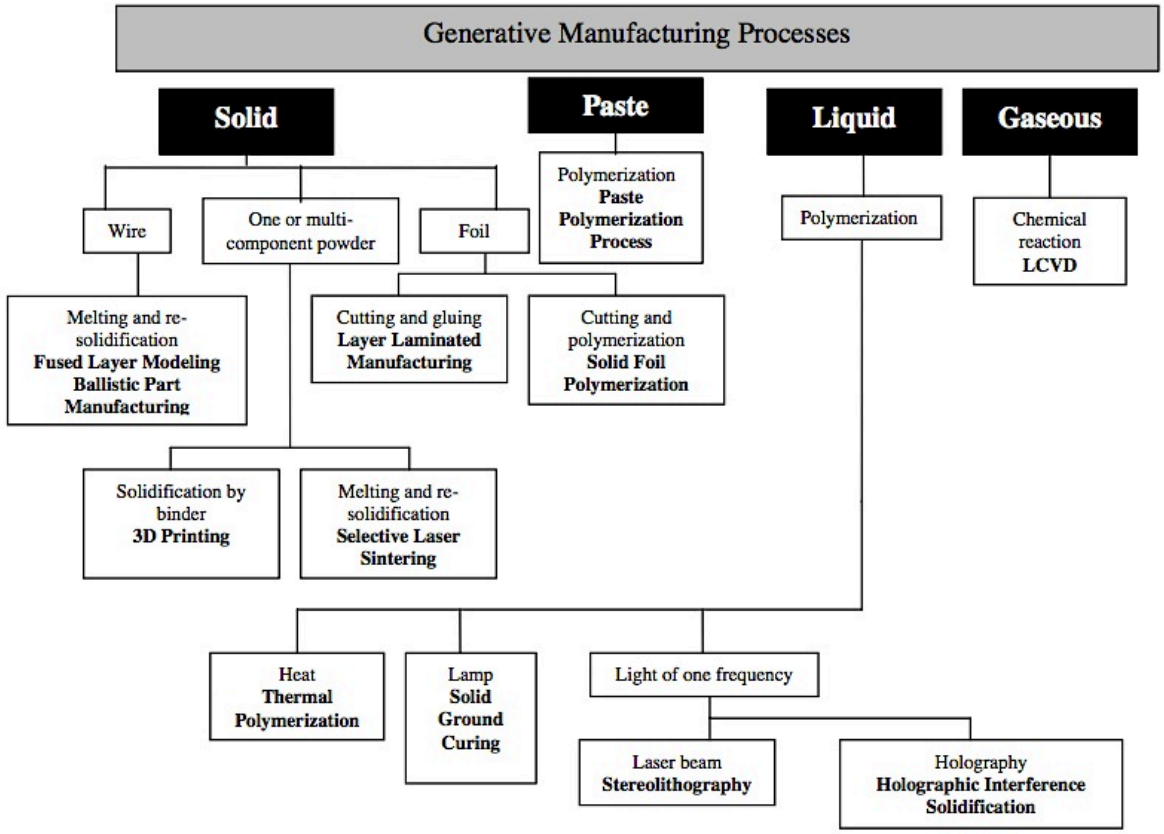

Figure 3: Classification of RP processes [4].

Some of the most important Rapid Prototyping processes that are described below are:

- Stereolithography (SL)
- Selective Laser Sintering (SLS)
- Fused Deposition Modeling (FDM)
- Laminated Object Manufacturing (LOM)

Stereolithography

In this process photosensitive liquid resin is used as a fundamental concept. This resin, when exposed to ultraviolet light, forms a solid polymer. Because of the concentration and scattering of beam, the reaction only happens near the surface, and voxels of solid polymeric resin are formed. A SL machine consists of a build platform (substrate), which is mounted in a vat of resin and a UV Helium-Cadmium or Argon ion laser. The laser scans the first layer and platform is then lowered equal to one slice thickness and left for a short time so that liquid polymer settles to a flat and even surface and inhibit bubble formation. Afterwards, the new slice is scanned. In new SL systems, a blade spreads the resin by traversing the vat. This ensures smoother surface and reduced recoating time. It also reduces trapped volumes, which are sometimes formed due to excessive polymerization at the ends of

the slices. When the complete part is deposited, it is removed from the vat and then excess resin is emptied which may take long time due to high viscosity of liquid resin. The green part is then post-cured in an UV oven after removing support structures. A typical schematic illustration of Stereolithography is shown in Fig. 4.

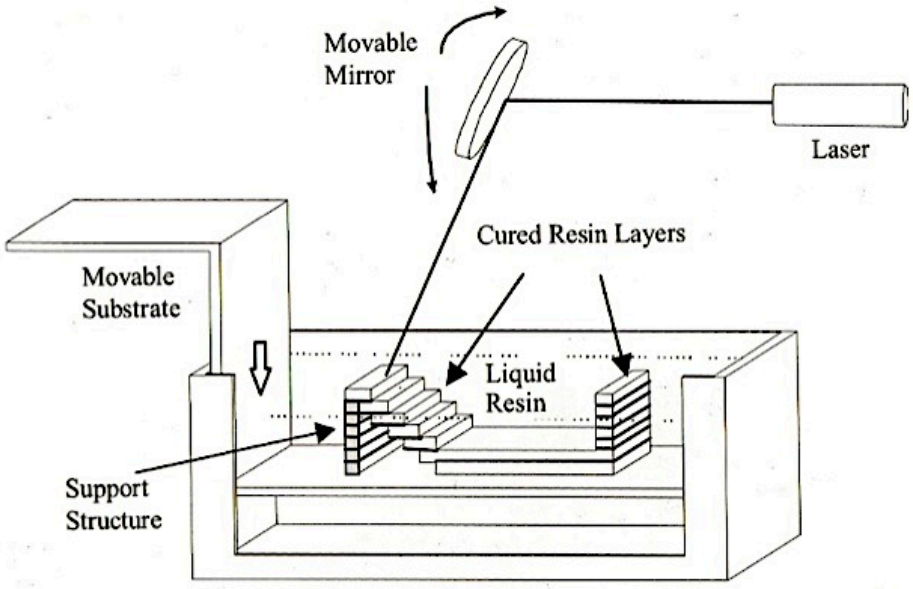

Figure 4: Stereolithography [4].

Build strategies have been developed to increase build speed and to decrease amount of resin by depositing the parts with a higher proportion of hollow volume. These strategies are developed as these models are used for making cavities for precision castings.

Selective Laser Sintering

In Selective Laser Sintering (SLS) process, fine polymeric powder like polystyrene, polycarbonate or polyamide etc. (20 to 100 micrometer diameter) is spread on the substrate using a roller. Before starting CO2 laser scanning for sintering of a slice the temperature of the entire bed is raised just below its melting point by infrared heating as to minimize thermal distortion and facilitate fusion to the previous layer. The laser is modulated in such a way that only those grains, which are in direct contact with the beam, are affected. Once laser scanning cures a slice, the bed is then lowered and the powder feed chamber is raised so that a covering of powder can be spread equally over the build area by counter rotating roller. In this process support structures are not required as the unsintered powder remains at the places of support structure. It is cleaned away and can be recycled once the model is complete. A typical SLS configuration is given in Figure 5.

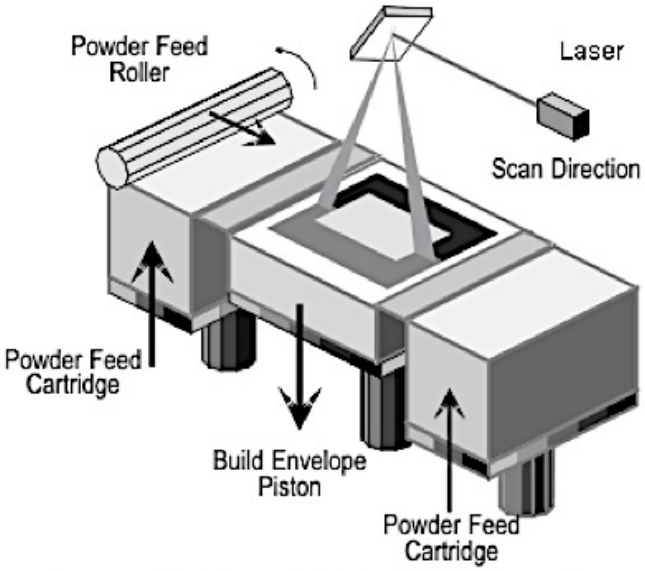

Figure 5: Selective Laser Sintering System [4].

Fused Deposition Modeling

In Fused Deposition Modeling (FDM) process a movable (x-y movement) nozzle deposits on to a substrate threads of molten material. The build material is heated slightly above its melting temperature so that it solidifies within a very short time (approximately 0.1 s) after extrusion and cold-welds to the previous layer as shown in Fig. 6.

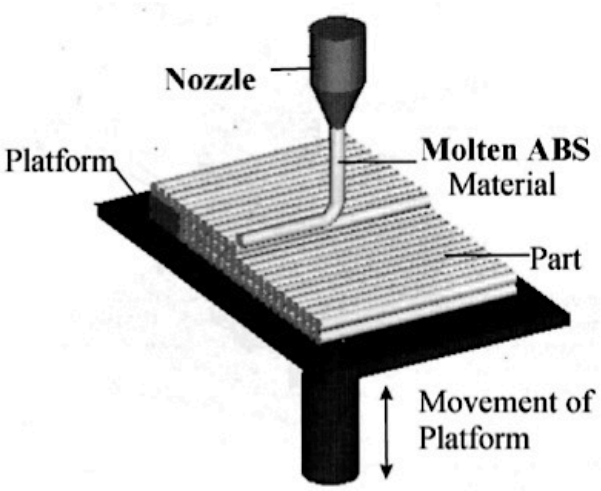

Figure 6: Fused Deposition Madeling Process [4].

The factors that need to be considered are various; steadiness of the nozzle, material extrusion rates, addition of support structures for overhanging features and speed of the nozzle head are quite few parameters that affect the slice thickness. More recent FDM systems include two nozzles, one for part material and other for the support material. The support material is relatively of poor quality and can be broken easily once the complete part is deposited and is removed from substrate. Even more recent FDM technologies have water-soluble support structure material.

Laminated Object Manufacturing

Fig. 7 illustrates a typical system of Laminated Object Manufacturing (LOM). The slices that are cut, require to be formed *by the supply roll of material* by using a 25-50 watt CO2 laser beam. New slices are bonded to previously deposited ones by using a hot roller, which activates a heat sensitive adhesive. The unwanted material is also hatched in rectangles to facilitate its later removal but still remains in place during the build to act as supports. After the completion of one slice, the platform can be lowered and the roll material can be advanced onto a second roller until a fresh area of the sheet lies over the part.

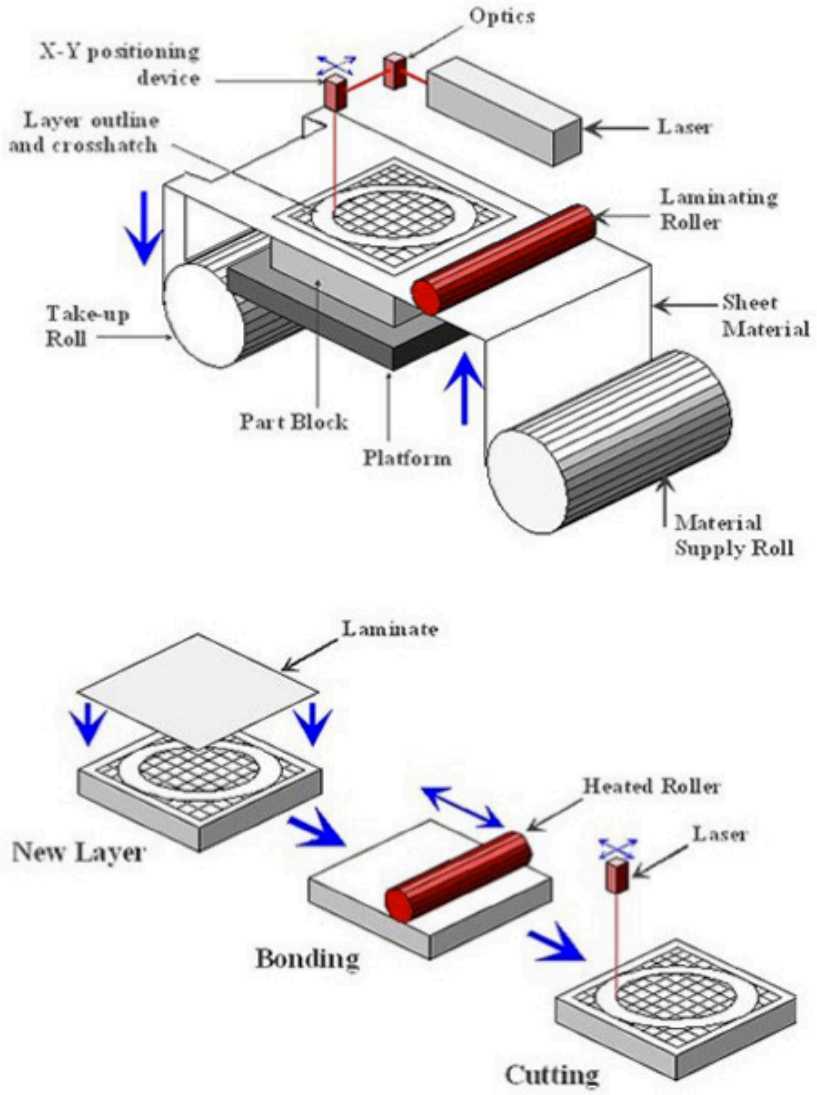

Figure 7: Laminated Object Manufacturing Process [4].

With this process, materials that are relatively cheaper like paper, plastic roll etc. can be used and parts of fiber-reinforced glass ceramics can be produced. It is in addition a very fast technique as large models can be produced and the building speed is 5-10 times faster as compared to other RP processes. One limitation of this process is that large amount of scrap is formed thus creating potential danger of fire hazards.

CHAPTER I.2

Direct Laser Metal Deposition

I.2.1 Introduction

In the current economic situation, with a free and globalized trade, the importance of producing new time and cost effective products increases. Particularly, the tooling processes, which are expensive and time consuming need to be reassessed. The new standards the market has forced concerning the geometric complexity, the number of variants and the amount of other requirements that characterize the new products, has reinforced the need to find new ways of producing these products. Two of the biggest challenges for manufacturing companies of the twenty-first century are reducing time and the international competitiveness. Immediate reactivity to customer requests are also critical and they have to be combined with high quality, low cost and better functionality than before. These factors push the manufacturing companies to find solutions both in technology and in organization.

Material Accretion Manufacturing (MAM), which consists of additive technologies, and the modern operational structures, are effective tools that contribute in reducing time and costs. They are most likely the best solution that western industry can take to survive the intense competition with other countries, as for example Asiatic and Eastern European ones, where labor has a very low cost, but nonetheless is able to achieve good quality products.

Among the various MAM technologies, which have offered the possibility to apply the basic concepts of Rapid Prototyping for the creation of finished products, the Direct Laser Metal Deposition (DLMD) process of metal powders stands out. The DLMD relate the group of technologies called Material Accretion Manufacturing (MAM), and, more precisely, is based on the principles of rapid prototyping (RP) and laser cladding. The MAM technologies start with a three-dimensional design to get the object in a single pass through an additive processing, that is overlapping each other layers with a small thickness. The purpose of the mechanical industry has always been to use the basic principles of rapid prototyping to direct manufacture metal parts with mechanical properties as close as possible to those of parts obtained with conventional processes.

I.2.2 Process and Process Parameters

Direct Laser Metal Deposition has been the main interest of a lot of researchers for several years and was finally introduced, in 1995-96, with three very similar processes. These processes are now acknowledged worldwide, under the names of Directed Light Fabrication (DLF), Light Engineered Net Shaping (LENS) and Direct Metal Deposition (DMD), developed respectively at the Los Alamos National Laboratory (Los Alamos, New Mexico, USA), at Sandia National Laboratory (Albuquerque, New Mexico, USA) and at the University of Michigan (Ann Arbor, Michigan, USA). The DLMD process combines powder metallurgy, solidification metallurgy, laser, CAD- CAM, CNC (Computer Numerical Control), rapid prototyping and sensors technologies. This process allows single step producing metal components, ready to use, without the need for dies, molds or tools and using a wide variety of metals, including those very difficult to work with conventional techniques **[6],[7],[8]**.

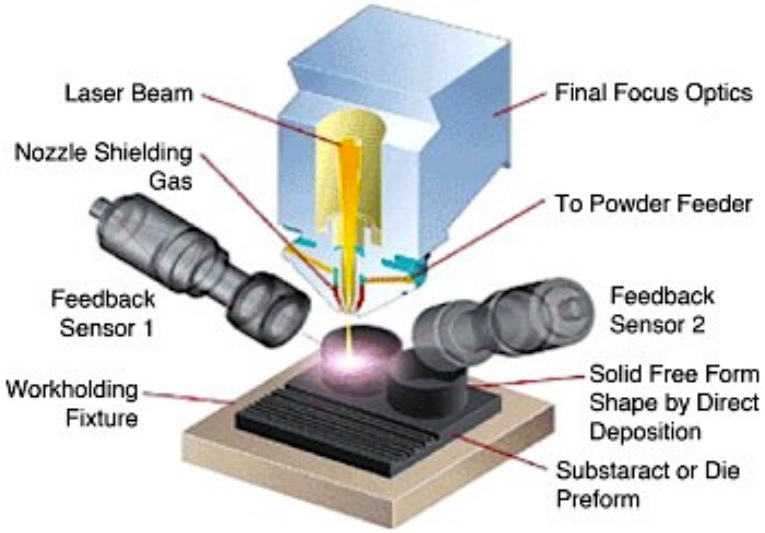

Figure 8: Schematic representation of the process [32].

The DLMD of metal powders is an additive process in which a metal powder is deposited on the base material, layer by layer, and melted with it. The process starts from the three-dimensional CAD representation of the part. Then it is fabricated by using the technique of layer by layer. There are two different processing solutions that can be adopted, depending on the type of system used; a 3-axis or a 5-axis CNC system. With the 3-axis systems the steps are the same to those described in Chapter 2, for all Rapid Prototyping processes, i.e initial conversion of the CAD files in STL files. The model obtained is later on equipped by supports, useful to tolerate overhangs, and finally subjected to the stage of slicing. In systems with 5 or more axis, in addition to translations along X, Y, Z, the head of the machine can perform rotations around the same directions. For these systems, which are increasingly popular, the slicing operation is carried out directly on 3D-CAD model, with layers having its normal always parallel to construction direction, which may differ from the Z axis. The biggest advantage of this method is that the conversion of 3D-CAD model into the STL format is not needed. In addition, with 5-axis systems, components that require the deposition of layers with different orientation with respect to the previous ones can be fabricated by angling the laser beam and nozzle that supplies powder or by angling the piece under construction. As a result, the axis of the laser beam is always normal to the plane of deposition.

The geometry of each layer is determined with the slicing and it is possible to define the path of the laser beam. Therefore, the movements of the machine head and of the worktable and the commands to control the laser and the powder feeder are defined. The influence of high thermal stresses and of surface tension, makes the tool path for the DLMD more complicated than that one of the traditional rapid prototyping processes. Thus, it is important to design an appropriate path, as it not only improves the quality of the final product, but also increases the efficiency of the manufacturing process. In the realization of the layers, DLMD technology incorporates laser cladding, a technique of metal surfaces coating performed by laser. The laser beam, through its heat energy, creates a molten pool with dimensions, on the XY plane, varying from half to five times the diameter of the focal spot, depending on the adopted power and scanning speed. A flow of metal powder is uninterruptedly injected in the molten pool, created on the substrate by the laser. Powder melts completely and then solidifies, making a very compact and welded to the substrate track. The beam-scanning path forms a set of tracks, one next to the other, with a designated amount of overlap. Most commonly, each track is started and stopped on the outer edges of

the piece until the entire first layer is completed. The heat stored in the substrate or in the previously deposited material also influences the size of the molten pool. If the heat loss happens very quickly the width of the molten pool decreases, and on the contrary, if the heat loss occurs very slowly the width of the molten pool increases. Thus, the size of the molten pool, otherwise interpreted as the properties of the final product, is heavily depended on the settings of the laser power and the processing speed.

The first layer is built on a metal substrate that is the construction base of the product. Usually, the substrate is made of the same material of the component that has to be built. Following the deposition of the first layer, laser head, that includes focusing lens, and powder delivery nozzle, move in the construction direction (Z direction in the case of 3 axis systems) depositing the second layer. In a similar repetitive manner, the process continues, line-by-line and layer-by-layer, until the entire component is built up.

PARAMETERS

The parameters that influence the quality of the products that can be obtained with DLMD are numerous and difficult to prioritize. A careful control of process parameters is crucial to achieve products with satisfactory dimensional accuracy and good mechanical properties.

The main process parameters are:

1. powder feed rate;
2. laser power;
3. scanning speed;
4. beam diameter;
5. layer thickness;
6. overlap percentage;
7. energy density.

The powder feed rate stands for the amount of powder per time unit that exits from the nozzle and it affects mainly the layer thickness: high flow rates result in very thick layers. In turn, the thickness of the deposited layer determines not only the dimensional and geometrical accuracies of the product, but its mechanical properties as well. Actually, if the same laser power is used, it becomes more difficult to obtain good adhesion between the layers when layer thickness increases.

The laser power depends on the type of laser used. Currently, the laser sources most broadly used for DLMD process are CO2 and Nd:YAG sources and the power of lasers ranges from 1 to 18 kW. The main difference between the CO2 and Nd:YAG lasers is the wavelength. The CO2 laser has a wavelength of 10.6 μm while that of the Nd:YAG laser is 1.06 μm. For most metals, the absorption of the laser energy increases when the wavelength decreases. Studies have shown that a greater depth of molten pool can be achieved through the use of a Nd:YAG laser due to increased energy absorption. However, most commercial machines are equipped with a CO2 laser because of its high efficiency, lower cost and it is more easily maintained than Nd:YAG laser.

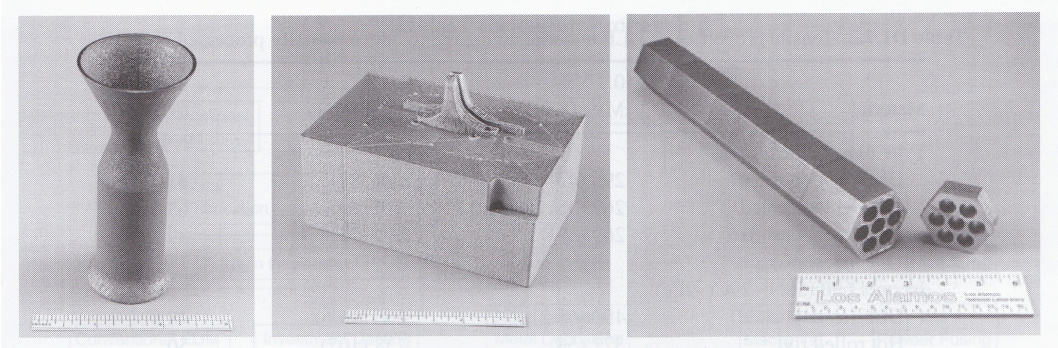

Figure 9 : Examples of components fabricated by the DLF process (left to right): a Ti-6Al-4V alloy rocket thruster, a 316 stainless steel injection die insert and an Inconel 690 high hexagonal conduit [6].

Scanning speed can be defined as the speed with which the laser beam finishes the tool path over the part that has to be built. Although high scanning speed decreases the time required to complete the sections it also affects negatively the quality of the final component. For example, high scanning speed can cause: differences in the height between the edges of the layers and deviation from the desired thickness.

The key parameter for the laser processing is the beam diameter. It determines the spot diameter, which is equal to the beam diameter at the focus, and, therefore, the size of the track. Consecutively, the surface roughness is affected as it is closely related to the size of the track. In addition, the beam diameter also affects directly the energy density.

The thickness of the layer is determined by the slicing of the CAD model. One of the greatest difficulties in the DLMD is to maintain the desired layer thickness, thus, it is preferable to use a feedback control system.

The overlap percentage is defined as the ratio between the area of overlap between two adjacent tracks and the total area of the track itself, measured on the work plane (Schneider, 1998):

$$\%O = \frac{Aoverlapped}{Atotal}$$

The overlap percentage affects the porosity and, therefore, the density and mechanical properties of the manufactured material.

As proven in several studies, the quality and mechanical properties of the DLMD components are strongly influenced by the size of the molten pool and by the residual stresses, which can be directly controlled from the laser energy input.

Energy density E [J/mm2], defined by the following equation, describes the laser energy input:

$$E = \frac{P}{hv}$$

where P is the laser power [W], h is the hatch spacing [mm], (the distance between the vectors drawn from the center of the laser spot in two parallel and consecutive tracks) and v is the scanning speed [mm/s]. In the event of overlapping zero, h becomes equal to the spot diameter.

I.2.3 Process Equipment

The equipment used for the DLMD process of metal powders consists of a set of subsystems that are interconnected. These subsystems provide a full control of laser power, speed, position of the spot, powder flow rate and size of molten pool.

The subsystems currently used are:

1. the control workstation;
2. the laser source;
3. the powder feeding system;
4. the multi-axis CNC system.

A feedback control system and a controlled atmosphere chamber may also be included in some systems.

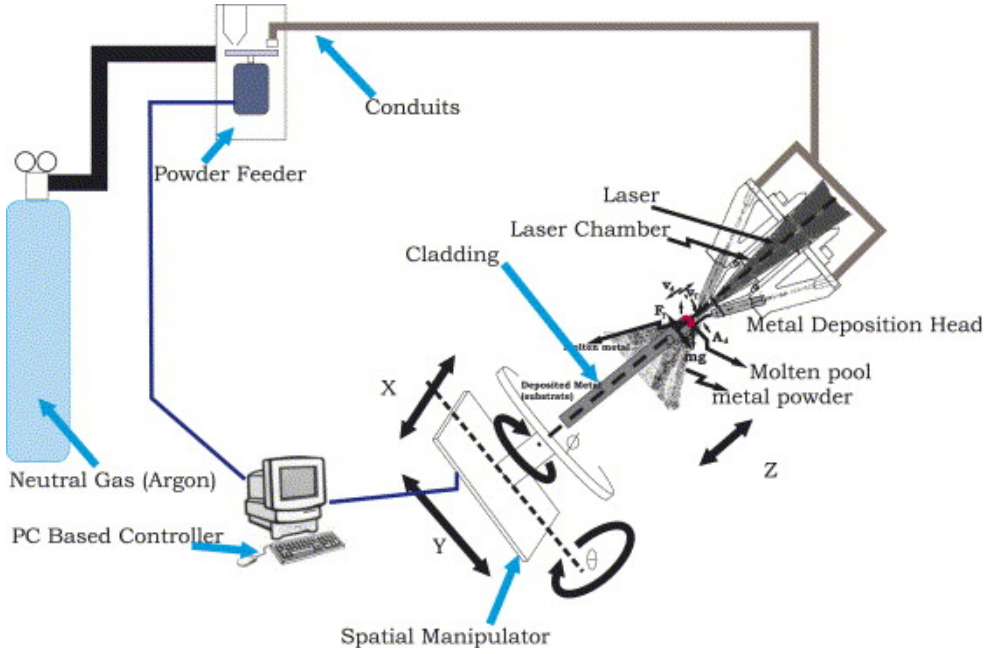

Figure 10: Components of the DLMD process combined [34].

The control workstation is a PC that collects the part data in the CNC instructions format, originated from 3D-CAD model by means of a CAD/CAM software. In addition, it communicates with all the subsystems and allows, therefore, the intelligent control of the entire deposition process.

The laser source that is used must have a high power, typically between 500 W and 6000 W, in order to melt both the metal substrate and the metal powder.

Through the powder feeding system the powder is available in the work area and can also be mixed with the several types of powders when simultaneous use is needed. It consists of some devices for the mass flow rate control, a mixer and a nozzle to deposit the material into the molten pool. In systems with several containers it is possible to produce mixtures of powders, filling each one with a different powder and combining them. The mixing of powders can be obtained either directly in the molten pool, feeding them simultaneously, or within the mixer. These two solutions make the process able to produce different types of alloys or to vary the composition of the material depending on the desired properties.

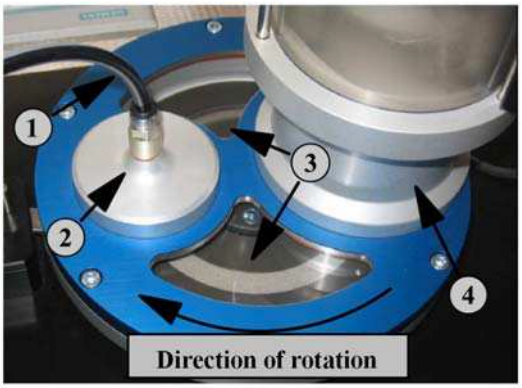

1. Powder feeding pipe
2. Powder outlet
3. Slot on the disc
4. Container

Figure 11: Disc powder feeder [8].

There are several mechanisms for the mass flow rate control that can be based on different operating principles. For example, one mechanism is constituted by a hopper, under each container, having a horizontal shaft with some caves on the lateral surface. The rotation speed of the shaft can be varied to control the mass flow rate. Another type of powder feeding system consists of a container from which the powder flows by gravity into a slot that is created on a rotating disc. The powder is transferred to a suction unit, which through a carrier gas flow, is sent to a nozzle. The parameters that influence the powder mass flow rate are the slot size and the rotating speed of the disc. The third type of powder feeding system consists of a pneumatic screw feeder; in this case the mass flow rate of powder depends on the rotating speed and on the size of the screw. Next the powder must be transferred to the work area: this can be done by means of a carrier gas (argon, helium, nitrogen) or simply by means of gravity. The powder feeding system ends with a nozzle that has to inject the powder into the molten pool. To increase the capture efficiency of powder by the molten pool, the nozzle has to be placed very close to the pool itself. This indicates that the nozzle is subjected to high thermal loads and, therefore, is usually made of brass. Consequently, it is also able to reflect the laser radiation that is back reflected from the molten pool.

Concerning the nozzle there can be several different configurations. There are two principal ones: with a coaxial supply and a lateral supply of powder. With the coaxial supply, the main advantages are the independence from the moving direction of the head, of the controlled heating of the powder before it goes into the molten pool and the high capture efficiency of powder by the molten pool. In this case, the powder moves coaxially to the laser beam. The nozzle (cone-shaped) consists of two internal annular interstices. The carrier gas, or primary gas, is used to transport powder outer the first interstice. A secondary gas, usually argon or helium, is injected into the inner interstice to perform various functions: to avoid wearing of powder flow, ensuring the captivity along the nozzle axis, and to prevent oxidation. However, some components may not be accessible by a coaxial powder nozzle. On the other hand, the lateral supply of powder allows the treatment of all types of geometries. Basically, the nozzles are lateral pipe with custom-made length, shape and diameter.

Component	Material	Deposition time (hr)	Deposition rate ($cm^3\ hr^{-1}$)	Deposition rate ($g\ hr^{-1}$)	Powder flow rate ($g\ hr^{-1}$)	Powder efficiency (%)
Rocket thruster	Ti–6Al–4V	0.75	12	55	431	13
	316 SS	0.87	9.8	77	822	6
Die insert	316 SS	57.7	7.2	59	822	7
Hexagonal conduit	Inconel 690	172	2.1	18	454	4
Plate ($2.6 \times 0.14''$)	Haynes 188	6.3	10.7	95	794	12
Rod ($0.75''$ diameter)	Inconel 690	15.6	7.2	59	277	21

Figure 12: Processing rates [6].

The multi-axis CNC system controls the position, the speed and the motion path of the laser spot. The motion path is determined either by slicing the STL model or directly from a 3D- CAD model, if the system has 3 or more axis (usually 5) respectively. The deposited powder mass tends to be irregular due to the oscillation of the laser power and to the difficulty of controlling the powder mass flow rate. This factors result in a flawed deposition, characterized by uneven surfaces and lack of adhesion between the layers. To regulate the height of the deposition a feed back control system can be used to control some of the variables, such as the energy density and powder flow rate. It usually consists of a detection height unit (Height Sensing Unit), a processing unit of the feedback signal (Signal Processing Unit) and an optical sensors apparatus with CCD cameras. The detection height unit elaborates the images from the optical sensors apparatus, which generally consist of at least two cameras in order to neutralize the effect of the laser head movement. Through the processing unit it is possible to repair an anomalous deposition. In the case of a lower than desired deposition, solving the problem may be by repeating the path on the same layer before moving to the next. On the other hand, a deposition greater than desired can be resolved reducing the laser power and the powder flow rate as quickly as possible. If the use of shielding gas ejected from the head is insufficient to have a good deposition, then the process can be performed in a sealed chamber in which there is a controlled atmosphere consisting of inert gases, such as argon, helium or nitrogen. Without this condition, the fabricated component may have extreme porosity and oxidation, with insufficient adhesion between layers and, consequently, very poor mechanical properties. When a controlled atmosphere chamber is used, DLMD becomes a free waste process. Truly, the powders not fused by the laser during the process can be saved through a suction system, filtered and reused. This characteristic makes it particularly attractive when it has to process very expensive or hazardous materials that require containment during processing.

I.2.4 Comparison with conventional manufacturing technologies: Advantages and Disadvantages

Metal parts are usually produced by means of thermo mechanical processes, including casting, rolling, forging, extrusion, machining and welding. Conventionally, to obtain the finished pieces multiple steps and heavy equipment, forms, dies and tools are required. The use of this equipment is justified and profitable in mass and in large sets production. When the part is unusual in form, has complex internal cavities or has to be made in small batches,

costs and time to prepare the production rapidly increase thus conventional technologies are practically not applicable.

On the other hand, the DLMD process fabricates the required components already with the final material, with mechanical properties close to or, in some cases, higher than those obtained with conventional processes. With DLMD there can be parts with extremely complex geometries, usually oversized of 0.025 mm. Following a quick cleaning, in order to achieve the tolerances and the surface finishes required, they are ready to use.

Using DLMD of metal powders chemical segregation is eliminated. This problem occurs in parts obtained by casting and to resolve it, homogenizing heat treatments and plastic deformations for the grain refinement are indispensable. Chemical homogenization is achieved by randomizing the composition by using powders as input material and by limiting chemical diffusion in the liquid state to the boundaries of the small molten pool that is used to deposit the entire component.

Moreover, the high solidification rate, which results from the narrow HAZ (Heat-Affected Zone), and the high temperature gradients that are generated around the molten pool, allows a fine grain microstructure. Another positive aspect of this process involves the production speed increasing. A study by the National Center of Manufacturing Science, Michigan, showed that the direct laser deposition of metal powders can reduce by 40% the time to produce a mold.

Another advantage of this technology is determined by the reduction of the labor required and of the equipment cost, since there is only one machine that runs the entire process automatically. An extra machine tool or EDM is only used later on to finish the piece. This results in a decrease of the floor area needed for the factory and for the warehouse.

Even compared to the use of CNC machine tools, DLMD is suitable because of at least further two advantages: there is no waste and the purity of the final component is higher. In fact, the processes performed by the CNC machine tools apart from the finished part, they also result in metal chips, fluids, lubricants for cutting and worn tools that need to dispose of. In the contrary, the DLMD process results only in the desired component. There are no wastes since this process can be achieved in a controlled atmosphere, with high purity inert gas. The powder that was not melted by the laser can be extracted and used again.

This feature makes DLMD particularly attractive especially when it has to use very expensive or hazardous materials.

Fig. 13 shows an example of how properties of finished products vary when different processes are used.

Material	0.2% YS[a] (MPa)	UTS[b] (MPa)	Elong. (%)
DLF 316 ss	296	579	41 (46)
316 ss (cast)	269	517	39
316 ss (wrought)	262	572	63
DLF inconel 690	448	669	49
Inconel 690 (wrought)	372	738	50
DLF Ti-6Al-4V	958	1027	6
Ti-6Al-4V (cast)	889	1014	10
Ti-6Al-4V (wrought)	827–1000	931–1069	15–20

YS[a] : Yield Strenght, UTS[b]: Ultimate tensile strength

Figure 13: Properties of DLF Deposited Materials Compared with Conventionally Processed [7].

CHAPTER I.3

Ti & Ti Matrix Composites

I.3.1 History and Production of Titanium

Titanium was first recognized by Wiliam McGregor, a clergyman and amateur mineralogist, in 1791, who detected the oxide of an unknown element in local ilmenite sand ($FeOTiO_2$). The name of the metal come form the German chemist Martin Heinritch Klaproth, who made similar observations in 1795 at the mineral rutile (TiO_2), thus naming the titanium element after the mythological first sons of the Earth, Titans. The first impure Ti was isolated in 1825 but the first production of Titanium was realized in 1937 in Luxembourg, when Kroll reacted $TiCl_4$ with molten magnesium under an atmosphere of argon. This discovery opened the way to the industrial exploitation of titanium.

The preparation of pure titanium is difficult because of its reactivity. Titanium cannot be obtained by the common method of reducing the oxide with carbon because a very stable carbide is readily produced, and, moreover, the metal is quite reactive toward oxygen and nitrogen at elevated temperatures. In the Kroll process, one of the ores, such as ilmenite ($FeTiO_3$) or rutile (TiO_2), is treated at red heat with carbon and chlorine to yield titanium tetrachloride, $TiCl_4$, which is fractionally distilled to eliminate impurities such as ferric chloride, $FeCl_3$. The $TiCl_4$ is then reduced with molten magnesium at about 800° C (1,500° F) in an atmosphere of argon, and metallic titanium is produced as a spongy mass from which the excess of magnesium. On the laboratory scale, extremely pure titanium can be made by vaporizing the tetraiodide, TiI_4 and decomposing it on a hot wire in vacuum **[5]**.

In short, the essential features of the process are as follows:

1. Briquette of TiO_2 with coke and tar and chlorinate at 800℃ to promote the reaction: $TiO_2 + 2Cl_2 + 2C \rightarrow TiCl_4 + 2CO$.
2. Purify $TiCl_4$ by fractional distillation.
3. Reduce $TiCl_4$ by molten magnesium or sodium under an argon atmosphere, one reaction being: $TiCl_4 + 2Mg \rightarrow Ti + 2MgCl_2$.

The most convenient source of titanium is the mineral rutile (TiO_2), which is found in beach sands along the eastern coast of Australia and in estuaries in Sierra Leone. Most of the titanium metal is extracted from rutile but in the future the major titanium source will be the mineral ilmenite which is much more plentiful and more complex at the same time. Currently, titanium metal accounts for only the 3% of all minerals production. The most common extraction procedure that is used now is known as the consumable-electrode arc furnace as shown in Fig. 14. The melting is carried out in a copper crucible by circulating water or a liquid sodium-potassium eutectic. Heat is then generated by a direct current arc that is struck between an electrode of titanium to be melted and a starting slung of this material contained in the crucible.

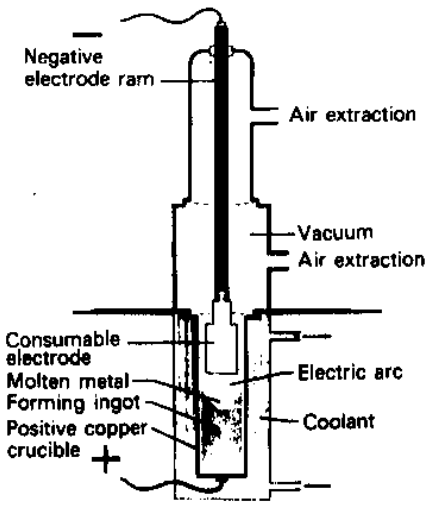

Figure 14: Consumable-electrode arc furnace for melting and refining titanium [5].

An advantage of the liquid alloy coolant is that it does not react with titanium if the electric arc drills the crucible, whereas water and steam can cause an explosion. The entire arrangement is encased in a vessel that can be evacuated where inert gas such as argon is introduced. Double and sometimes triple melting is carried out to improve the homogeneity of the ingots. Titanium alloys are usually used for critical rotating parts of gas turbine engines and for this reason, special attention must be given in order to eliminate the inclusion of castings which may serve as sites for the initiation of fatigue cracks in components such as forged compressor discs.

Overall, the energy consumed in making pure titanium sponge is greater than that required for producing any other form of metals in ingots form. Impressively, it is about 70% higher than the energy needed to extract an equally weighted aluminium and as much as 14 times the energy required to produce steel. A more ecological solution would be to produce titanium by the electrolysis of fused salts, but this method is not very useful from a commercial scope. Likewise, techniques involving carbothermic and plasma reduction of Ti compounds are still applicable only in laboratories. Conventional arc melting process, however, tends to become more economical. A typical example would be the Kobe Company in Japan that has decreased the operation time by using higher voltage and current.

I.3.2 Properties of Titanium

Titanium is widely distributed and constitutes 0.44 percent of the Earth's crust. The metal is found combined in practically all rocks, sand, clay, and other soils. It is also present in plants, animals, natural waters as well as meteorites and stars.

Pure titanium is ductile, about half as dense as iron and less than twice as dense as aluminum; it can be polished to a high lustre. The metal has a very low electrical and thermal conductivity and is paramagnetic (weakly attracted to a magnet) **[1], [5], [9], [10], [11]**.

Titanium has two crystal structures which are categorized according to the temperature status of the metal; below 883° C (1,621° F) there is the hexagonal-close-packed (hcp) structure (*alpha)* and above 883° C, the body-centred-cubic (bcc) structure *(beta)*. More precisely, at 882,5° C, titanium undergoes an allotropic transformation from low-remperature hcp structure (α) to a bcc (β) structure that remains stable until the melting point. This transformation allows the prospect of having alloys with α, β or mixed α/ b microstructures.

Titanium is important as an alloying agent with most metals and some nonmetals. Some of these alloys have much higher tensile strengths than does titanium itself. Titanium has excellent corrosion-resistance in many environments because of the formation of a passive oxide surface film (TiO_2) even up to 535°C. There is no noticeable corrosion of the metal despite exposure to seawater for more than three years. Titanium resembles other transition metals such as iron and nickel in being hard and refractory. Its combination of high strength (up to 700°C), low density (it is quite light in comparison to other metals of similar mechanical and thermal properties), and excellent corrosion-resistance make it useful for many parts of aircraft, spacecraft, missiles, and ships. Titanium has a very good resistance to fracture in low temperatures (below 0°C) and this is also a reason why it is used in prosthetic devices, as is does not react with fleshy tissue and bone.

Although at room temperatures titanium is resistant to tarnishing, at elevated temperatures it reacts with oxygen in the air. This is no detriment to the properties of titanium during forging or fabrication of its alloys; the oxide scale is removed after fabrication. In the liquid state, however, titanium is very reactive and reduces all known refractories.

I.3.3 Titanium alloys

I.3.3.1 Classification of Ti Alloys

The alloying elements of titanium are classified as neutral, α-stabilizers and β-stabilizers according to their influence on the β-transus temperature. The α-stabilizing elements extend to the α phase field at higher temperatures, while β stabilizing elements shift the β phase field to lower temperatures.

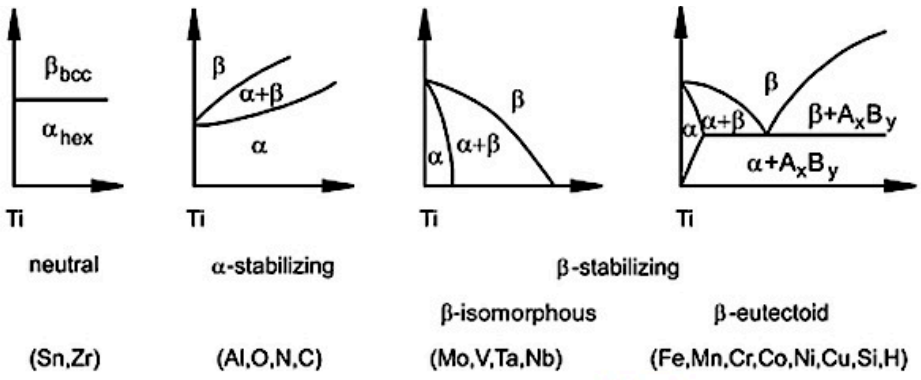

Figure 15: Influence of alloying elements on phase diagrams of Ti alloys (schematically) [1].

Among the α-stabilizers, aluminium is by far the most important alloying element of titanium. The interstitial elements oxygen, nitrogen and carbon also belong to this category. In addition to extending to the α phase field to higher temperatures, the α-stabilizers develop a two phase α + β field. α-stabilizing elements are subdivided into β-isomorphous and β-eutectic elements. Of these, the β-isomorphous elements e.g. Mo, V, and Ta, are by far more important due to their much higher solubility in titanium. On the other hand, even very low volume fractions of β-eutectic, e.g. Fe, Mn, Cr, Co, Ni, Cu, Si and H, can lead to the formation of the intermetallic compounds. Sn and Zr are considered neutral elements since

they have (nearly) no influence on the α/β phase boundary. As far as strength is concerned, they are not neutral since they primarily strengthen the α-phase.

Usually, titanium alloys are classified as α, α+β, and β alloys, with further subdivision into near-α and metastable β alloys. A three-dimensional schematic phase diagram, as shown in Fig. 16, which is composed of two phase diagrams with an α- and a β-stabilizing element respectively, outlines the aforementioned.

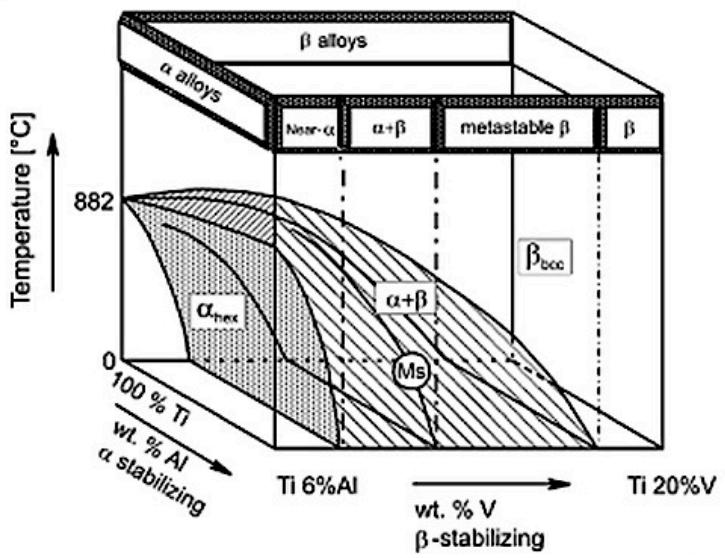

Figure 16: Three-dimensional phase diagram to classify Ti alloys [9].

According to Fig. 16 , the α- alloys comprise commercially pure (cp) titanium and alloys exclusively alloyed with α-stabilizing and/or neutral elements. If minor fractions of β-stabilizing elements are added, they are referred to as near-α alloys. The α+β alloys, the most widely used alloy group, follow the following class: at room temperature these alloys have a β volume fraction ranging from about 5 to 40%. If the proportion of β-stabilizing elements is further increased to a level where β no longer transforms to martensite upon fast quenching, the alloys are still in the two-phase field and the class of metastable β-alloys is reached. It should be noted that these alloys can still reveal an equilibrium α volume fraction of more than 50%. Finally, the single-phase β alloys mark the end of the alloying scale of the conventional titanium alloys.

The most important and by far intensively investigated titanium phase diagram is the system Ti-Al (Fig. 17). Apart from the α and β phases, which are the most significant for the conventional titanium alloys, several intermetallic phases are present, such as $a_2 \cdot Ti_3Al$, $\gamma \cdot TiAl$, $TiAl_2$ and $TiAl_3$.

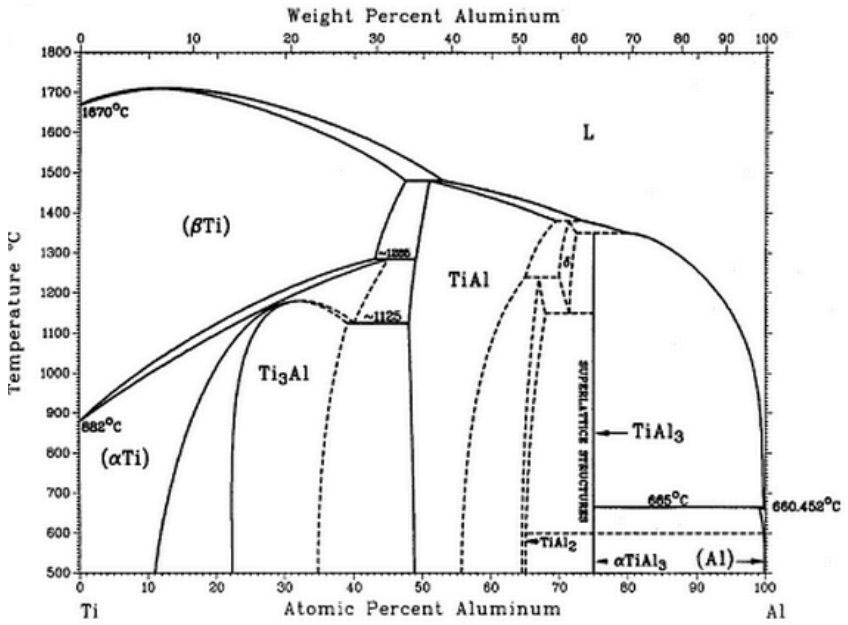

Figure 17: The Ti-Al phase diagram [9]

I.3.3.2 Basic Principles of heat treatment

Although, α-alloys show little response to heat treatment, it is essential to examine the general principles that are involved, even if they relate mainly to the α/β and β groups. This is possible by considering the effects of alloy content on the β to α transformation in a typical binary β-isomorphous system, as shown in Fig. 18 where it is also included a schematic diagram which depicts trends in tensile strength with respect to alloy content resulting from different heat-treatment procedures. The strength of the annealed alloys increases gradually and linearly as alloy content, or percentage of β-phase, increases. It should be noted that the β-phase in these alloys does not transform during cooling to room temperature. However, for alloys quenched from the β-phase field, a more complex relationship exists between strength and composition that depend on the transformation of β to the martensitic-form of the α-phase, entitled α′. If the concentration of the solute is low, some strengthening occurs as a result of this transformation, but the effect is much less than that traditionally found for martensitic reactions in ferrous materials. What is more, there is little change when martensitic α′ is tempered or aged. The maximum strength that can be obtained from this β to α′ transformation happens at a composition for which the martensite finish (Mf) temperature reaches the room temperature.

If the solute content is increased above this level then there will be a progressive increase in the amount of metastable β that is retained on quenching from the α or α+β phase fields, and in addition, the strength of the quenched alloys is gradually decreased to a minimum level at a composition at which the martensite start (Ms) temperature ocurs at room temperature, i.e. 100% metastable β (Fig. 18: shaded area).

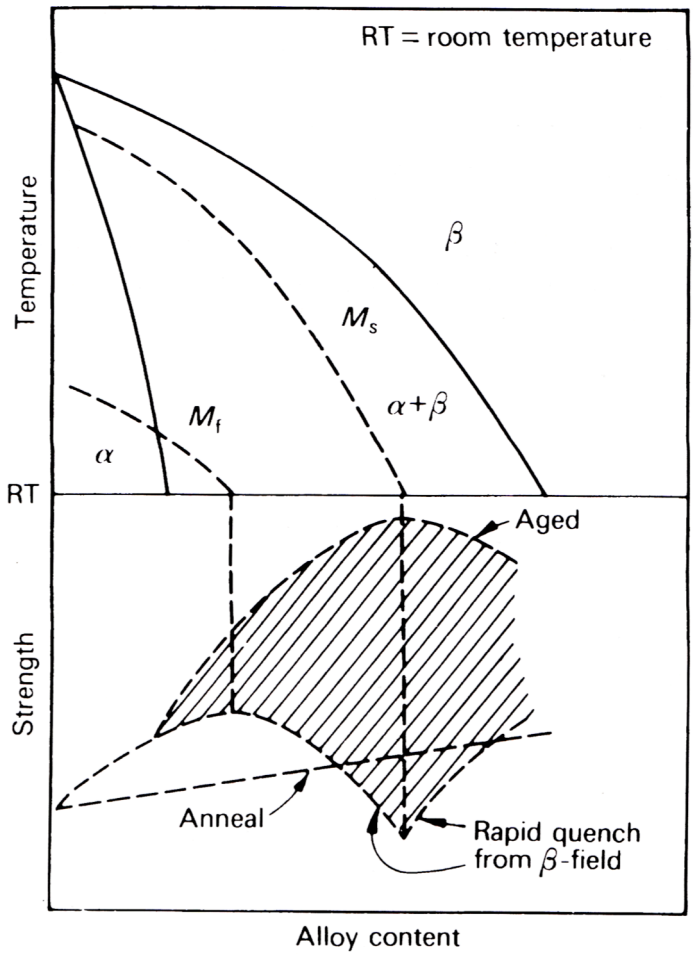

Figure 18: Schematic diagram for the heat treatment of β-isomorphous titanium alloys (from Morton, P. H., *Rosenhain Centenary Conference on the Contribution of metallurgy to Engineering Practice.* The Royal Society, London, 1976) [5].

I.3.3.3 Characteristics of titanium alloys

I.3.3.3.1 α alloys

The stabilizing elements aluminium and oxygen and the neutral elements tin and zirconium are the main substitutional alloying elements which dissolve the α-phase. They all cause solid solution hardening and increase tensile strength by between 35 and 70 Mpa for each one per cent of the added element. Apart from the composition, the properties of α titanium alloys depend also on processing history, because this history controls the grain size and the preferred orientation (texture). By comparison to α+β and β alloys, the properties of α titanium alloys have more direct composition dependence. Generally, the sheet products show a continuous variation of the yield strength and the elastic modulus between the longitudinal and transverse directions. This variation is due to the crystallographic texture which is always present in α titanium alloys. In addition, elasticity increases in Ti-Al alloys, presumably because Al is a substitutional element which contracts the α phase lattice. In the Ti-Al system, elevated temperature ageing of alloys with an aluminium content above 5-6% can lead to the formation of a finely ordered phase (α_2) which is coherent with the lattice of

the α-phase over a wide temperature range. This phase has the general Ti_3X formula with a hexagonal structure. Oxygen, in contrast, is an interstitial element in the α phase and has essentially no effect on modulus of elasticity, as seen in Table 1. In order to strengthen single phase titanium alloys such as the α phase alloys, there are relatively few options and there are practical limits to the extent to which they can be used. The basic mechanisms for strengthening α phase alloys are solid solution strengthening, both by interstitials (oxygen, carbon, and nitrogen) and substitutional elements (aluminum, tin, and zirconium), grain size strengthening, texture strengthening, and precipitation hardening by α_2 phase formation.

Material	E (GPa)	σ0.2 (Mpa)	UTS (MPa)	Elong. (%)	σ0.7 (Mpa) (R=-1)	σ0.2/ σ0.7
Grade 1	105	170	240	24	-	-
Grade 2	105	275	345	20	-	-
Grade 3	105	380	445	18	280	0.73
Grade 4	105	480	550	15	350	0.73

Table 1: Typical mechanical properties of CP titanium [38].

Among these possibilities, solid solution strengthening by interstitials (oxygen in particular) leads to strain localization. Solid solution additions and very small grains both restrict the operation of deformation twinning thus reducing the formability of the material. Precipitation hardening by α_2 phase also results in strain localization that can severely reduce the tensile ductility of the material.

I.3.3.3.2 Near α-alloys

Alloys of this class possess higher room temperature tensile strenght than the fully α-alloys and show the greatest creep resistance of all titanium alloys at temperatures that exceed 400℃. They are composed of α-phase and of small amounts of β-phase which are disseminated into the α-phase mass. The creation of these dispersions is succeeded with the limited (1-2%) inclusion of elements that stabilize phase β. This class was developed to meet the demands for higher operating temperatures in the compressor section of aircraft gas turbine for improved performance and efficiency.

I.3.3.3.3 α/β alloys

The limitations in strenght that can be developed in a fully-α alloys because of the reactions that occur in the order at higher solute contents combined with difficulties that are presented during hot-forming, led to the early investigation of compositions containing both the α-and β-phases. They have the greatest commercial value among the family of Titanium alloys, with one of the most important representative of this group being the composition of Ti-6Al-4V which makes more than half the sales of all titanium alloys both in Europe and the United States. The improved formability and the relatively high tensile strength that they offer gives them a great advantage that even balances the reduced creep strength in high temperatures (above 400℃) as well as the reduced weldability. They contain 4–6% of β–stabilizers which allow substantial amounts of β to be retained on quenching from the $\beta \rightarrow \beta + \alpha$ phase fields, e.g. $Ti - 6Al - 4V$.

Ti-6Al-4V

Ti 6Al-4V and Ti 6Al-4V ELI are the most widely used titanium alloys and account for more than half of all the titanium sponge used worldwide. Of this usage, the 80% is attributed for aerospace applications and the remainder is found in defense, marine, medical, chemical, and other industries.

The chemical composition of the alloy is shown in Table 2. Aluminium reduces density, stabilizes and strengthens the α-phase while vanadium provides a greater amount of the more ductile β phase for hot–working. This alloy is popular because of its strength (1100 MPa), creep resistance at 300℃ fatigue resistance and castability. Due to the β-phase, which has a body–centred cubic crystal structure, similarly to ferritic iron, it has a ductile–brittle transition temperature. The transition temperature tends to be above room temperature and as a result, the cleavage fracture is dominating at ambient temperatures.

Element	Ti	Al	V	Fe	O	N	H
Wt.%	Balance	6.27	4.19	0.20	0.18	0.012	0.0041

Table 2: Chemical Composition of Ti-6Al-4V [39].

As shown in Fig. 19 depending on thermal heat treatments, two phase *α/β* alloys can be obtained in several different temperatures. The technologically important microstructures are first the equiaxed *α+β* morphologies generated by deforming and subsequently recrystallizing the lamellar microstructures in the *α+β* phase field. Secondly, the bimodal microstructures with primary *α* grains surrounded by a fine lamellar microstructure produced by performing recrystallization treatments or annealing the equiaxed microstructures in the high temperature region of the *α+β* phase field and thirdly, the fine lamellar microstructure (also known as Widmanstatten *α*, or transformed *β*) that is produced by quenching from the *β* phase field followed by annealing in the *α+β* phase field.

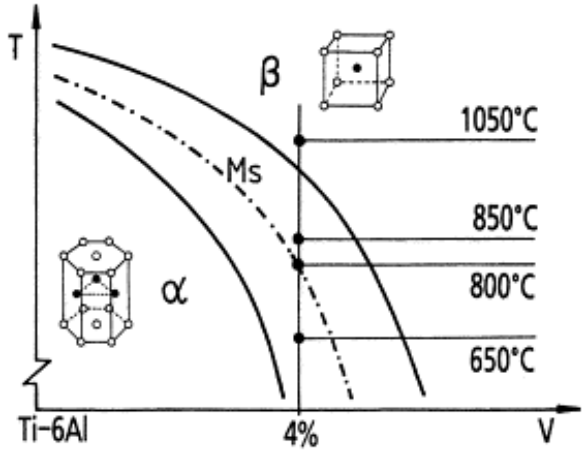

Figure 19: Ti–6Al–4V phase diagram in the *α+β* region of interest for *α/β* processing options [35].

I.3.3.3.4 Metastable β alloys

Beta alloys are characterized by high hardenability with the metastable beta phase being completely reserved on air cooling of thin sections or water quenching of thick

sections. As expected, alloys of metastable beta systems are richer in beta stabilizers and leaner in alpha stabilizers than α/β alloys. They attracted early attention due to their superior forming characteristics anticipated from the body-centered cubic structure. In addition, they offer the advantage of beign cold-formed in a relatively soft condition and then strenghtned by age-hardening. Temperatures of 450 to 650 ℃ are used to partially transform the metastable beta phase to alpha.

One disadvantage that might be encoutered is that because of the high contents of β-stabilizing elements, although it increases the hardenability of the alloy, it is likely that it may cause some problems with ingot segregation thus increasing the density of the alloy. Moreover, beta alloys have lower creep strenght and lower ductility in the aged condition. However, even though tensile ductility is lower, the fracture of an aged beta alloy is in general higher than of an aged alpha-beta alloys of comparable yield strenght.

Noticable yield strenghts, about 1172 Mpa (170 ksi) with very good toughness (K_{Ic} = 40 ksi$\sqrt{in}$) have been reported for the beta alloy Ti-10V-2Fe-3Al. Generally, the class of beta alloys serves a great need for titanium components that are to be fabricated in moderate-temperature applications.

Fig. 20 shows a concise comparison between the main titanium alloy groups, concerning their various characteristics.

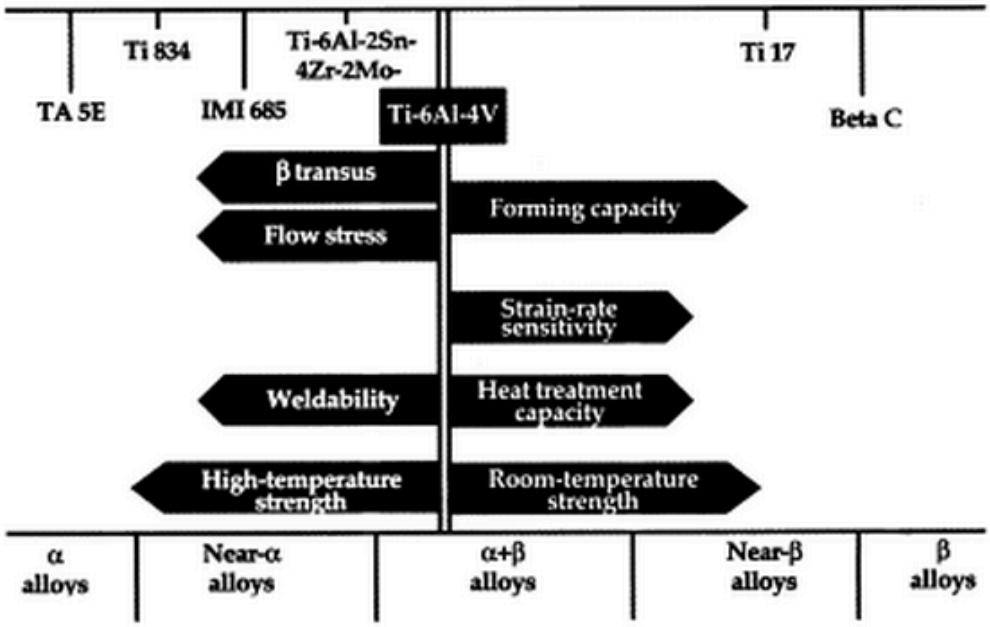

Figure 20: Main characteristics of different titanium alloy family groupings [36].

I.3.4 Metal Matrix Composites

I.3.4.1 General

Metal composite materials have found application in many areas of daily life for quite some time. These materials are produced *in situ* from the conventional production and processing of metals. Cast iron with graphite or steel with a high carbide content, as well as tungsten carbides, consisting of carbides and metallic binders, are quite a few of the

composite materials that belong to this group. For many researchers the term metal matrix composites is often associated with the term light metal matrix composites (MMCs). Significant progress in the development of light metal matrix composites has been achieved in recent decades, so that they could be introduced into the most important applications. Particularly in traffic engineering in the automotive industry, MMCs have been used commercially in fiber reinforced pistons and aluminum crank cases with strengthened cylinder surfaces as well as particle-strengthened brake disks.

These advanced materials open up unrestrained possibilities for modern material science and development; the characteristics of MMCs can be designed into the material, custom-made, dependent on the application. Taking this into account, metal matrix composites fulfill all the anticipated conceptions of the designer. These material groups are often used as constructional and functional materials, especially if the property profile of conventional materials either does not reach the increased standards of specific demands, or is the solution of the problem. The advantages of the composite materials are only realized when there is a reasonable cost – performance relationship in the component production as MMC's technology is in competition with other modern material technologies, for example powder metallurgy.

Moreover, the possibility of combining various material systems (metal – ceramic – non- metal) gives the opportunity for limitless variations. The properties of these new materials are basically determined by the properties of their single components. The distribution of the composite materials into groups of various types of materials are shown in Fig. 21.

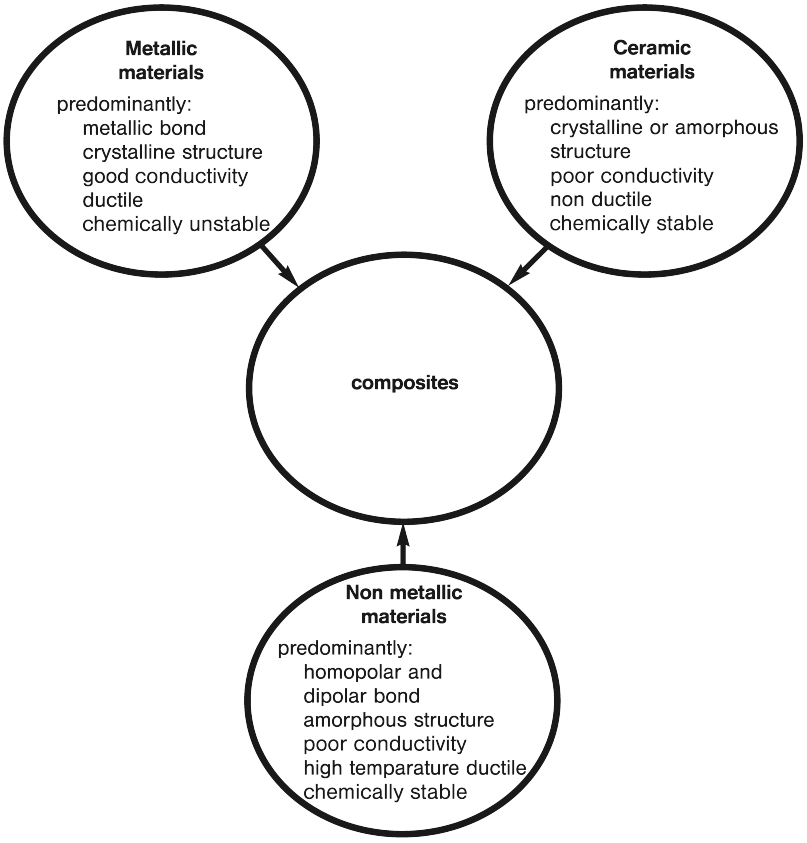

Figure 21: Classification of the composite materials within the group of materials [37].

The reinforcement of metals can have many different purposes. In order to improve of the component properties, reinforcements of light metals open up the possibility of application of these materials in areas where weight reduction has first priority. The main improvements and developments that are introduced by this technology are:

- ✓ Increase in yield strength and tensile strength at room temperature and above while maintaining the minimum ductility or rather toughness,
- ✓ Increase in creep resistance at higher temperatures compared to that of conventional alloys,
- ✓ Increase in fatigue strength, especially at higher temperatures,
- ✓ Improvement of thermal shock resistance,
- ✓ Improvement of corrosion resistance,
- ✓ Reduction of thermal elongation.

In summary, the aforementioned advantages illustrate the possibilities of extending the application area, substituting of the common materials and advancing the optimization of component properties. Depending on the application, different development objectives are given, which slightly differ from those mentioned before. For instance, in medical technology, mechanical properties, like extreme corrosion resistance and low degradation as well as bio-compatibility are expected. Moreover, application areas like traffic engineering, are very cost orientated and conservative and the industry is not willing to pay extra costs for the use of such materials. For all these reasons metal matrix composites are only at the beginning of the evolution curve of modern materials. (Fig. 22).

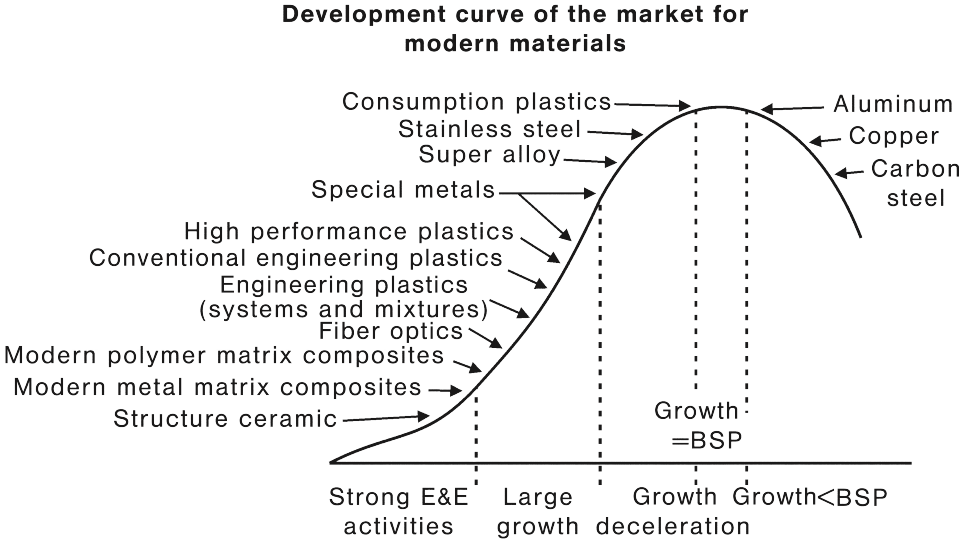

Figure 22: Development curve of the market for modern materials [37].

Fig. 23 shows a classification of the metal matrix composites which takes under consideration the type and contribution of reinforcement components in particle-, layer-, fiber- and penetration composite materials. Fiber composite materials can be further classified into continuous fiber composite materials (multi- and monofilament) and short fibers or, rather, whisker composite materials.

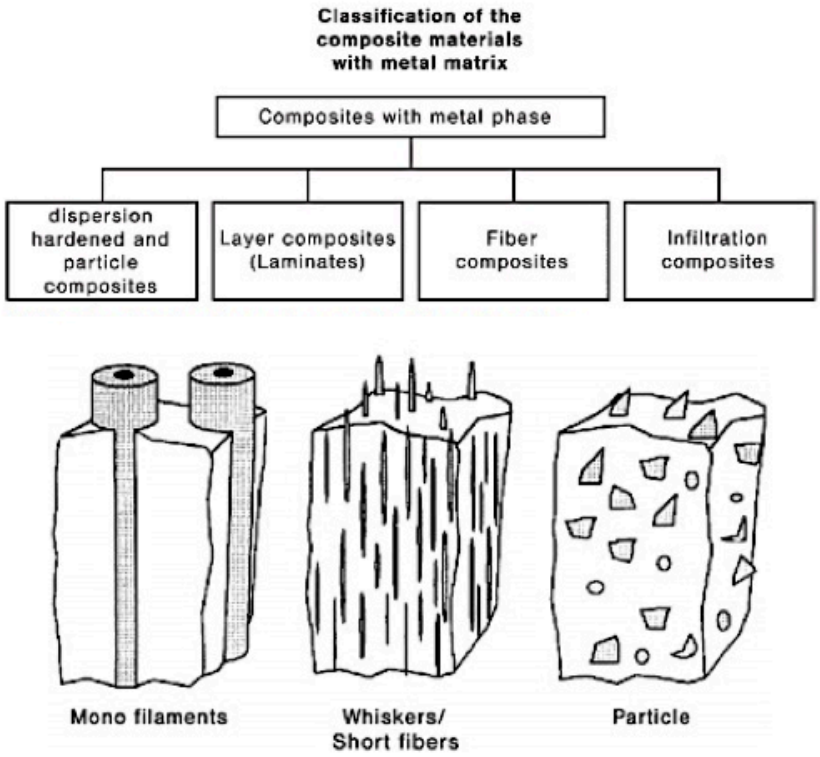

Figure 23: Classification of composite materials with metal matrixes and schematic presentation of three shapes of metal matrix composite materials [37].

I.3.4.2 Titanium Matrix Composites

The selection of the most suitable matrix alloys is mainly determined by the intended application of the composite material. With the development of light metal composite materials that are mostly easy to process, conventional light metal alloys are applied as matrix materials. In the zone of powder metallurgy special alloys can be applied because of their advantage of fast solidification during the powder production. Those systems are free from segregation problems that arise in conventional solidification. Titanium metal matrix composites (MMCs) offer potential advantages for structural applications, as they combine the high strength, high temperature capability, and oxidation resistance of titanium with an increase in stiffness provided by the ceramic reinforcement. They have the advantage of having an isotropic behavior, being cheaper to manufacture and more amenable to subsequent processing and component forming operations. Of potential reinforcing phases for titanium, including TiB, TiB2, SiC, Al2O3, and TiC, TiB offers the best equilibrium of stiffness, stability, and similarity of thermal expansion coefficients. The benefits these composites offer over conventional titanium alloys including increased stiffness, good creep performance, fatigue resistance, and wear resistance.

I.3.5 Uses and Applications of Titanium

As previously mentioned, titanium is a metal that is widely used in industry and manufacturing. Due to the advantages that it provides it is used in highly specialized industries that can in addition afford and justify the high cost. Few of the main utilizers of titanium are the following:

- Aerospace Industry

Due to their light weight and temperature resistance properties, Ti is used for building aircraft turbine disks, blades, and airframe structural components.

- Petrochemical Uses

Due to its high level of corrosion resistance and heat tolerance, titanium stock is often used in the petrochemical industry in heat exchangers and reactors.

- Medical Application

Due to its biological compatibility with human bone and tissue, titanium rod and wire are ideal materials for medical implements. Titanium suppliers commonly provide stock for dental implants, prosthetic devises, as well as bone and joint replacement procedures.

- Recreational Uses

Titanium distributors are quickly finding more widespread uses for titanium tubing in recreational products, including sports equipment such as bicycles, golf clubs, and tennis racquets. Titanium sheet and wire is now an attractive alternative to other special metals used in the jewelry industry, particularly in wedding jewelry.

CHAPTER I.4

DLMD of Ti-6Al-4V/TiC composites and analysis of microstructure- Bibliographical Review

I.4.1 Comparison between powder and wire feeding in DLMD

Direct Laser Metal Deposition [DLMD] is a novel manufacturing technique that provides a single-step and waste-free process to fabricate near net shape components. In every research attempted, various combinations of the different critical parameters are explored in order to achieve the best solutions regarding the microstructures and mechanical properties achieved.

One of the principal parameters is the deposition technique that is used. There are two possibilities currently explored, the powder feeding system and the wire feeding system.

W.U.H Syed and **A. J. Pinkerton [15],** in their study they explore the differences that resulted in the microstructures as well as in the mechanical properties between the samples that were wire-fed and the powder-fed ones. All the other related processing parameters were kept identical during the experiments.

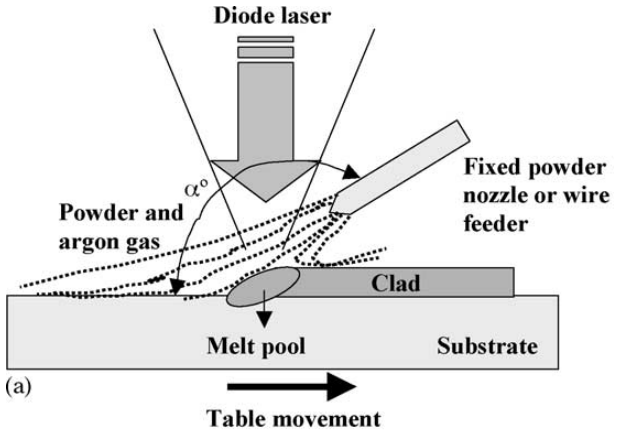

Figure 24: Schematic diagram for wire/powder feeding-rear feeding [15].

For the realized experiments the deposition materials were the 316L stainless steel wire of 0.8 mm diameter (composition of steel: 0.03%C, 2.0% Mn, 1.0% Si, 16.0-18.0% Cr, 10.0-14.0% Ni, 2.0-3.0% Mo) or powder with a particle size of 53-150 μm both supplied via a lateral feed nozzle along with argon gas as the protection gas (Fig. 24).

According to the experimental results, there cannot be a definite answer on to whether powder feeding is better than wire feeding. Depending on the characteristics examined, both of the two deposition methods present advantages. More precisely, the parameters concerning the surface roughness, the feeding direction, location and angle, the microstructures, the morphological characteristics and the deposition efficiency were discussed.

The most interesting results regarding wire feeding were that it has better deposition efficiency and approximately 25% less surface roughness than powder feeding. However, there are no significant differences in the microstructures and morphologies observed. Both samples remained austenitic in phase and the microstructure was mainly dendritic, cellular with no cracks. Only some porosity was observed with the powder feeding and some cavities for both deposition methods, at laser powers lower than 900 W and more than 1200 W (Fig. 25).

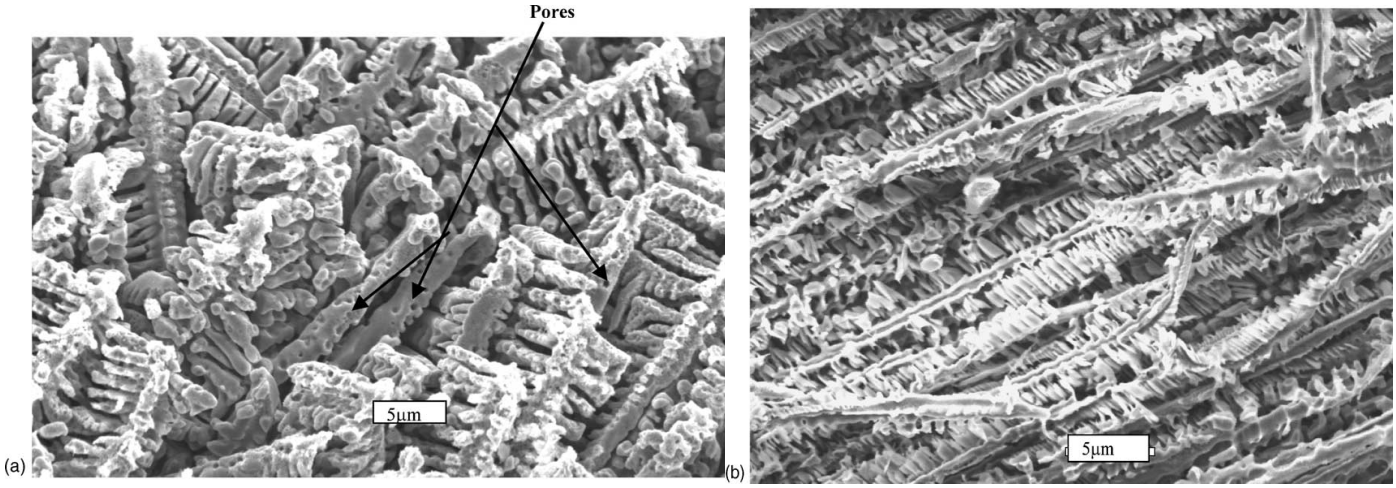

Figure 25: SEM of wire and powder feed samples, (a) powder fed part top layer and (b) wire fed part top layer [14].

Another possibility for the DLMD method is to have simultaneous powder and wire deposition (Fig. 26). **F. Wang, J. Mei, H. Jiang, and X. Wu [12],** used for their experiments synchronized deposition of TiC powder in different percentages and Ti-6Al-4Vwire.

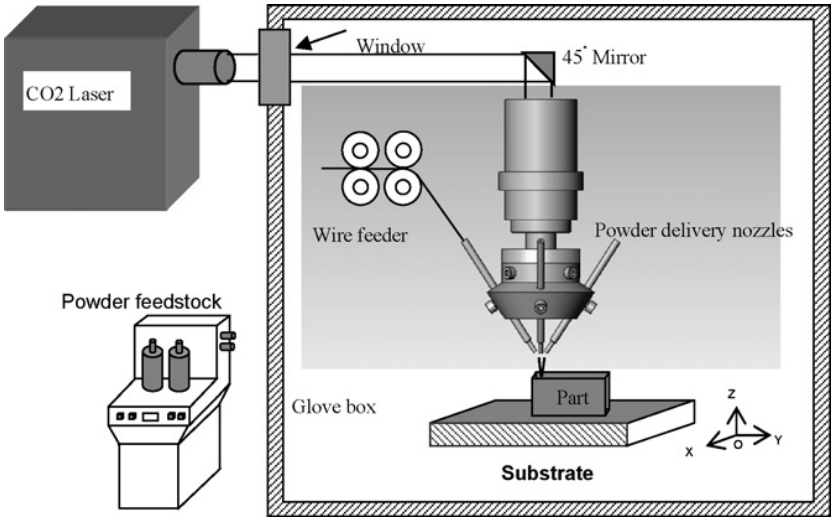

Figure 26: Schematic of direct laser fabrication with simultaneous powder and wire feed [12].

According to their results, one of the problems they encountered was the different power-requirements needed to melt powder and wire. The amount of power needed to melt wire is significantly greater.

The main reason for this is that the powder is melted both by the laser irradiation and the liquid molten pool. In contrast, the wire used needs higher laser power because it sticks to the surface of the built pass if the laser power is very low. In addition, when too much powder is fed into the laser, part of the laser is shielded and reflected by these 'extra' powders engaging the power required to maintain the temperature in the molten pool, thus leaving un-melted particles in the build part. The aforementioned are some complications that need to be taken into to account when using simultaneous wire and powder feeding. Other than that, the results concerning the microstructure are positive as later discussed, thus making this deposition method successful for the fabrication of a compositionally graded TiC/Ti6Al4V material.

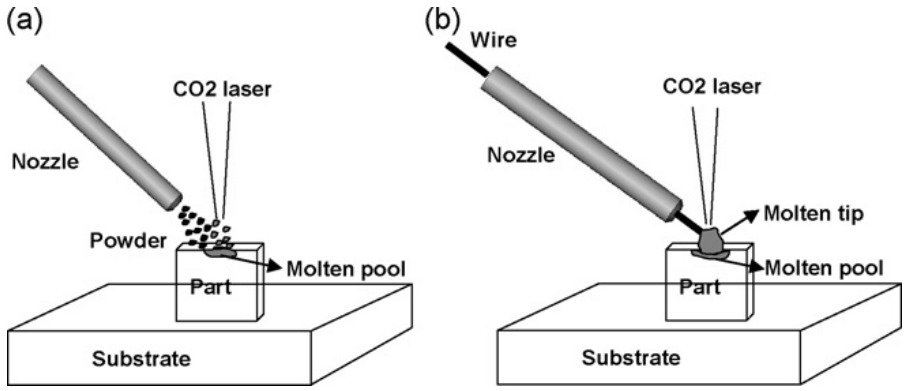

Figure 27: Schematics of the process of laser melting powder and wire. (a) Direct laser fabrication with powder feed; (b) direct laser fabrication with wire feed [12].

I.4.2 Influence of TiC reinforcement in DLMD Ti-6Al-4V composites

As previously mentioned in Chapter 4, in manufacturing technologies of metal matrix composites, metal reinforcements are used to improve the properties of the final component. One of the most common reinforcements for the Ti-6Al-4V composite is TiC (Fig. 28). Several studies have been conducted to investigate the effect of carbon content on the microstructure and properties of the TiC/ Ti-6Al-4V composites. In addition, a critical parameter is the percentage of the TiC particles added to the mixture-an issue also widely discussed among the scientific society.

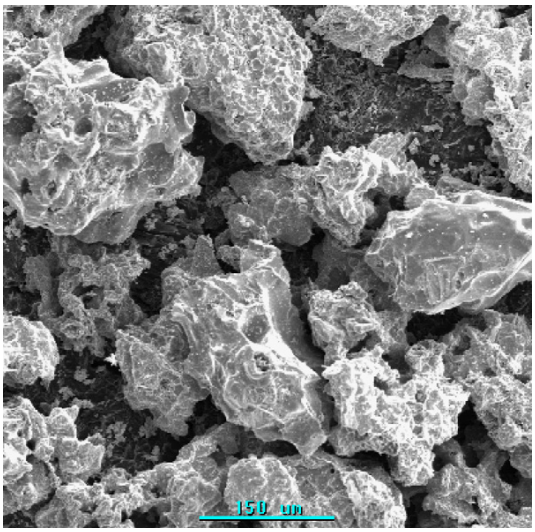

Figure 28: SEM morphology of the TiC particulates [22].

For better understanding the influence TiC particles have on Ti-6Al-4V composites, it is important to first investigate the Ti-C system phase diagram.

M.J. Hamedi, M.J. Torkamany, J. Sabbaghzadeh [21] examined the Ti-C system shown in Fig. 29 and its reaction to the laser processing. According to their results, during the laser surface processing, a cloud of plasma is created on top of the surface including the substrate, pre-coated material and shielding gas. Consequently, as a result of the generated high temperature at the surface (temperature reaches to 2500–3000 °C - COMSOL's^{TM} analysis) Ti (T_m=1670 °C and T_b=3287 °C) will be found in liquid or vapor phase. TiC formation possibility is about 10–19% of carbon weight percent at the temperature range of 1648–3000 °C according to the phase diagram of TiC.

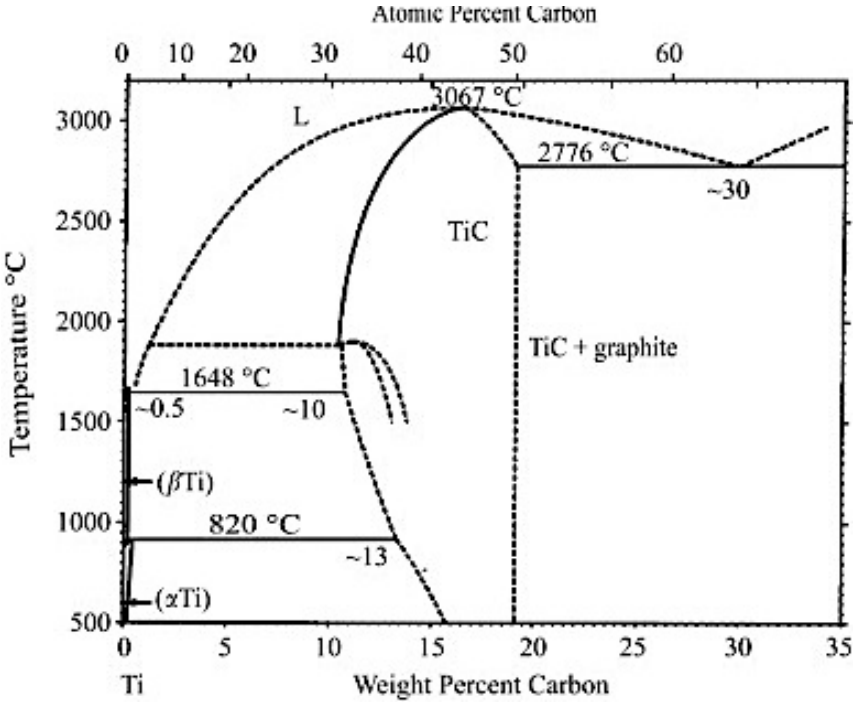

Figure 29: Ti-C phase diagram [21].

X. Wang, P. Gai [17], state that TiC particles are useful for wear resistance and they are widely used to improve surface characteristics. By controlling the growth of TiC crystal with heat treatment during the fabrication, the properties of the final composites can be significantly improved. In order to examine the importance of the carbon presence to the properties of the final product, the authors tested samples with 0,15%, 0,20%, 0,40%, 0,80%, 1,40% and 2,00% carbon content of the TiC/Ti-6Al-4V composites. In a comparative way, results regarding the morphology are shown in Fig. 30. There is a uniform distribution of the TiC particles in the matrix alloys.

More precisely, when the carbon content is about 0,15-0,20% TiC particles have a short-bar shape. This formation still continues while the carbon content increases and it gradually transforms into a feather-like, wheat-shape TiC. When the TiC content reaches 1,40%, TiC is still mainly of short-bar shape but in combination with the dendritic shape that starts to appear. Dendritic TiC is well developed when carbon content finally reaches 2,00%. Concerning the hardness, the authors resulted that there is a straight analogy between the hardness and the carbon content. This means that with the increase of the TiC percentage, the hardness of the composites also increases.

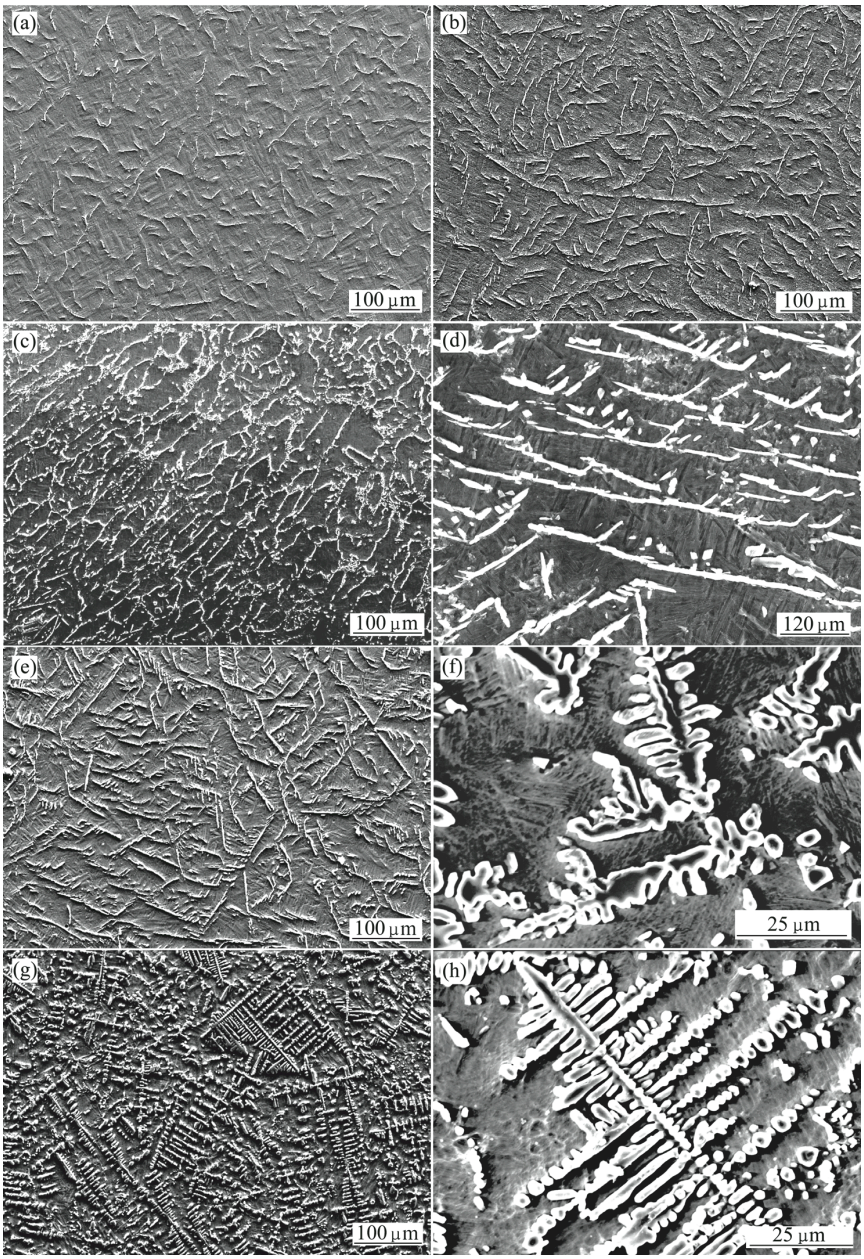

Figure 30: Morphologies of TiC in TiC/Ti-6Al-4V composites with different content of carbon: (a) 0.20%C; (b) 0.40%C; (c), (d) 0.80%C; (e), (f) 1.40%C; (g), (h) 2.00%C [17].

This also can be explained with the phase diagram. The crystal structure of TiC is fcc. From the phase diagram, we can see that the peritectic point is about 0,80% C. When the carbon content of the composites is less than 0,80% during equilibrium crystallization, there is no dendritic TiC as primary TiC translates into β-Ti completely through peritectic reaction. When it comes to TiC/Ti-6Al-4V composite, the growth of TiC depends on solid state diffusion of Ti, Al, V and C. Due to the limitation of diffusion velocity and distance, TiC is prone to form short-bar shape and distributes in β -Ti. When eutectic reaction begins, α -Ti nucleates and grows at grain boundaries of β-Ti primarily. Then, the short-bar shape TiC in β -Ti transfers to grain boundaries or triangular grain boundaries of α-Ti.

D. Liu, S.Q. Zhang, A. Li, H.M Wang [19], examined the tensile properties of the composites as a function of the TiC volume fraction. The samples they used consisted of TA15 spherical powders (Ti-6Al-2Zr-1Mo-1V (wt%)) mixed with TiC powders of 5%, 10%,

15% volume percentages. According to their results, in the cases that TiC reinforcements exceeded 5%, the mechanical properties of the final product were not improved when compared to the monolithic matrix. Table 3 shows that as the percentage of the carbon content increases from 5% to 10%, both the yield strength (YS) and the ultimate tensile strength (UTS) of the composites decrease significantly. In addition, the ductility and the elongation also deteriorate as the TiC percentage increases.

Sample	YS (MPa)	UTS (MPa)	Elongation (%)
LMDed 5%TiC/TA15	925.87 ± 61.72	1085.97 ± 44.80	4.32 ± 1.78
LMDed 10%TiC/TA15	845.27 ± 121.76	897.14 ± 117.25	1.23 ± 0.18
LMDed 15%TiC/TA15	806.38 ± 34.92	886.05 ± 69.90	1.33 ± 0.04
LMDed TA15 [24]	837.50 ± 45.96	931.50 ± 37.48	18.20 ± 2.40
Cast BT20JI [25]	784	882–1127	≥5
Forged TA15 plate [26]	855	930–1130	6–12

Table 3: Room temperature tensile properties of the LMDed TiC/TA15 composites [19].

As for the wear resistance, **F. Wang, J. Mei, H. Jiang, and X. Wu. [12]** found that the sliding-wear resistance is not improved when the volume fraction of TiC reinforcements is less than 15 vol.%. This happens because most of the TiC precipitates along the Ti6Al4V matrix grain boundaries, and very little TiC could be found in the grains. The materials in the grains are easily cut because of their low hardness. Therefore, the wedges generated from the steel ball and composites during the sliding process remove them. While TiC in the composites increases (volume fraction of TiC reinforcements larger than 24%), TiC particles not only precipitate along the grain boundaries but also precipitate in the grains. In this case, during the sliding process, the wedges contact more TiC reinforcements rather than soft matrix so that sliding wear resistance is improved as shown in Fig. 31.

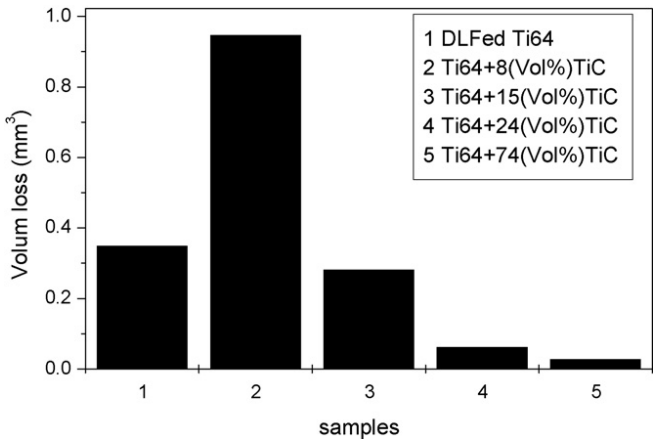

Figure 31: Wear volume loss of Ti6A4V and Ti6Al4V with TiC particles reinforced specimens [12].

Furthermore, to understand the importance of the laser power as an essential parameter in the process, **D. Gu, Y. Shen, G, Meng [23],** investigated the morphologies of the formed TiC grains under different laser powers ranging from 700W to 900W. Fig. 32 displays the crystal growth mechanisms behind the microstructural developments at different laser parameters. As a result of their research, the authors concluded that the consecutive

changes of the formed TiC grain were as follows: by increasing the laser power-i.e increasing the process temperature- the original laminated shape grain initially took an octahedron shape, then an truncated near-octahedral shape and in the end a near-spherical shape.

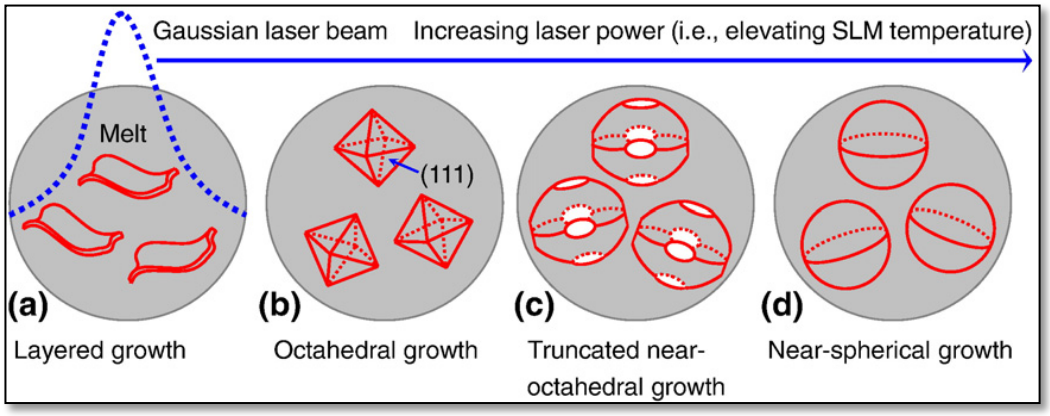

.
Figure 32: Schematic of growth mechanisms of TiC grains during SLM [23].

I.4.3 Microstructures observed at DLMD Ti-6Al-4V/TiC composites

As already introduced in chapter 5.2, the microstructures of the composites that are seen after the DLMD fabrication, depend on a lot of parameters, one of the most critical one being the percentage of the carbon content in the mixture.

C. Mitchell et al. [16], particularly focused on the effects the processing conditions have on the microstructure of the final composite. More precisely, laser power, scan speed and powder feed rate were the center of their research. The effects of each parameter are not straightforward but nonetheless they made some very interesting observations.

In summary, by increasing the laser power and the powder feed rate α and β laths are also increased. In the contrary, the size of α and β laths decrease with the increase of laser scanning speed as shown in Fig. 33 - Fig. 35.

(a) 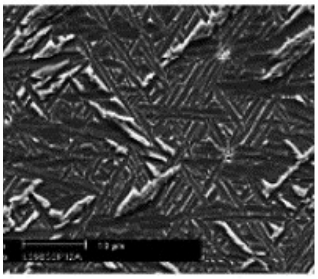 (b) 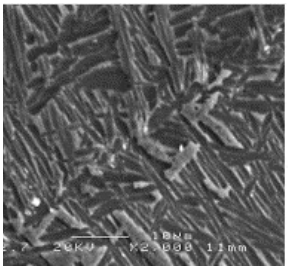

Figure 33: SEM micrographs showing the increased size of α and β laths with increase of the laser power: (a) 390 W and (b) 516 W. Scan speed=300 mm/min and powder feed rate=12 g/min [16].

(a) 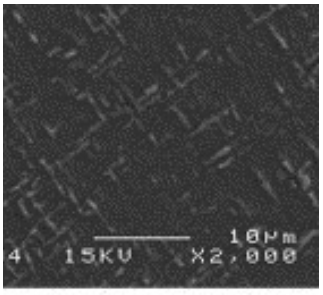 (b) 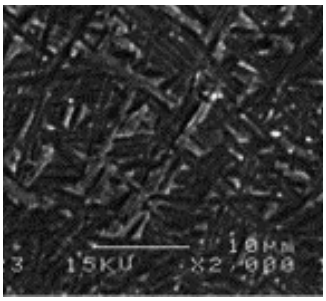

Figure 34: SEM micrographs illustrating increased size of α and β laths for powder rates (a) 12 g/min and (b) 24 g/min [16].

(a) 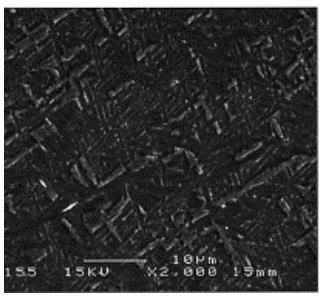 (b) 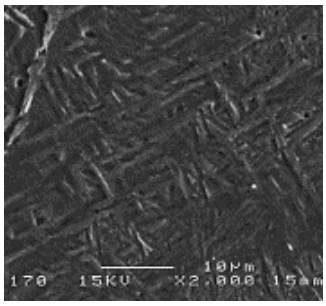

Figure 35: SEM micrographs illustrating that the size of columnar grains and the size of α and β laths decrease with increase of laser scanning speed from (a) 600 mm/min to (b) 900 mm/min at a given powder feed rate of 18 g/min and a laser power of 432 W [16].

I.4.4 Previous Work at École Nationale Supérieure d'Arts et Métiers [ENSAM]

The current project serves to further advance and continue the research that was previously done by **A. Mbaye (2011) [27]** and **A. Racle (2010) [28]** at the ENSAM's PIMM laboratory regarding the Direct Laser Metal Deposition of Ti6Al4V-TiC and the connection between the laser parameters and the microstructures of the manufactured samples.

A. Racle studied two different cases: for the first set of experiments the composition of the powder was 15% TiC and 85% of Ti6Al4V whilst at the second set of experiments the percentage of the TiC particles in the powder's composition was 30%. Three different laser powers were applied; 350 W, 400 W, 450 W and the mass feed rate was constant at 1 gr/ min. Numerical simulation using the COMSOL program was applied to better understand the heat

evolution during the creation of the walls for the fabricated samples. The principal results that were obtained during the aforementioned study were the following:

- For the lower velocities (200 mm/min), the distribution of the unmelted particles is located more to the center of the cross section for the samples with 15% of TiC and more to the edges (of the same view) for the samples with 30% of TiC
- On a level of homogeneity, the most homogenous microstructures were observed for the most important laser power i.e. 450 W and at the lower velocity i.e. 200 mm/min
- A more important density of the primary TiC dendrites is observed closer to the last layers (the hotter ones) whereas closer to the substrate (first layers) fine eutectique TiC can be found

A.Mbaye in his study focused on two different laser powers i.e. 350 W and 450 W, the same two different velocities that were studied by A. Racle (200 mm/min and 400 mm/min) and a powder's mass feed rate constant at 2 gr/min. The laser's propagation was of guassian type the percentage of the TiC particles in the composition of the powder was 10% and the powders' grain size spectrum was 50-100 μm. The most significant results that were obtained through A. Mbaye's study were the following:

- Although there has been some changes to the principal DLMD paremeters used during the fabrication, no significant differences were observed in comparison with the results of A. Racle.
- Regarding the mechanical properties, the presence of the TiC particles attributed an increase to the model of elasticity.
- Although the change to the parameters used did not result in better homogeneity along the microstructure of the samples as anticipated, the presence of TiC did affect positively the surface quality resulting to less rough surfaces with less 'waves'.

II. EXPERIMENTAL PROCEDURES

II.1 Introduction

For the realization of the current thesis project, the experiments were conducted at the *Process and Engineering in Mechanics and Materials laboratory* (PIMM) of the École Nationale Supérieure d'Arts et Métiers (ENSAM) (member of the ParisTech) under the ERASMUS program.

The experimental procedure is primarily divided into two parts. The first part consists of the manufacturing of the samples using the direct metal deposition technology (DLMD) at varying conditions and the second part consists of the analysis of the microstructure and the mechanical properties of the acquired samples. Both parts are more extensively presented at the following paragraphs.

II.2 Direct Laser Metal Deposition

Eight samples were fabricated at the first part of the project using the Direct Laser Fabrication facility of the Power Laser Application Laboratory (LALP) of ENSAM's Processes and Engineering in Mechanics and Materials Laboratory (PIMM). The substrate for all the samples was pure Ti6Al4V and the power of the laser applied was stable at 500 W. Furthermore the mass feed rate of the powder was aimed to remain stable for all the samples at the state of 1.5 gr/min. Small inclinations from the desired rate were achieved. Two different velocities were studied: 200 mm/min and 400 mm/min. An important variation in comparison with the two prior thesis projects that were realized at the PIMM's Laboratory by A. Mbaye and A. Racle under the MAGIS Master Program[2] is that half of the samples, after the first simultaneous deposition of the laser and powder (i.e after the formation of the first layer) they were remelted at a 600 W laser power without any powder deposition. The goal was to study the effects of the remelted TiC particles to the properties and microstructrure of the formed wall.

Another important novelty that was proposed throughout the realization of this project was the laser's beam profile. In contrast with the two previous projects, where the beam's propagation was of Gaussian type, Top Hat propagation was introduced to investigate whether this would have notable advantages to the final product. A generalized comparison of the two profiles is shown at Fig. 36.

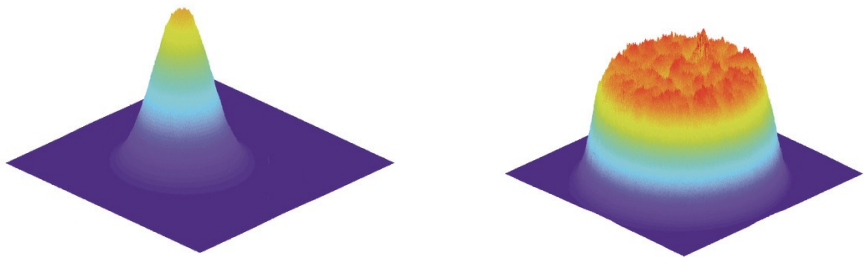

Figure 36: Comparison of the two laser beam profiles; a) Gaussian b) Top Hat.

[2] http://www.lmt.ens-cachan.fr/MAGIS/

The Top-Hat distribution was obtained by modifying the optical device in the laser head using a focusing lens of 280 mm, a collimating lens of 100 mm and an optical fiber of 600 μm. In turn, the magnification was 280/100=2.8 and the spot size becomes 600 x 2.8 = 1.68 mm. The use of a uniform distribution was expected to modify advantageously microstructures by limiting temperatures in the fusion zones, and providing a better energy distribution along the width. On the other hand, a Top-Hat distribution minimizes thermal gradients and reduces Marangoni convection flow.

The schematic of the DLMD facility as well as PIMM's DLMD facility are shown at Fig. 37. and at Fig. 38, 39.

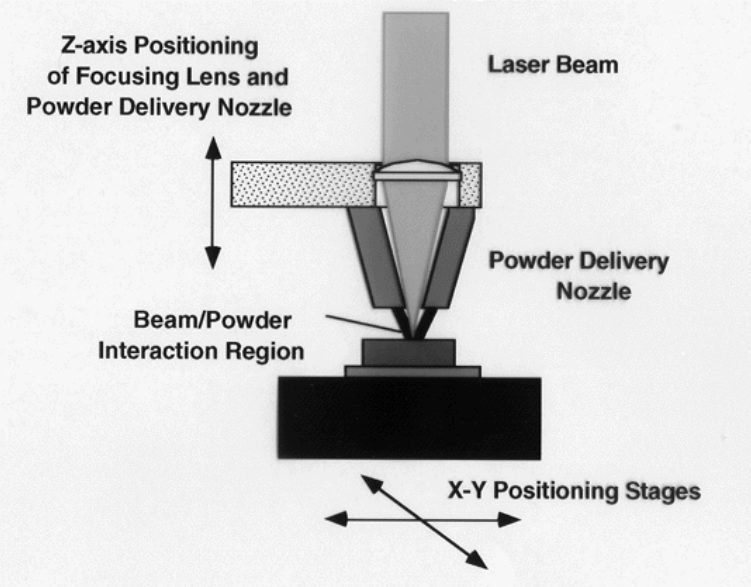

Figure 37: Schematic of the experimental setup for the laser powder deposition[3].

[3] http://www.wtec.org/loyola/rp/06_03.htm, <Mon. 21st 2013>

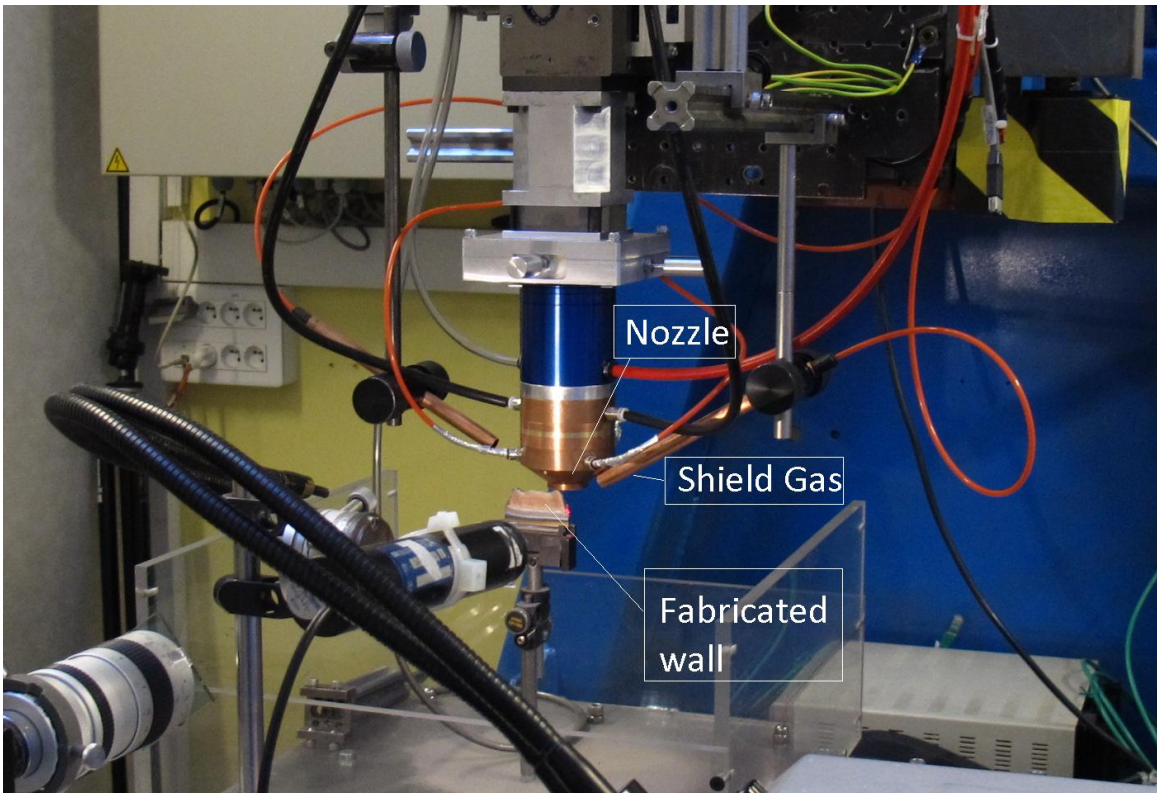

Figure 38: PIMM's DLMD facility.

Figure 39: Powder feeder.

The composition of the powder was 10% TiC and 90% Ti6Al4V. The powder was premixed prior to the deposition at the TURBULA Shaker-Mixer machine for about twenty minutes in order to achieve homogeneity among the particles of the two substances. The grain size spectrum was 50-75μm. To obtain this size, the powder was sieved for a

considerable amount of time at a sifting machine and later observed at the optical microscope to ensure that the size of the grains satisfied the aforementioned limitations. (Fig. 40)

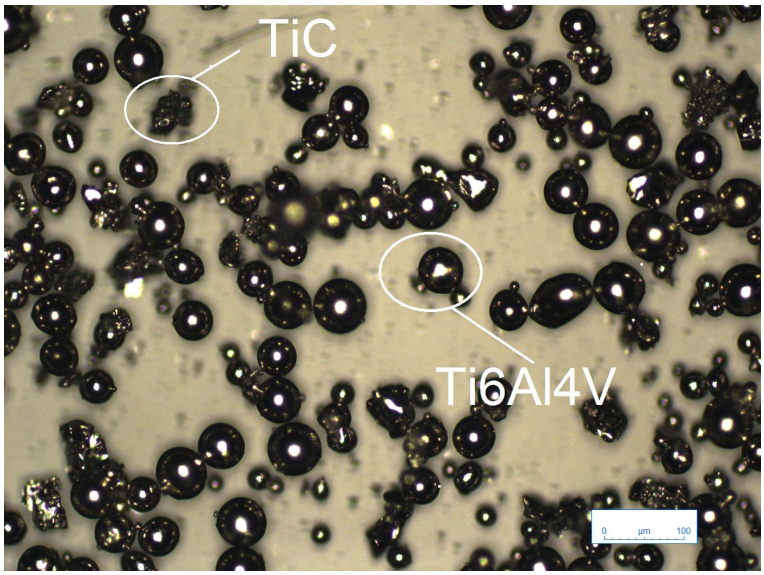

Figure 40: Powder composition after the mixing process.

Table 4 introduces the characteristics and the different parameters among the fabricated samples. Images of the samples that were manufactured are shown in Part II.

	Name of Sample	Remelting	Velocity (mm/min)	Power (W)	Powder's Flow Rate (gr/min)
i.	TOP_P_1	no	200	500	1,4913
ii.	TOP_P_2	no	400	500	1,5038
iii.	TOP_P_3	no	400	500	1,4
iv.	TOP_P_4	no	200	500	1,45
v.	TOP_L_1	yes	200	500/600*	1,47
vi.	TOP_L_2	yes	400	500/600*	1,5038
vii.	TOP_L_3	yes	400	500/600*	1,4738
viii.	TOP_L_4	yes	200	500/600*	1,45

* = remelting power

Table 4: Parameters of the manufactured samples during DLMD.

All of the eight samples were afterwards edited with the required processes in order to be appropriately prepared to proceed to the desired analysis.

Samples' Preparation

The samples after their manufacturing were adequately prepared in order to be ready for the analysis. The steps that were executed are the following:

- ⇨ All the samples were cut in three parts each one being about 15 mm long (with the height and width remaining that of the samples) at the Struers-Discotom 6 cut-off machine with the cutting paper 20S25 which is the appropriate for Titanium cutting.
- ⇨ The samples were later mounted in carbon or copper resines at the Mounting MecaPress 3 machine. The ones that were scheduled to be observe at the EBSD, were mounted in a copper resin to achieve higher conductivity, but it was concluded that this did not make a significant difference in the end.
- ⇨ After the mounting, the samples were grinded with SiC papers (80 to 4000) at the Struers Terga-Force 5/ Terga Pol-31 machine and then polished at a 9 μm and 1 μm diamond suspension.
- ⇨ The samples that were observed at the EBSD, underwent the following specific preparation as it is extremely important to prepare the surface very well due to the high sensitivity of the analysis:
  - SiC Papers 1200 to 4000
  - Spray diamond 3 μm, 1 μm and 0,25 μm
  - OPS suspension for 30 minutes
- ⇨ For the XRD analysis, the samples underwent nearly the same preparation that was required for the EBSD. The sole difference was that spray diamond was limited to 3 μm and 1 μm only.

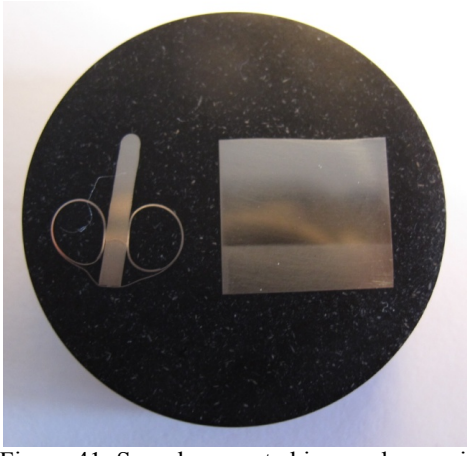

Figure 41: Sample mounted in a carbon resin (40 mm Ø)

Figure 42 Sample mounted in a copper resin (30mmØ)

II.3 Analysis of the Surface condition, the Microstructure and of the Mechanical Properties

The goal of the project was to examine the manufactured samples and to investigate from a multiple scope how the chosen parameters affected the microstructure and mechanical properties of the final products. The following measurements were realized:

i. Analysis of the surface condition with Roughness Measurements

The roughness measurements were realized using PIMM's DEKTAK® 150 Stylus Surface Profiler. All the samples went through a 2D surface analysis of 4mm length at the left, middle and at the right side of the surface in order to compare any differences that might occur. In addition, for all the samples apart from the TOP_L_2 (because its wall's height was not sufficient) went through a Map Scan to obtain a 3D analysis of a 4 mm x 4 mm surface area.

ii. Optical Microscopy observation

All the samples were observed at PIMM's optical microscopes Olympus BH2-UMA and Leica Leitz DMRM after being grinded and polished (see 'Samples' Preparation' p. 52-53). Mosaic photos of the samples were taken using the micro hardness machine's microscope to acquire better results. More photos were taken for the less oxidized samples that present better results in comparison with the others. These are the same four samples for which we also tested the micro hardness.

iii. Scanning Electron Analysis Observation (SEM)

PIMM's Scanning Electron Microscope HITACHI 4800 II was used to examine the microstructure of the samples TOP_P_4 (longitudinal direction) and TOP_L_4 (longitudinal direction) as these two sample present the best results in terms of homogeneity. Furthermore, separate powder particles of TiC and of Ti6Al4V were analyzed after being embedded on a cooper resin to facilitate the observation

iv. Electron BackScatter Diffraction Measurement (EBSD)

What is EBSD and how does it work?

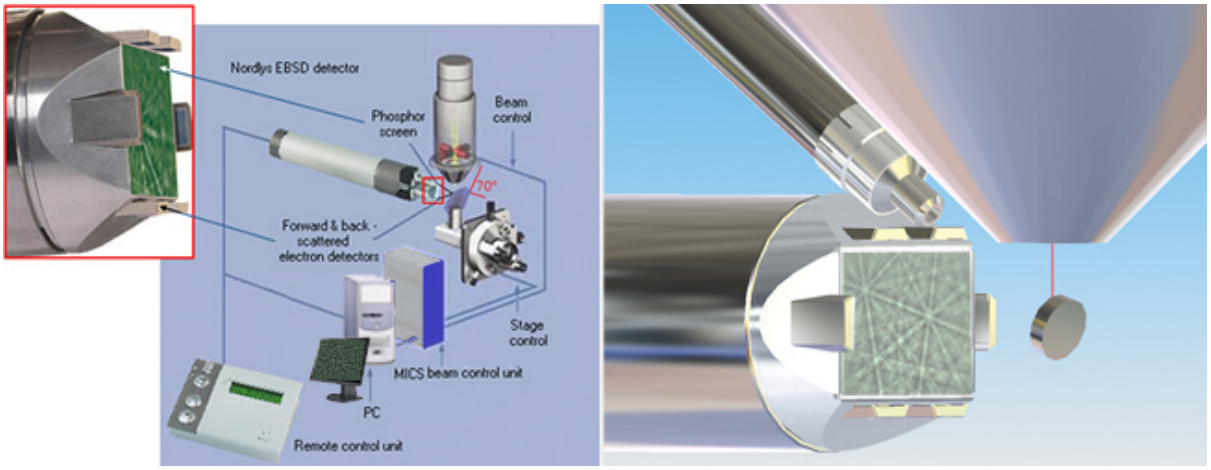

Figure 43 a): Experimental set up of EBSD [31].

Electron backscatter diffraction (EBSD), also known as backscatter Kikuchi diffraction (BKD), is an SEM based microstructural-crystallographic technique to measure the crystallographic orientation. EBSD provides quantitative microstructural information about the crystallographic nature of metals, minerals, semiconductors, and ceramics—in fact most inorganic crystalline materials. It reveals grain size, grain boundary character, grain orientation, texture, and phase identity of the sample under the beam.

In EBSD a stationary electron beam strikes a tilted crystalline sample and the diffracted electrons form a pattern on a fluorescent screen. This pattern is characteristic of the crystal structure and orientation of the sample region from which it was generated. An example of such a pattern is shown here. The bands in the pattern are referred to as Kikuchi bands (fig. 43 b)) and are directly related to the crystal lattice structure in the sampled region. As such, analyzing the pattern and bands can provide key information about the crystal structure for the measured phase. It is a very powerful tool for microstructural characterization **[29], [30], [31].**

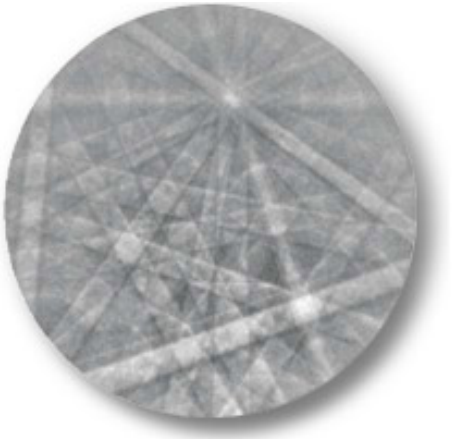

Figure 43 b): Kikuchi bands[4]

[4] "Introduction to Orientation Imaging Microscopy". <Wed.13March 2013>. http://www.stanford.edu/group/snl/SEM/OIMIntro.htm#configuration

The EBSD measurements were realized at the University Paris-Sud 11 at Orsay town by T. Baudin[5] and F. Brisset[6]. A ZEISS SUPRA 55VP SEM was used for the measurements. The high sensitivity of the instrument requires the best possible surface preparation of the samples. For this reason, the samples were adequately prepared with the help of J. Hoarau[7].

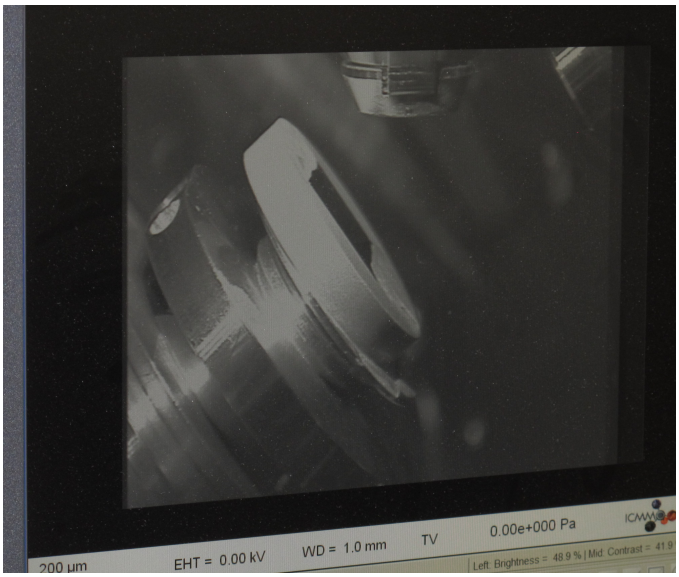

Figure 44: Sample during the process of EBSD analysis.

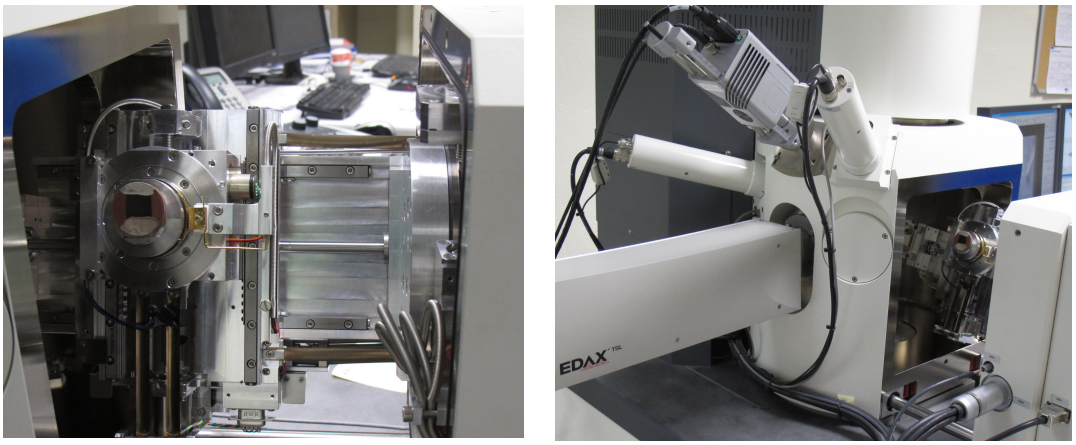

Figure 45: EBSD facility at the Laboratoire de Physico-Chimie de l'Etat Solide [LPCES] at the Institut de Chimie Moléculaire et des Matériaux d'Orsay [ICMMO], Université Paris-Sud XI.

[5] Research Director of the Laboratoire de Physico-Chimie de l'Etat Solide [LPCES] at the Institut de Chimie Moléculaire et des Matériaux d'Orsay [ICMMO], Université Paris-Sud XI
[6] Research Senior Scientist at ICMMO, Université Paris-Sud XI
[7] Technical Assistant at the LPCES- ICMMO

vii. X-Ray Diffraction Measurement (XRD)

PIMM's PANalytical's X'Pert PRO Materials Research Diffraction system was used to make the XRD analysis. Si, TiC and Ti6Al4V powders were first used as a sample to ensure the accuracy of the instrument and to verify the imposed settings. Afterwards, the samples TOP_P_4, TOP_L_4 and TOP_L_3 were examined.

vi. Hardness measurement

The hardness of the samples was measured using PIMM's Clemex CMT.HD ST-2000 Microhardness Automatic Tester. As it can be seen from Table 4, half of the samples were manufactured under the same conditions. (TOP_P_1 same as TOP_P_4, TOP_P_2 same as TOP_P_3, TOP_L_1 same as TOP_L_4 and TOP_L_2 same as TOP_L_3). Samples TOP_P_1, TOP_P_2, TOP_L_1, TOP_L_2, present higher levels of oxidation and thus for the following analysis, the less oxidized samples were used i.e. TOP_P_4, TOP_L_4, TOP_P_3, TOP_L_3.

The indents were made vertically at the edges of each sample to the longitudinal sense so that it would not affect the surface area in order to later perform the EBSD analysis. During the measurement, the applied force was 500 gf and the size of each indent was roughly 40 μm x 40 μm so that is could cover a relatively larger surface.

At the final stages of the project, even after the EBSD analysis, additional micro hardness analysis were made to further investigate the micro hardness properties in a wider zone of the samples. Those additional measurements were made only for the samples TOP_L_3 which at the first measurements presented significant differences in comparison to the other samples. This time, the indents were made horizontally first close to the top layers and then close to the substrate (see Part III).

viii. Tensile Tests

For the tensile tests, three new samples were fabricated with DLMD. The parameters used for their fabrication can be found at Table 5. The DLMD parameters are similar to the first set of samples in order to have a complete image of the sample's characteristics manufactured under the same conditions with all the other analysis. Fig. 46 presents the geometry of the samples before the realizations of the tests.

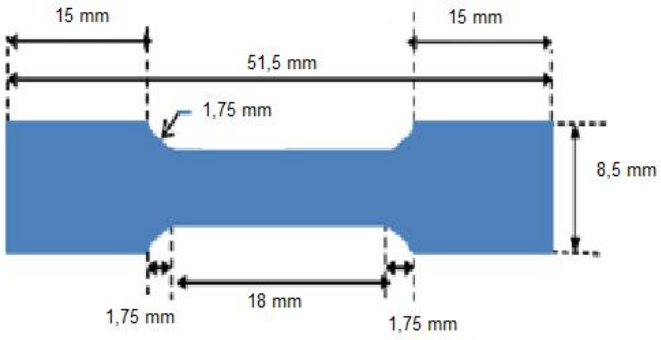

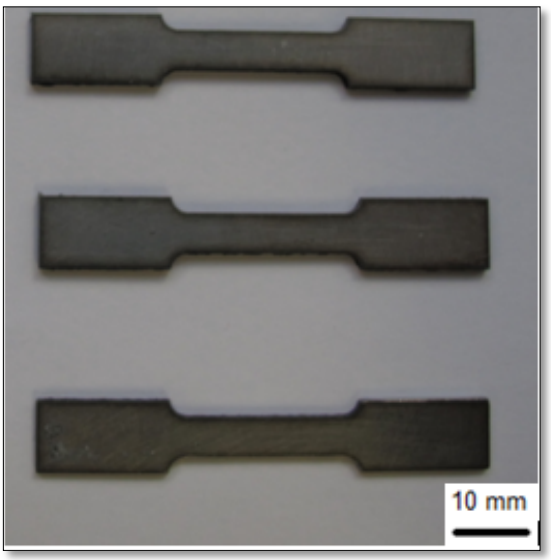

Figure 46: Dimensions and samples ready for the tensile tests.

The tests were realized using the INSTRON 5881 machine and the Instron Bluehill software. The samples acquired the desired geometry with laser cutting. The machine used was PIMM's TRUMF Laser HL201P, the laser type was Nd-Yag and the laser power Pcut.= 10 kW. The maximum load for the tensile tests was 50 kN and the static load cell weight was 5 kg. The velocity under which the experiments were realized was 0.2 mm/min.

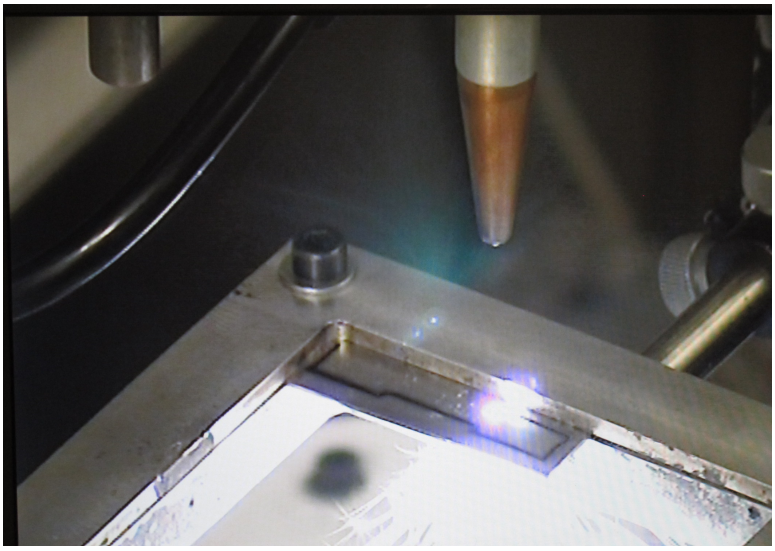

Figure 47: Sample cut with laser to achieve the desired geometry for the tensile tests.

	Tr_P_1	Tr_P_2	Tr_L_1
DLMD Parameters			
Velocity (mm/min)	400	400	400
Laser Power (W)	500	500	500
Powder's Flow Rate (gr/min)	1,55	1,57	1,51
Refusion at 600 W	No	no	yes
Wall's characteristics			
Length (mm)	57	56	57
Height (mm)	19	16	19
Width (mm)	2,4	2,3	2,4

Table 5: Parameters of the manufactured samples for the tensile tests.

III. RESULTS

III.1 Macroscopic Observations

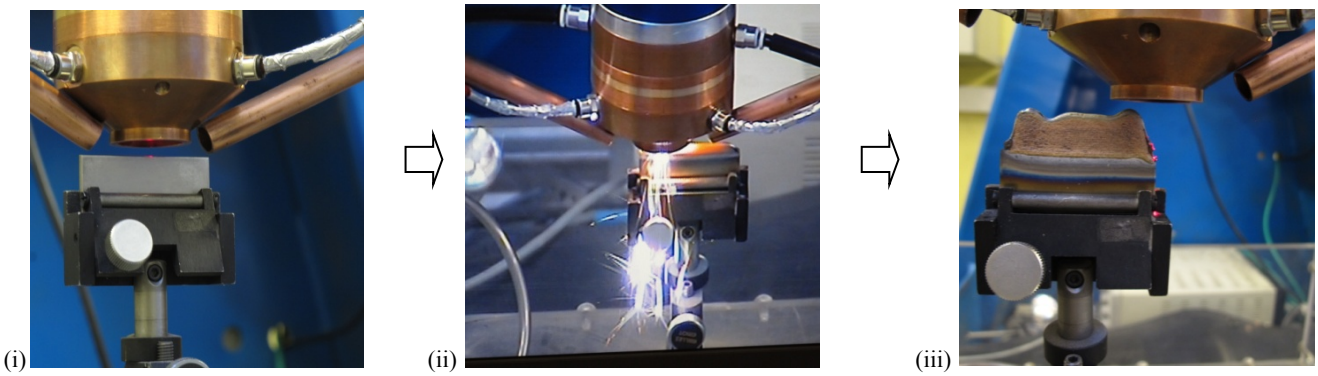

Figure 48: DLMD in progress.

Fig. 48 shows the occurred stages through the Direct Laser Metal Deposition [DLMD]. Picture (iii) shows the first sample that was fabricated with simultaneous laser-powder deposition at 500 W followed by an only-laser deposition at 600 W. (TOP_L_1). It can be seen that it is very oxidized. This most likely happened because of an insufficient deposition of the Argon shield gas. Table 6 presents the geometrical characteristics of all the eight samples that were fabricated and Fig. 49.1 – Fig 49.8 presents the manufactured walls.

Samples that were not remelted:

Figure 49.2: TOP_P_1

Figure 49.1: TOP_P_4

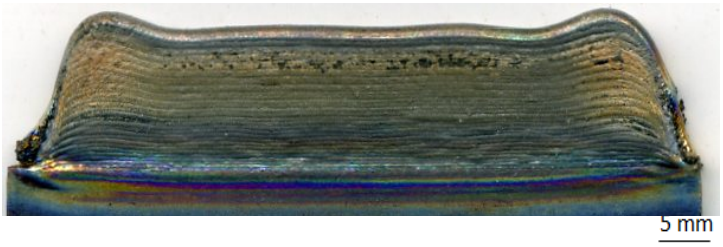

Figure 49.3: TOP_P_2

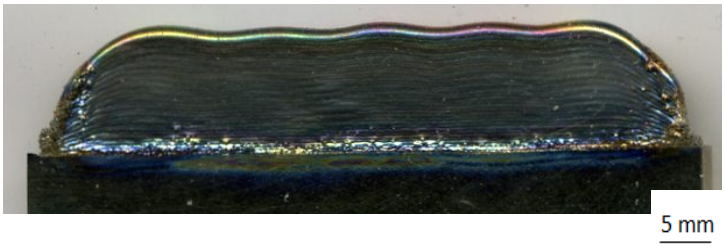

Figure 49.4: TOP_P_3

Samples that were remetled:

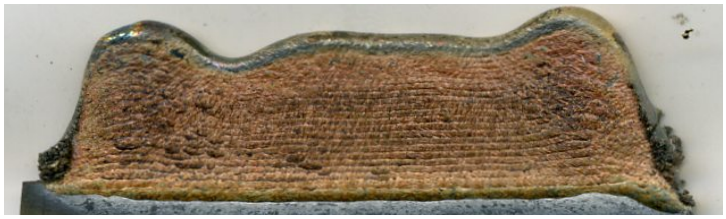

Figure 49.5: TOP_L_1

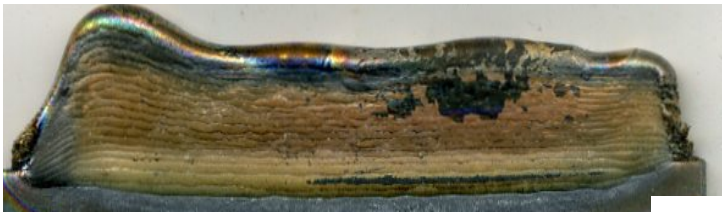

Figure 49.6: TOP_L_4

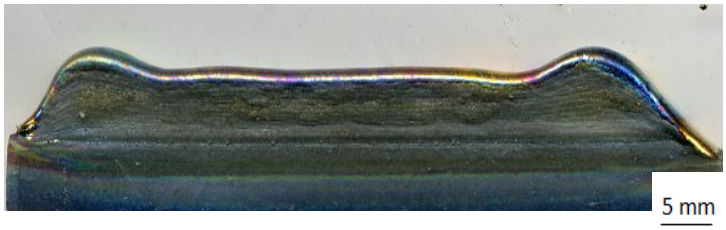

Figure 49.7: TOP_L_2

Figure 49.8: TOP_L_3

Although the samples named ‘1’ and ‘4’ and the samples named ‘2’ and ‘3’ were manufactured under the same parameters concerning the velocity of the laser beam, the morphology of the walls still present some differences.

	TOP_P_1	TOP_P_2	TOP_P_3	TOP_P_4	TOP_L_1	TOP_L_2	TOP_L_3	TOP_L_4
Wall's characteristics								
Length (mm)	45	45	45	46	42	43	41	44
Height (mm)	13	10	10	11,5	13	5	11	7,5
Width (mm)	2,51	1,91	2,15	2,4	2,6	2,09	2,13	2,59
Number of Layers (N)	26	35	36	26	26	14	37	17
Wall's mass (gr)	5,7435	3,9155	5,25	5,6883	6,2002	1,7202	4,3177	3,7602

Table 6: Geometrical Characteristics of fabricated walls.

- Table with overall characteristics of the samples

	TOP_P_1	TOP_P_2	TOP_P_3	TOP_P_4	TOP_L_1	TOP_L_2	TOP_L_3	TOP_L_4
DLMD Parameters								
Velocity (mm/min)	200	400	400	200	200	400	400	200
Laser Power (W)	500	500	500	500	500	500	500	500
Powder's Flow Rate (gr/min)	1,4913	1,5038	1,4	1,45	1,47	1,5038	1,4738	1,45
Refusion at 600 W	no	no	no	no	yes	yes	yes	yes
Wall's characteristics								
Length (mm)	45	45	45	46	42	43	41	44
Height (mm)	13	10	10	11,5	13	5	11	7,5
Width (mm)	2,51	1,91	2,15	2,4	2,6	2,09	2,13	2,59
Number of Layers (N)	26	35	36	26	26	14	37	17
Wall's mass (gr)	5,7435	3,9155	5,25	5,6883	6,2002	1,7202	4,3177	3,7602

Table 7: Overall characteristics of the samples

III.2 Analysis of the surface condition with Roughness Measurements

As mentioned at the Experimental Procedures chapter (Part II), for every sample there has been a measurement of the surface roughness. Table 8 shows the six parameters that characterize the quality of the surfaces that were studied in regard to roughness (Ra, Rt, Rp) and waviness (Wa,Wt, Wp).

In summary, the definitions of the roughness and waviness coefficients are **[1]**:
Roughness includes the finest (shortest wavelengths) irregularities of a surface and generally results from a particular production process or material condition. The main coefficients are the Ra, Rp and Rt:

Ra: the average absolute deviation of the roughness irregularities from the mean line over one sampling length,

Rp: the highest peak in the roughness profile over the evaluation length,

Rt: Rp+Rv, where Rv is the depth of the deepest valley in the roughness profile over the evaluation length.

Waviness, includes the more widely spaced (longer wavelength) deviations of a surface from its nominal shape.

	Ra	Rt	Rp	Wa	Wt	Wp
TOP_P_1	2,19 μm	200,94 μm	147,17 μm	28 μm	228,19 μm	106, 87 μm
TOP_P_2	0,57 μm	43,5 μm	14,18 μm	12,2 μm	100,8 μm	52,87 μm
TOP_P_3	0,55 μm	33,41 μm	19,62 μm	11,2 μm	92,78 μm	55,7 μm
TOP_P_4	0,52 μm	30,61 μm	15,37 μm	9,3 μm	99,51 μm	53,99 μm
TOP_L_1	1,43 μm	51,45 μm	21,81 μm	16,8 μm	132,74 μm	66,64 μm
TOP_L_3	0,56 μm	50,16 μm	27,94 μm	10,1 μm	92,2 μm	54,03 μm
TOP_L_4	0,69 μm	39,19 μm	22,57 μm	21,1 μm	143,35 μm	82,11 μm

Table 8: Roughness results.

Fig 50. illustrates all the results from the 3D scans. In general, it can be observed that the samples that were remelted present higher values of surface roughness. A possible explanation for this could be that these samples were exposed to the experimental environment for a longer period, thus they were more oxidized and their surface quality was affected. In addition, another plausible explanation would be that the increased waviness that is observed at the samples that were remelted is due to the convection current, which is originated from the remelting.

In general, the surface finish values are much better than those achieved on pure Ti6Al4V at similar DLMD conditions (nearly factor 2 to 3 decrease of roughness values). This indicates a tension effect of carbon in the Ti matrix that eventually acts as smoothening of the surface.

⇨ Samples without remelting. [Laser Power = 500 W]

All the maps shown below represent a surface area of 4000 μm x 4000 μm at the center of each sample respectively.

TOP_P_1 ; v= 200 mm/min

Ra=2,19 µm Rt= 200,94 µm Rp= 147,17 µm
Wa= 28 µm Wt=228,19 µm Wp= 106,87 µm

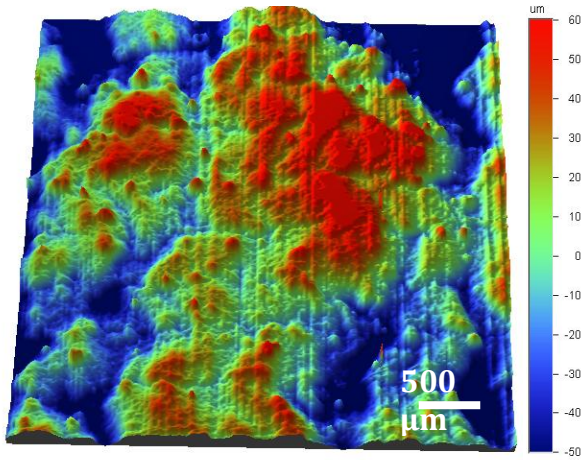

TOP_P_2 ; v= 400 mm/min

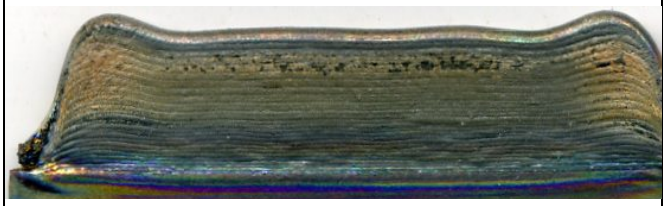

Ra= 0,57 µm Rt= 43,5 µm Rp= 14,18 µm
Wa= 12,2 µm Wt= 100,8 µm Wp= 52,81 µm

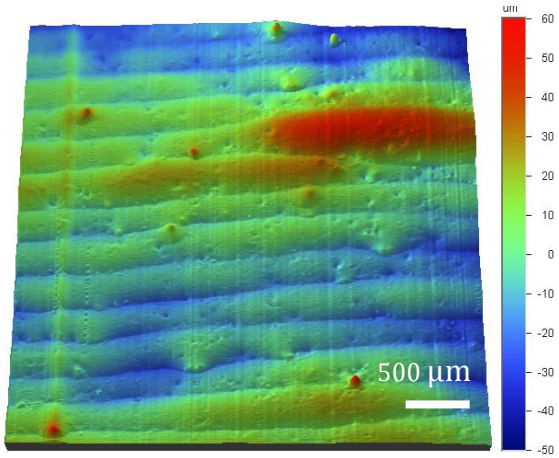

TOP_P_3 ; v= 400 mm/min

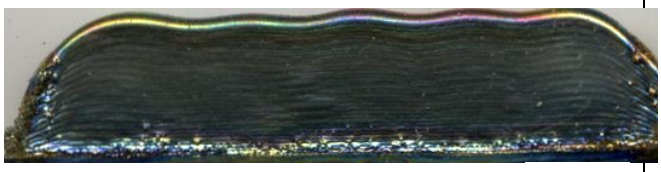

Ra= 0,55 µm Rt= 33,41 µm Rp= 19,62 µm
Wa= 11,2 µm Wt= 92,78 µm Wp= 55,7 µm

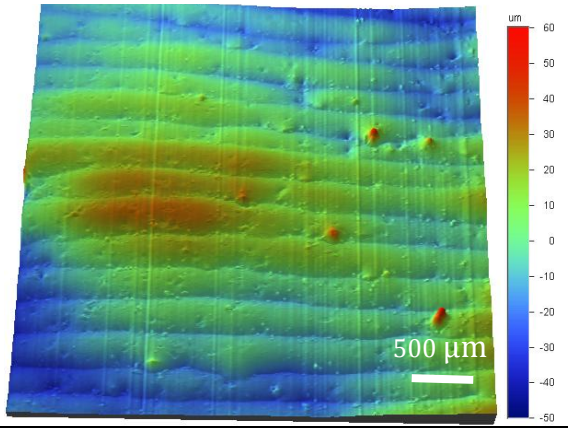

TOP_P_4 ; v= 200 mm/min

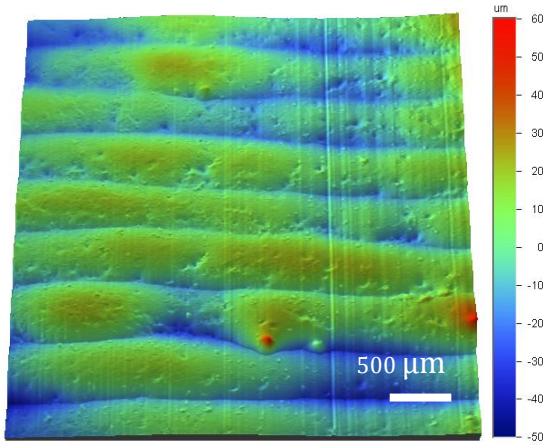

Ra=0,52 µm Rt= 30,61 µm Rp= 15,37 µm
Wa= 9,3 µm Wt= 99,51 µm Wp= 53,99 µm

⇨ Samples with remelting [Powder-Laser Power = 500 W, Refusion Power = 600 W]

TOP_L_1 ; v= 200 mm/min

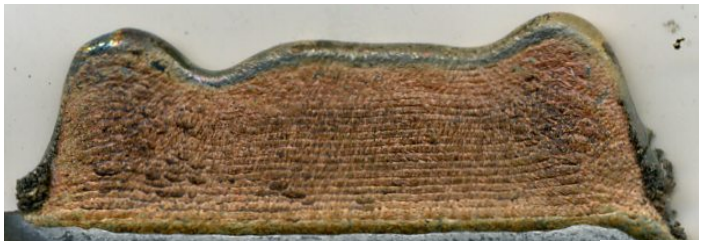

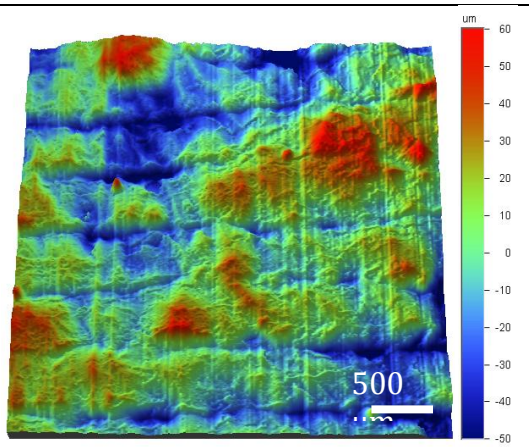

Ra=1,43 µm Rt=51,45 µm Rp=21,81µm
Wa=16,8 µm Wt=132,74 µm Wp=66,64µm

TOP_L_3 ; v= 400 mm/min

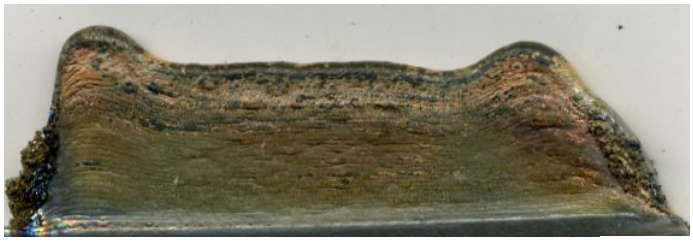

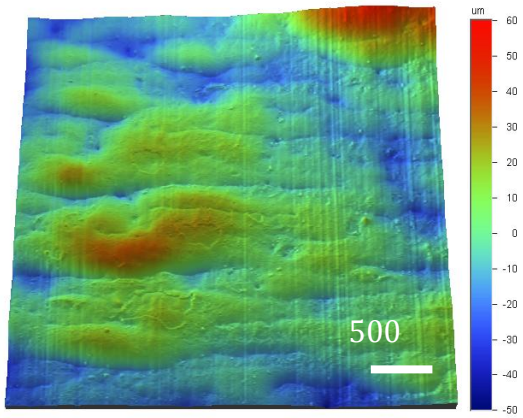

Ra= 0,56 µm Rt= 50,16 µm Rp= 27,94 µm
Wa=10,1 µm Wt= 92,2 µm Wp= 54,03 µm

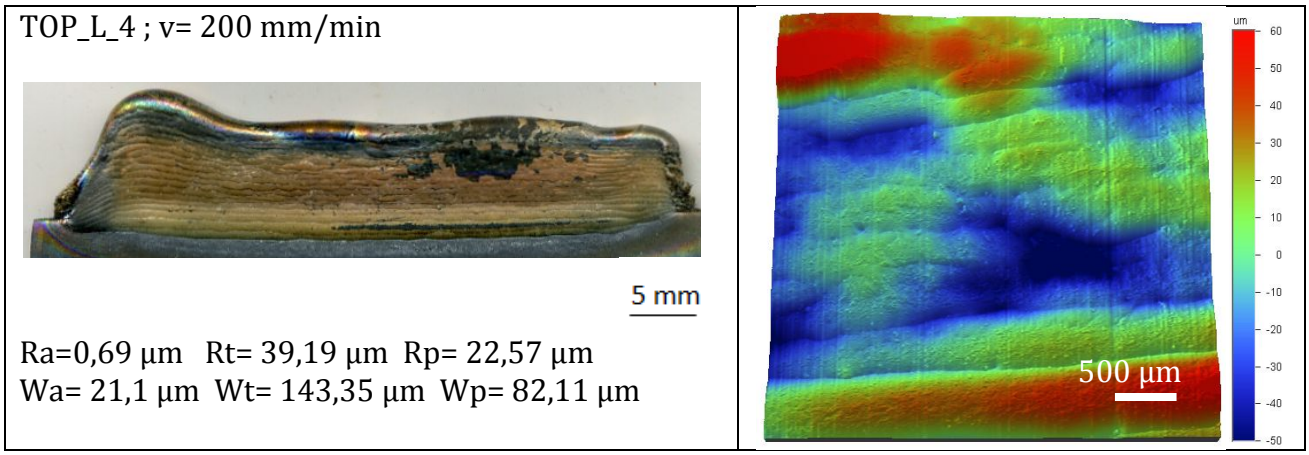

Figure 50: Roughness results: 2D and 3D scan results.

III.3 Analysis of the Microstructure

III.3.1 Optical Microscope (OM) and Scanning Electron Microscope (SEM) Observations

One of the main goals of the current project was to investigate the homogeneity of the microstructures that were created after the process. The principal outcome from the overall observations is that the samples that were remelted present better homogeneity regarding the distribution of the dendrites in the Ti matrix. In addition, there are less unmelted particles in contrast with the samples that were not remelted.

Another important outcome is that there are no significant differences between the samples of a same category. For instance, there are samples that were not remelted (one category) but were manufactured with different parameters (velocity) but still they do not present any notable differences to their microstructure. Fig. 51 shows a representative microstructure of the samples that was not remelted. Partially or completely unmelted particles are observed.

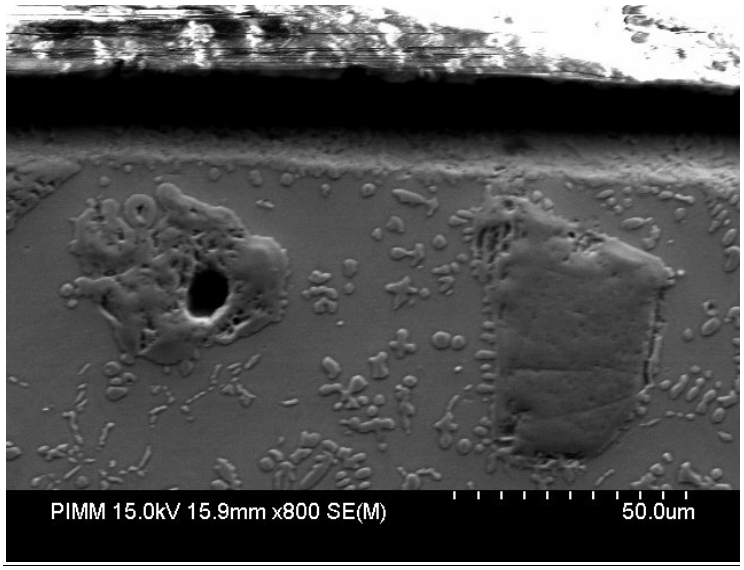

Figure 51: SEM Observation: Sample TOP_P_4 : TiC partially melted and unmelted particles.

The distribution of the dendrites is homogenous and there is no preferred orientation (Fig. 52 - Fig.55). An attempt to determine the percentage of the unmelted particles and the percentage of the dendrites in relation to the matrix shows that there are very few unmelted particles in comparison with the overall matrix (6%) and the dendrites are very homogenously distributed along the matrix as their percentage reaches 43% (Fig. 56, 57).

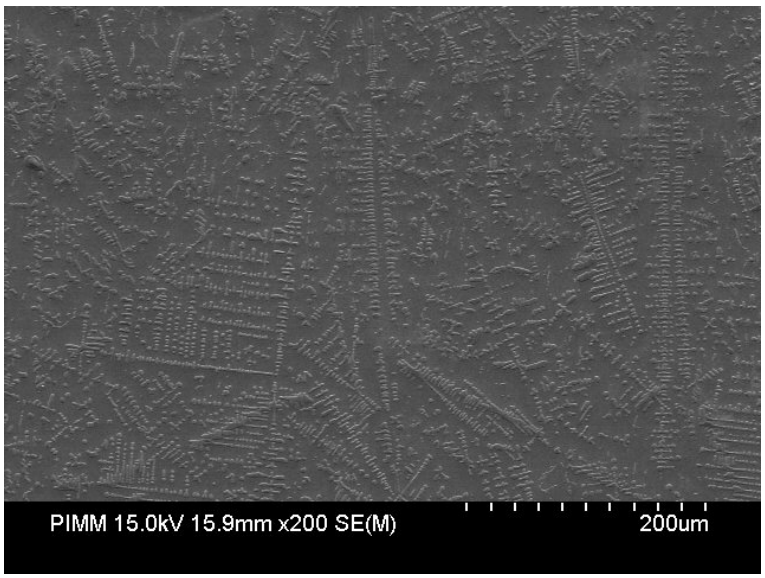

Figure 52: SEM Observation: Sample TOP_P_4: longitudinal view; center.

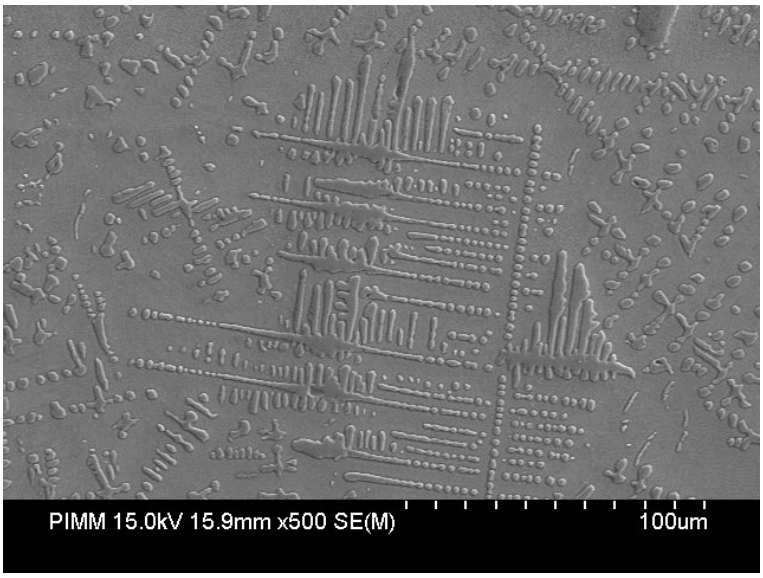

Figure 53: SEM Observation: Sample TOP_P_4: longitudinal view; center.

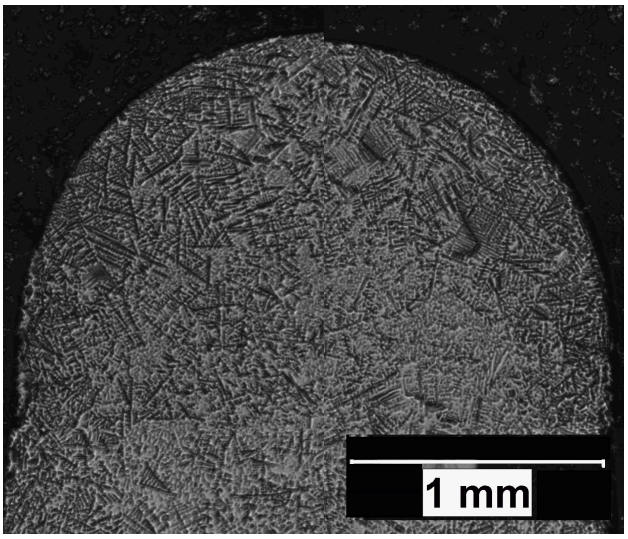

Figure 54: OM observation: Sample TOP_L_4 : transversal view; top.

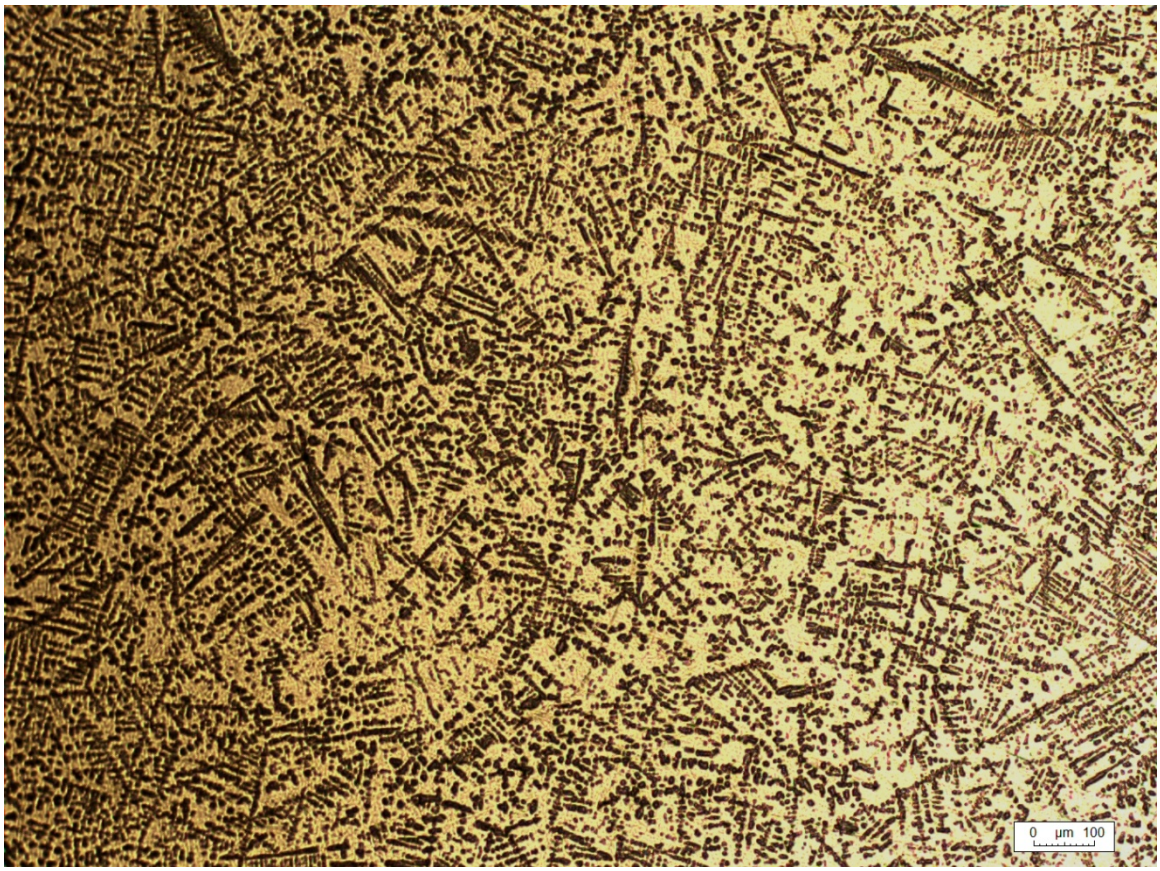

Figure 55: OM Observation: Sample TOP_L_1: section view; center.

- Determination of the percentage of the TiC dendrites in comparison to the Ti6Al4V matrix and of the percentage of the unmetled TiC in comparison to Ti6Al4V using IMAGE J software.

In order to estimate the percentage of the dendrites formed in the Ti matrix, the IMAGE J software was used. The basic concept of the estimation consisted first of making the difference between the dendrites and the matrix more evident by removing the color of the microscope image. As a result, dendrites were illustrated with black color and the remaining white areas represented the Ti matrix (fig. 56). Afterwards, by using the appropriate IMAGE J's command (*make binary)*, we resulted at an estimation of the ratio black to white, which we used as a scale to evaluate the percentage of the dendrites along the matrix.

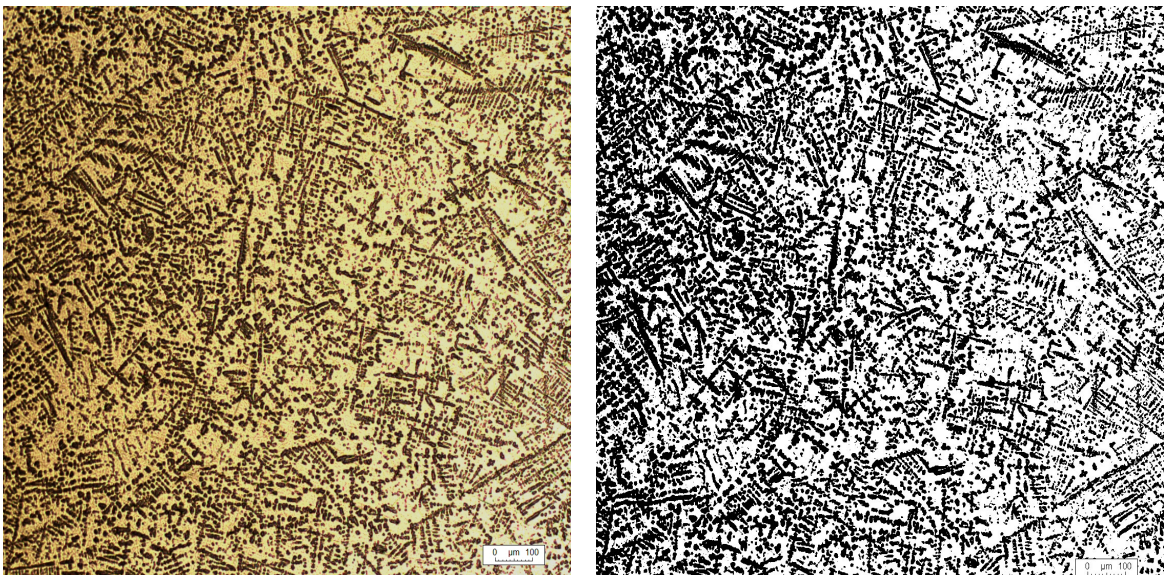

Figure 56. Sample TOP_L_1; Calculation of TiC dendrites : Ti6Al4V matrix ratio.

According to the acquired results, the percentage of dendrites (ratio black to white) in comparison to the Ti matrix was calculated to be 43%. This is a satisfactory outcome as it proves that dendrites are uniformly distributed along the Ti matrix.

Another important factor was to estimate the percentage of the unmelted TiC particles that remained after the fabrication. Likewise, we tried to isolate the umelted particles along the Ti matrix to later estimate them again as a ratio of black to white (fig. 57).

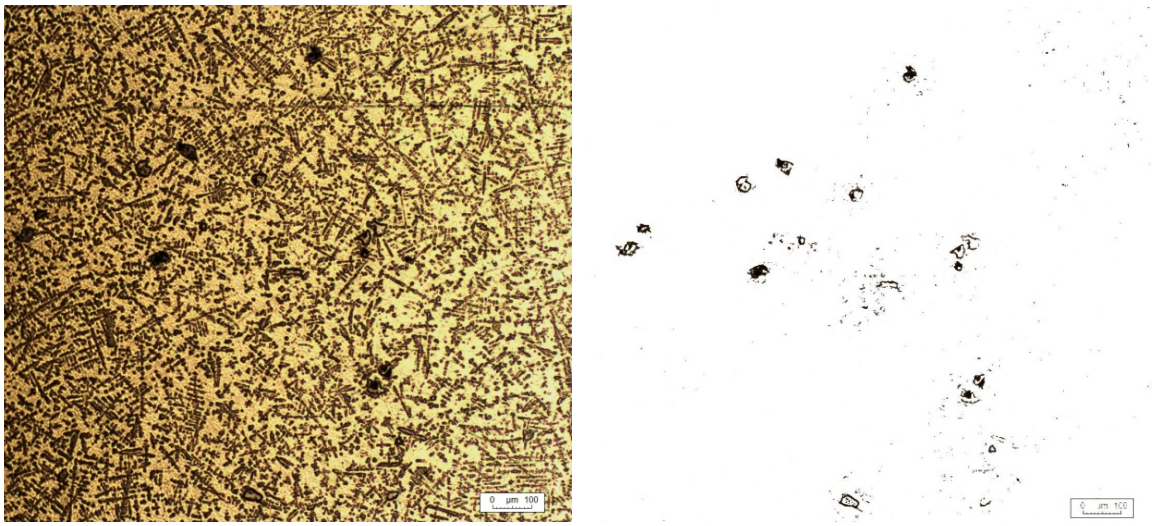

Figure 57. Sample TOP_L_1; Calculation of unmelted TiC : Ti6Al4V ratio.

According to the acquired results, the percentage of the unmelted particles as of a ratio black to white was calculated to be 6 %. This percentage is quite adequate.

- SEM and EDS results of the TOP_P_4 sample and TiC, Ti6Al4V powder grains.

Energy Dispersive Spectroscopy (EDS) allows one to identify what is the composition and the relative proportions (Atomic % for example) of the samples observed with the SEM. During EDS, a sample is exposed to an electron beam inside a scanning electron microscope (SEM). These electrons collide with the electrons within the sample, causing some of them to be knocked out of their tracks. The vacated positions are filled by higher energy electrons which emit x-rays in the process. By analyzing the emitted x-rays, the elemental composition of the sample can be determined.[8]

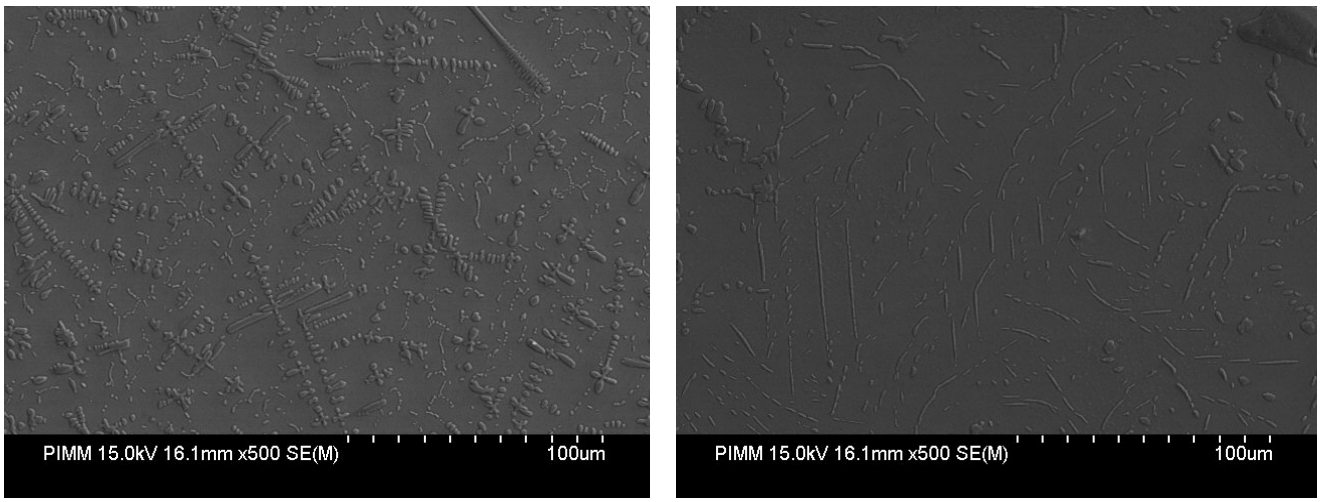

Figure 58: SEM Observation: Sample TOP_P_4; Comparison of the microstructure observed at the top center of the sample (left) to the substrate (left).

[8] "EDS Analysis Service". Tue. 12 March 2013. <http://www.semlab.com/edsanalysis.html>.

The results obtained from the EDS analysis at the SEM microscope, are shown below:

⇨ Dendrites grown along the Ti matrix:

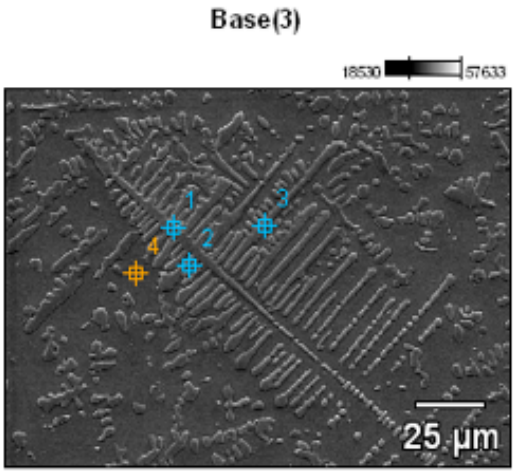

Image Name: Base(3)

Accelerating Voltage: 15.0 kV

Magnification: 700

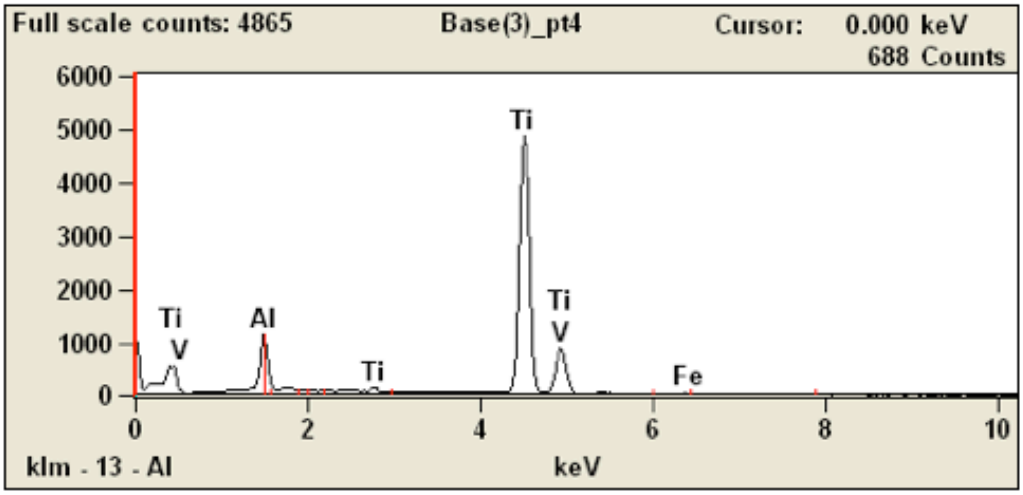

Weight %

	Be-K	C-K	Al-K	Si-K	Ti-K	V-K	Fe-K	As-K	Br-K
Base(3)_pt1	6.1	4.9	0.6	0.6	87.8				
Base(3)_pt2		2.8	2.8	0.5	91.7			2.2	
Base(3)_pt3	7.4	7.8		0.5	82.3				2.0
Base(3)_pt4			5.2		88.5	5.7	0.6		

Weight % Error (+/- 1 Sigma)

	Be-K	C-K	Al-K	Si-K	Ti-K	V-K	Fe-K	As-K	Br-K
Base(3)_pt1	+/-0.7	+/-0.9	+/-0.1	+/-0.1	+/-0.5				
Base(3)_pt2		+/-0.2	+/-0.1	+/-0.0	+/-0.5			+/-1.3	
Base(3)_pt3	+/-0.5	+/-0.4		+/-0.0	+/-0.4				+/-6.0
Base(3)_pt4			+/-0.1		+/-0.5	+/-0.3	+/-0.1		

Atom %

	Be-K	C-K	Al-K	Si-K	Ti-K	V-K	Fe-K	As-K	Br-K
Base(3)_pt1	22.9	13.8	0.7	0.7	61.8				
Base(3)_pt2		10.1	4.6	0.8	83.3			1.3	
Base(3)_pt3	25.3	20.2		0.5	53.2				0.8
Base(3)_pt4			8.9		85.4	5.2	0.5		

From the results displayed above, it is clear that we have well formed dendrites. Point 1 represents the main axis of the dendrite and points 2, 3 correspond to the arms of the dendrite. Point 4 represents the matrix. According to the results, as expected, along the matrix no parts of carbon (C) were found. In contrast, the presence of C is evident at points 1-3 which justifies the fact that well developed dendrites appear at this spot.

A possible explanation for the presence of other elements that logically should not appear here -such as Be and Si- would be that maybe these elements are the result of the sample's preparation (use of SiC papers during grinding) or because of a misdetection of the machine, which is always a potential factor for mistakes to all the experimental projects.

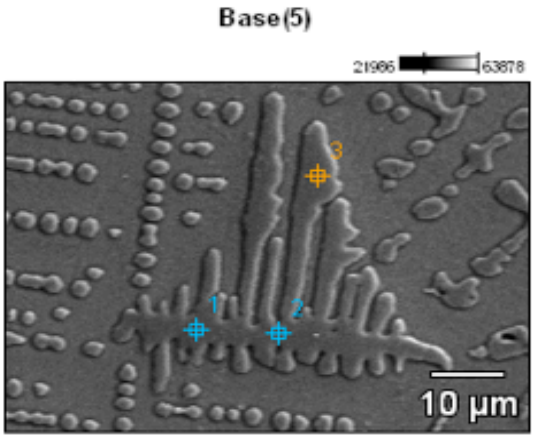

Image Name: Base(5)

Accelerating Voltage: 15.0 kV

Magnification: 1800

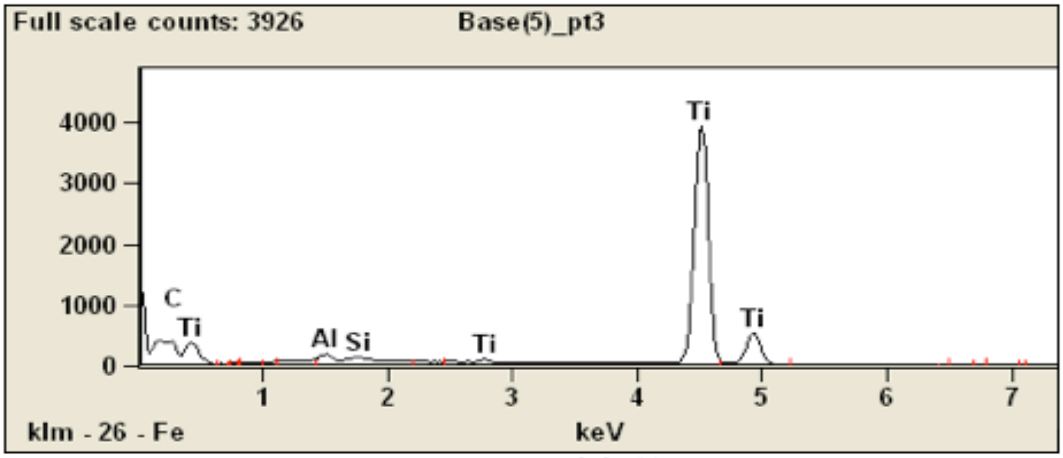

Weight %

	C-K	Al-K	Si-K	Ti-K
Base(5)_pt1	4.4	0.6	0.4	94.5
Base(5)_pt2	4.6	0.6	0.8	94.0
Base(5)_pt3	4.6	0.8	0.3	94.4

Weight % Error (+/- 1 Sigma)

	C-K	Al-K	Si-K	Ti-K
Base(5)_pt1	+/-0.4	+/-0.0	+/-0.0	+/-0.5
Base(5)_pt2	+/-0.4	+/-0.1	+/-0.0	+/-0.5
Base(5)_pt3	+/-0.4	+/-0.0	+/-0.0	+/-0.5

Atom %

	C-K	Al-K	Si-K	Ti-K
Base(5)_pt1	15.3	1.0	0.7	83.0
Base(5)_pt2	16.0	1.0	1.2	81.9
Base(5)_pt3	15.9	1.2	0.5	82.5

To examine the accuracy of the EDS results, we also examined a Ti6Al4V and a TiC particle. The results are satisfactory; for the Ti6Al4V particle we get the correct percentages of each of the main elements and for the TiC particle, the results are also acceptable. Although the obtained results are adequate, TiC particles often present large C/Ti changes because of the possibility of a non-stoichiometric re-crystallization of TiC. As a result, EDS analysis sometimes fails to measure C content correctly resulting at some Ti: 0.65, C: 0.35 stoichiometries.

⇨ Ti6Al4V particle:

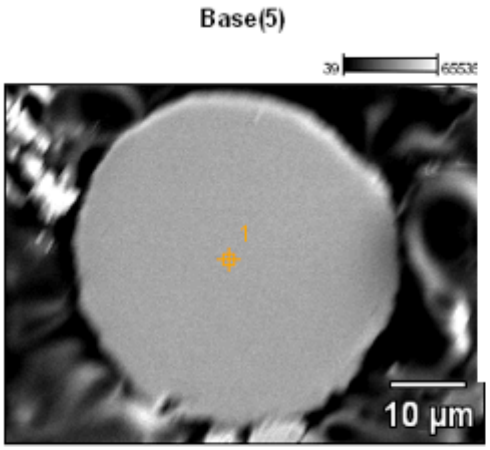

Image Name: Base(5)

Accelerating Voltage: 15.5 kV

Magnification: 2000

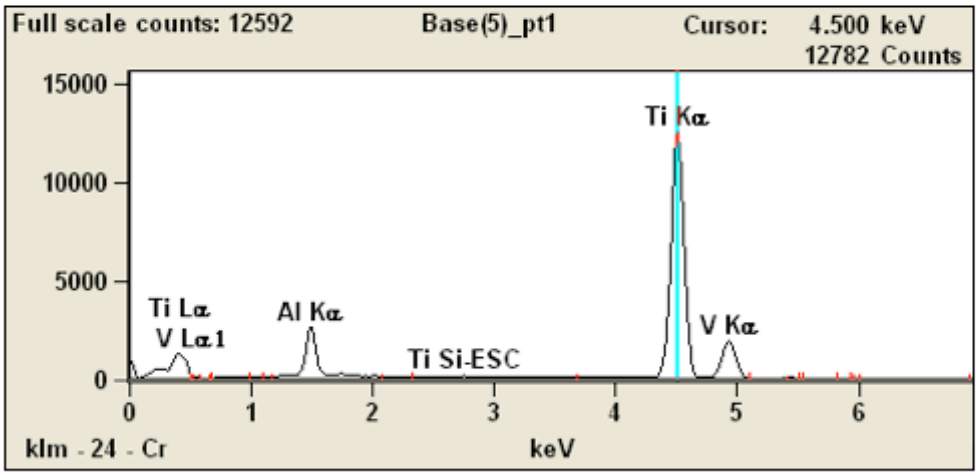

Weight %

	Al-K	Ti-K	V-K
Base(5)_pt1	5.2	90.7	4.0

Weight % Error (+/- 1 Sigma)

	Al-K	Ti-K	V-K
Base(5)_pt1	+/-0.1	+/-0.3	+/-0.2

Atom %

	Al-K	Ti-K	V-K
Base(5)_pt1	8.9	87.4	3.7

⇨ TiC particle:

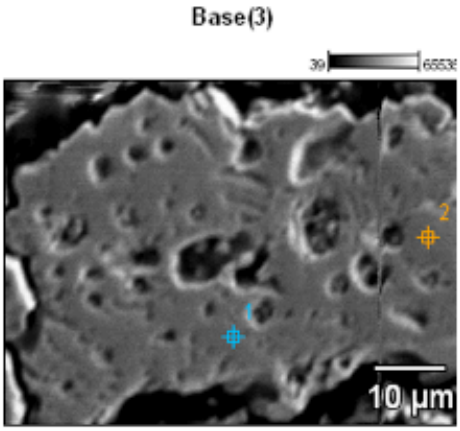

Image Name: Base(3)

Accelerating Voltage: 15.5 kV

Magnification: 2000

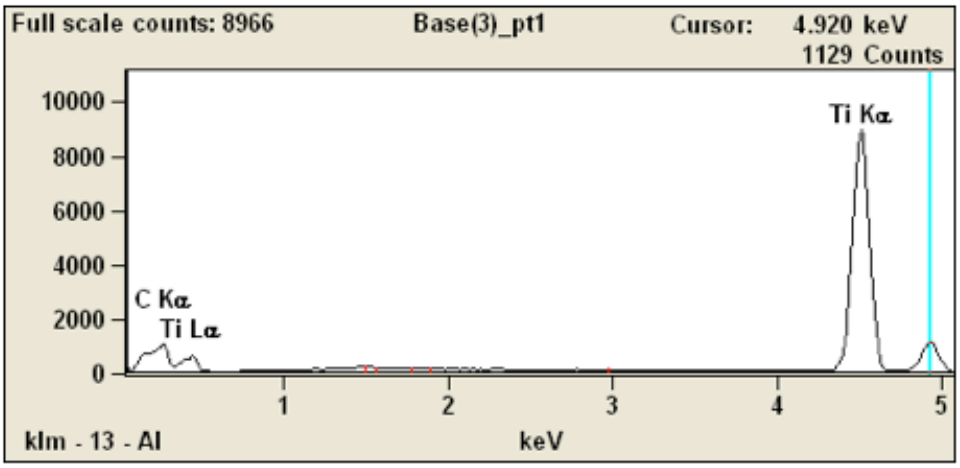

Weight %

	C-K	Ti-K
Base(3)_pt1	8.2	91.8
Base(3)_pt2	7.9	92.1

Weight % Error (+/- 1 Sigma)

	C-K	Ti-K
Base(3)_pt1	+/-0.4	+/-0.4
Base(3)_pt2	+/-0.4	+/-0.4

Atom %

	C-K	Ti-K
Base(3)_pt1	26.2	73.8
Base(3)_pt2	25.4	74.6

To better understand the nucleation of the dendrites and also the differences between the samples that underwent a remelting in comparison with the ones that did not, we had EBSD analysis. The remelting factor is the most significant one and this is the reason why most of the attention is focused on examining this effect. The differences in velocity among the samples (200 mm/min compared to 400 mm/min) do not present very important differences. Slightly better results are presented at the samples that were fabricated with 200mm/min velocity and for this reason the EBSD analysis was realized for these samples.

III.3.2 Electron BackScatter Diffraction Measurement (EBSD)

At EBSD analysis, each color represents a different crystallographic orientation. The cartography of the analysis that was completed within the context of the current project was 180 x 440 μm for the TOP_L_4 sample which corresponds roughly to one layer and for the sample TOP_P_4 the cartography was 150 x 775 μm to try and portray more than one layers.

The findings from this analysis were that one dendrite is expanded to more than one Ti matrix which makes the material more brittle.

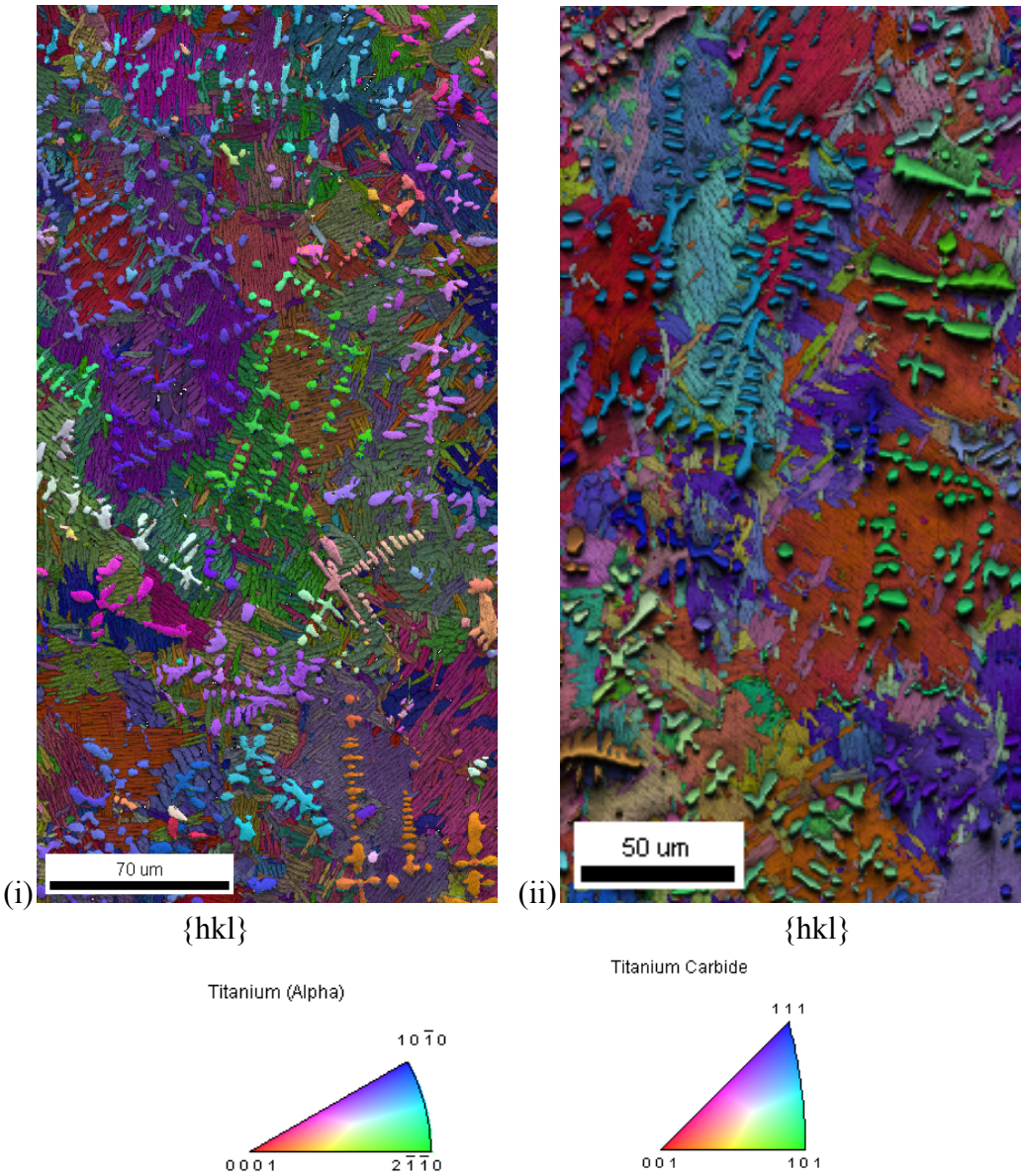

Figure 59: EBSD results for the samples: (i) TOP_L_4 (longitudinal view) (ii) TOP_P_4 (section view).

Furthermore, for the remelted samples, the presence of the small dendrites is a lot less than for the non-remelted sample which is very important.

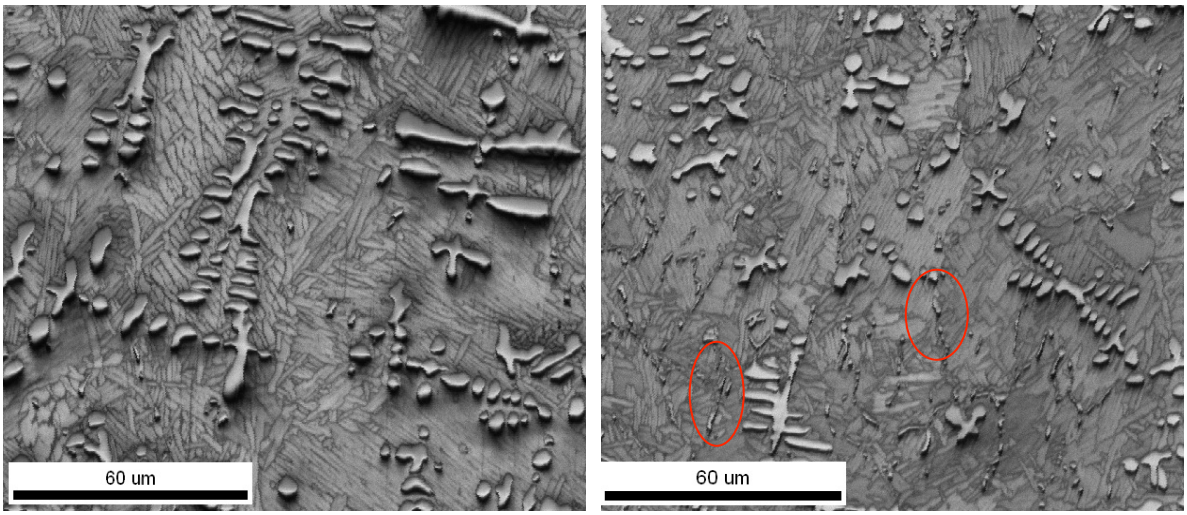

Figure 60: TOP_L_4 (left) presents a lot less small TiC than TOP_P_4 (right).

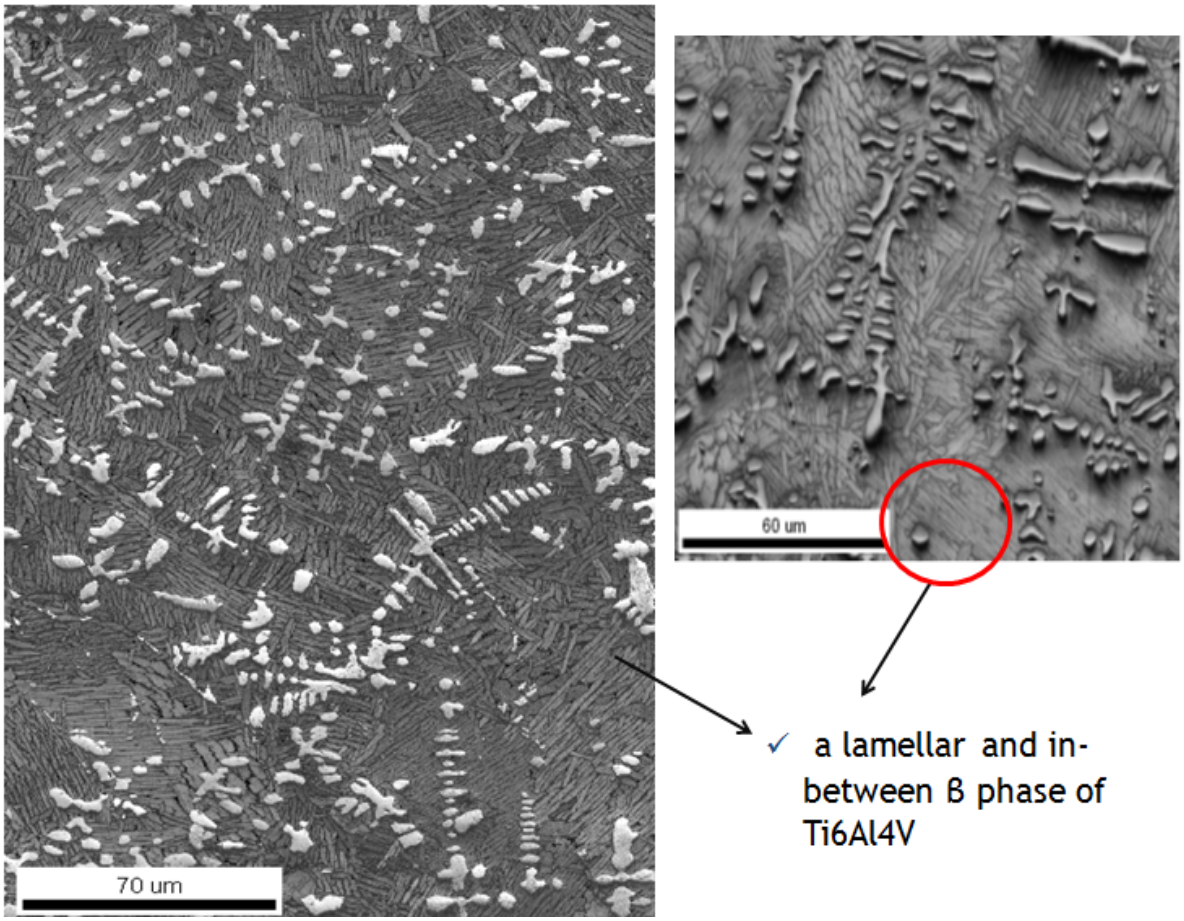

Figure 61: Ti matrix observed with EBSD

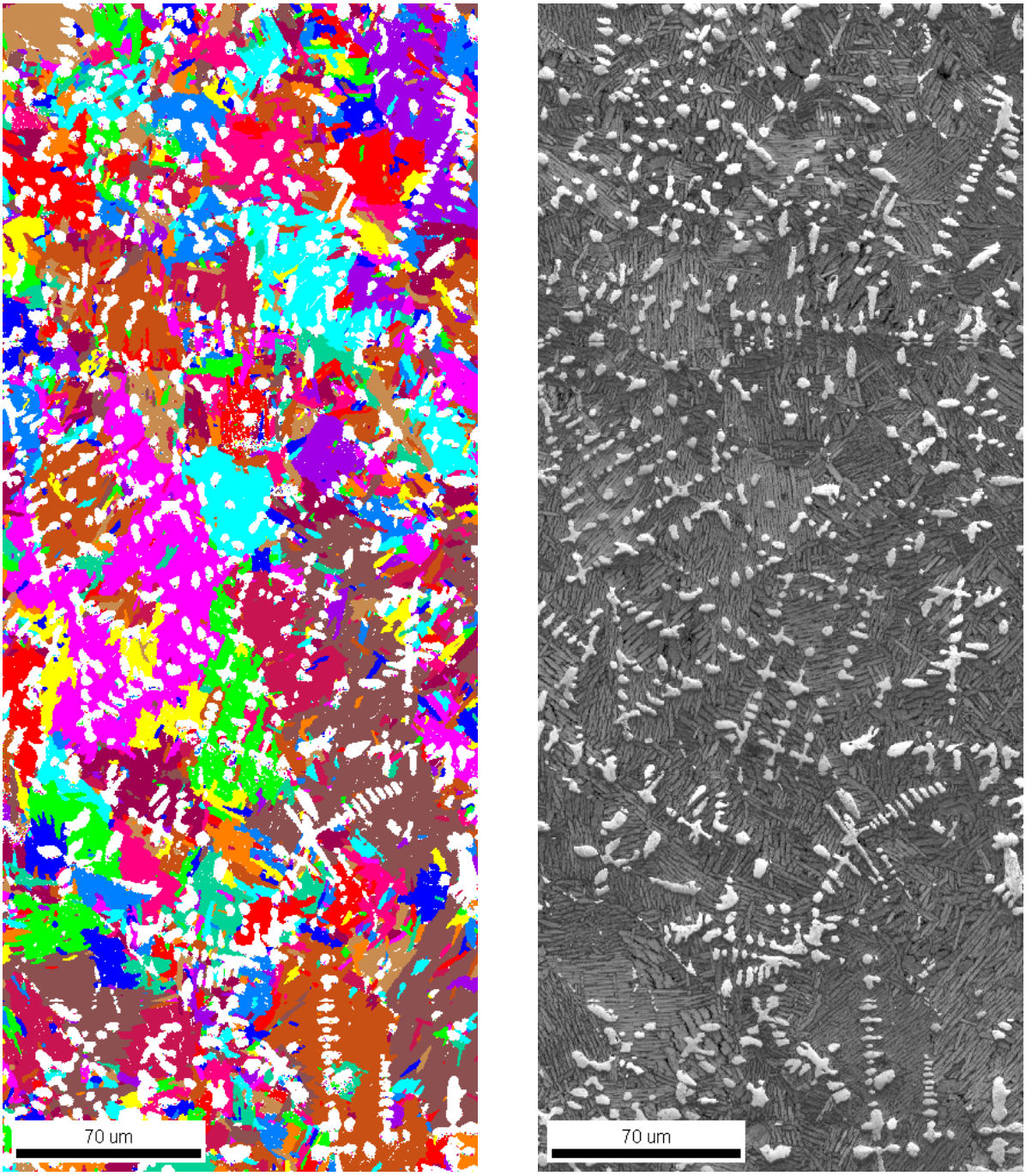

Figure 62: Criterion of 15° (left image)- Sample TOP_L_4

A number that expresses how well the simulated EBSP[9] overlays the actual EBSP is the mean angular deviation (MAD) that is given in degrees specifying the averaged angular misfit between detected and simulated Kikuchi bands. A grain boundary map can be generated by comparing the orientation between each pair of neighboring points in an OIM scan. A line is drawn separating a pair of points if the difference in orientation between the points exceeds a given tolerance angle.

[9] Electron Backscatter Patterns

An alternative way to determine the percentage of the TiC presence in the matrix, in comparison to Ti6Al4V, is by using the **OIM™ Data Analysis of EBSD results** as shown in Fig. 63 and Fig. 64. in addition to using the IMAGE J software as previously done (see pages 67-68). Although EBSD is a very precise analysis method, the results regarding the measurement of the percentage are not very accurate, nonetheless it is worth displaying them to illustrate an extra method in determining the TiC-Ti6Al4V ratio.

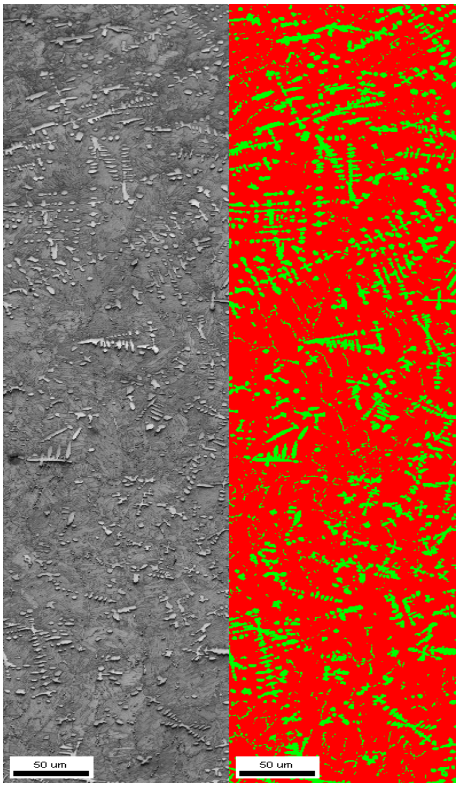

Phase	Total Fraction
Titanium (Alpha)	0.821
Titanium Carbide	0.179

Figure 63: Sample TOP_P_4

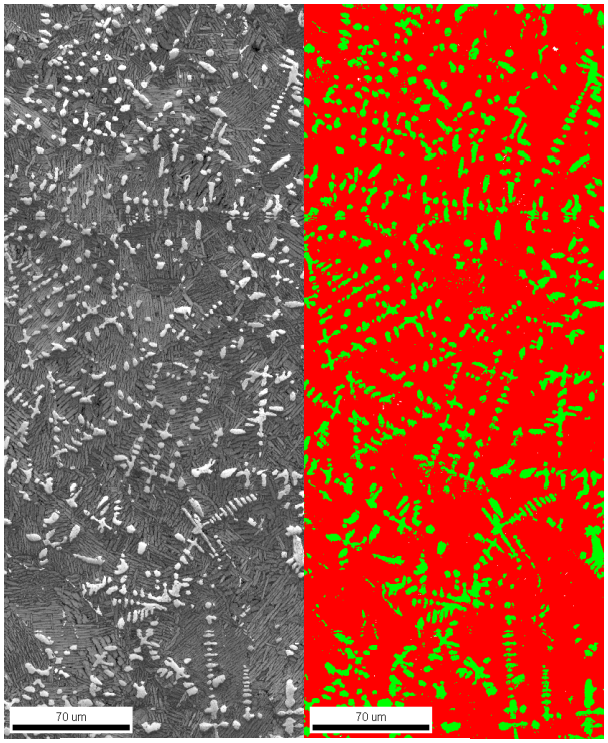

Phase	Total Fraction
Titanium (Alpha)	0.834
Titanium Carbide	0.166

Figure 64: Sample TOP_L_4

The experimental results display a percentage of the carbide element in the composition of the samples to be as little as 17.9% for the TOP_P_4 (sample that did not go under a remelting) and 16.6% for the TOP_L_4 (sample remelted). When compared to the results that were obtained with the IMAGE J software there is an important difference. Taking into account though that the area of the samples examined with the IMAGE J software was much larger, we tend to consider these outcomes more reliable and just.

III.3.3 X-Ray Diffraction Measurement (XRD)

The XRD analysis serves to identify the crystallographic phases of the samples. The XRD measurements, otherwise called Theta-2 Theta scans, were made to scan all lattice spacing present in the material. At the diagram below, the results for the sample TOP_L_4, TiC and pure Ti powder are displayed together to compare the phases.

It is clear that the peaks of the sample's measurement are very close to the ones of the composites of the samples. The small inclinations are justified because of the impact of the process on the material.

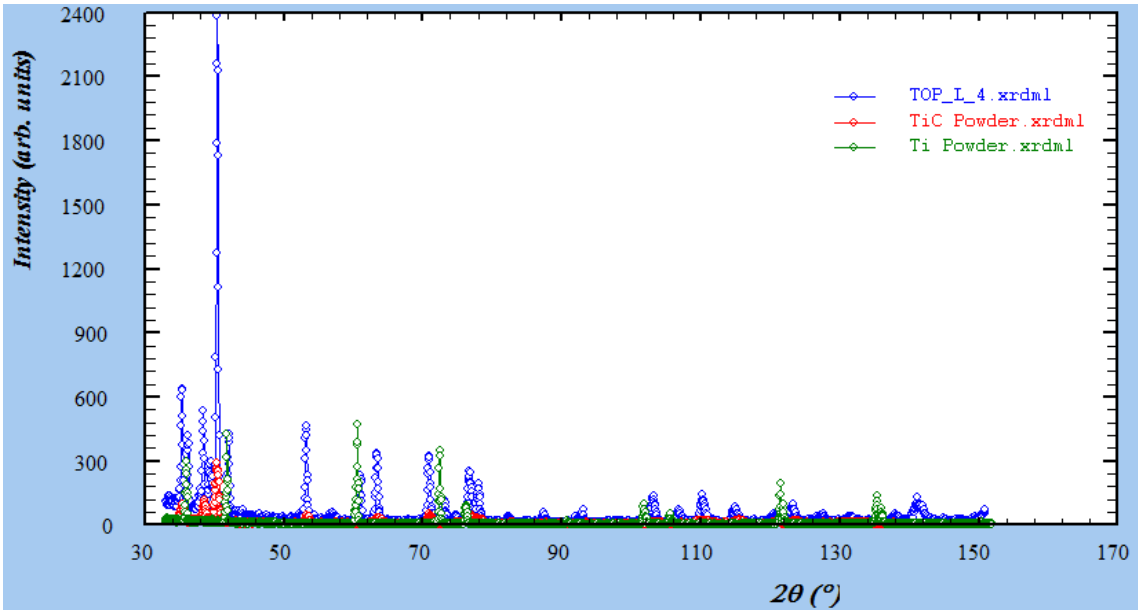

Figure 65: Diagram I=f (2θ) obtained after the diffraction of sample TOP_L_4, TiC and pure Ti powder.

III.4 Analysis of Mechanical Properties

III.4.1 Hardness measurement

- Location and size of imprints for micro hardness measurements

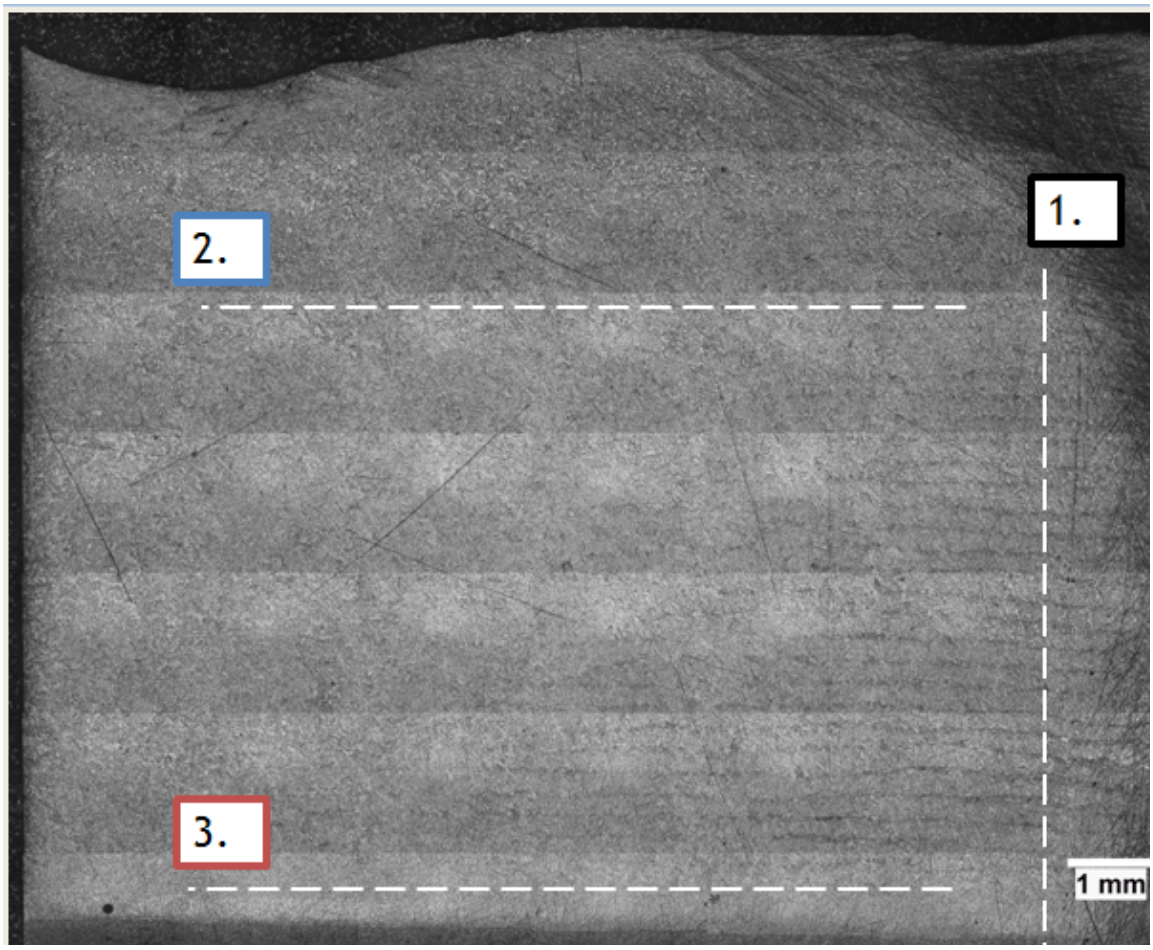

1. = same for all the samples

2. + 3. = only for sample TOP_L_3 for further examination

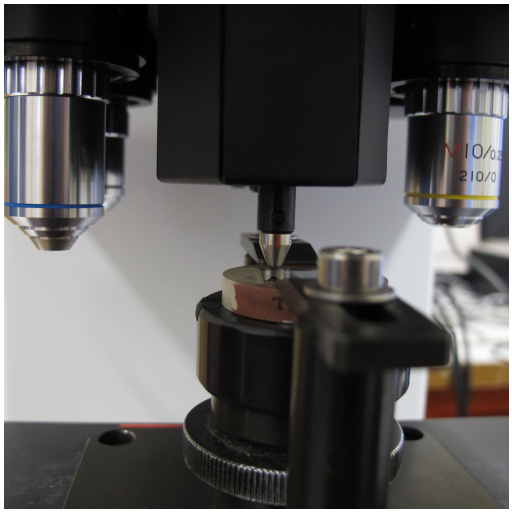

Figure 67 (left): Sample during the hardness measurement.

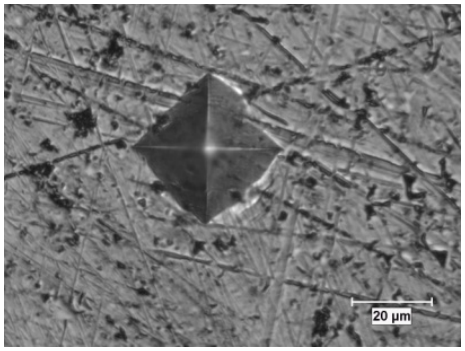

Figure 66: Size of an imprint

From the results obtained from the micro hardness measurements, it is clear that the presence of the TiC particles increases significantly the hardness of the samples. As the size of the imprints are about 40 μm (Fig. 66) and the TiC grain size spectrum is 50-75 μm it is very likely that the imprints could be made on TiC unmelted particles, something that can greatly modify the results. This is also a possible explanation for the unusual high values that were observed for the sample TOP_L_3 which can more clearly be seen at Table 9 and Table 10. The peak demonstrates an important difference in the obtained values in comparison with the other samples.

Sample	Hardness value [HV]		
	average	max	min
Pure Ti6Al4V	418	435	393
TOP_P_3	479	592	435
TOP_P_4	481	505	422
TOP_L_3	562	636	471
TOP_L_4	481	570	390

Table 9: Results from the micro hardness measurements.

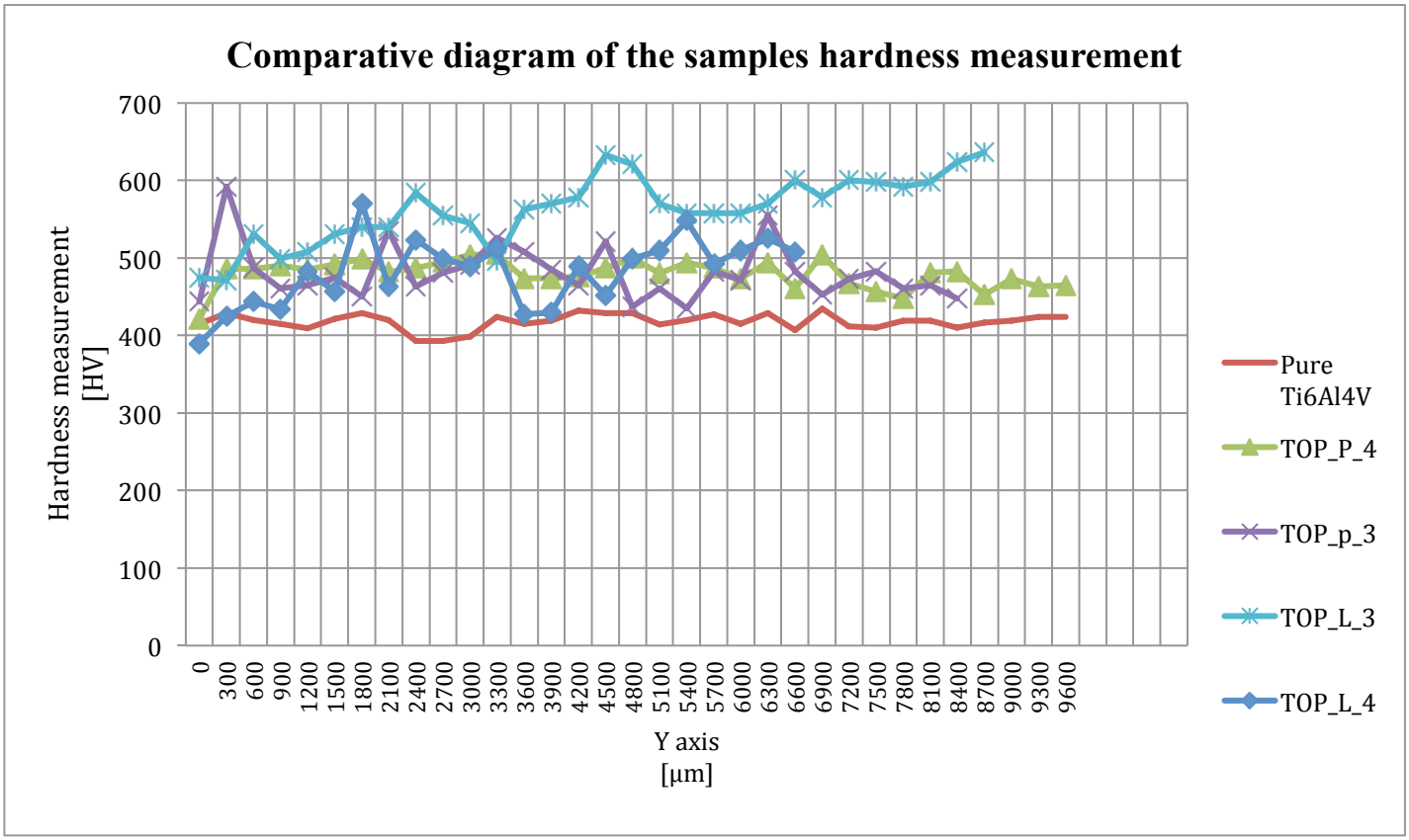

Table 10: Comparative diagram of all the samples tested.

For the reasons previously stated, we repeated a micro hardness measurement for the sample TOP_L_3 to investigate whether these results were systematic or more likely random with an explanation like the one given before. This time the measurements were made horizontally once closer to the substrate and then closer to the upper layers (see 'Location and size of imprints for micro hardness measurements' on page 77).

a)

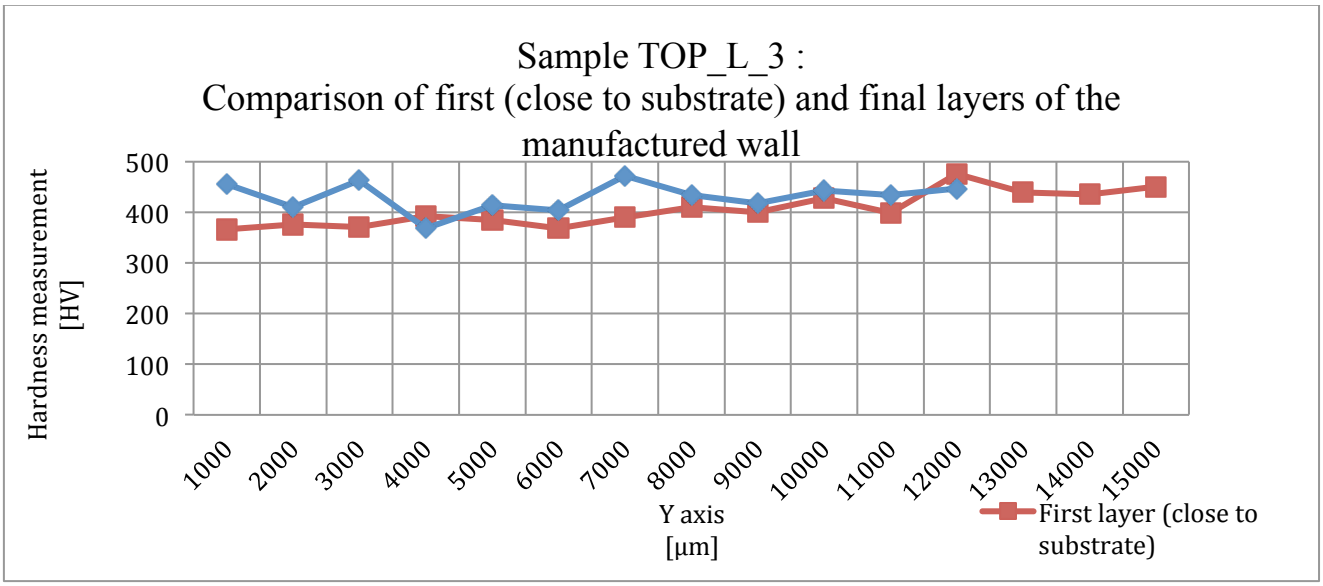

b)

Location of Measurement	Hardness value [HV] average	max	min
First layers; close to substrate	405	475	366
Final layers; top of the wall	430	471	368

Table 11: Micro hardness results in different horizontal locations (a) and average values (b) for the sample TOP_L_3.

The average values are now closer to the rest of the samples. In addition, a slight difference is noticed between the measurement close to the substrate and the measurement closer to the top layers. This result could be explained because of the annealing phenomena of Ti; top layers present more *β phase* which is harder than the *a phase* (primary phase of Ti) which is more likely observed closer to the substrate.

Concerning the principle parameters used during the experiments the following outcomes were extracted:

- Remelting Factor: No significant differences were observed regarding the effect of the remelting factor on the hardness results of the samples.

- Velocity Factor: Samples that were fabricated with velocity 200 mm/min present slightly better results regarding the hardness.

III.4.2 Tensile Tests

As aforementioned, for the realization of the tensile tests, three new samples were fabricated under the same conditions (see Table 5, Part II). Fig. 68 illustrates the walls of the newly manufactured samples and Fig. 69 presents the results of the roughness measurements.

Figure 68: Samples for tensile tests (from top to bottom) : Tr_P_1, Tr_P_2, Tr_L_1

Tr_L_1 ; v= 400 mm/min

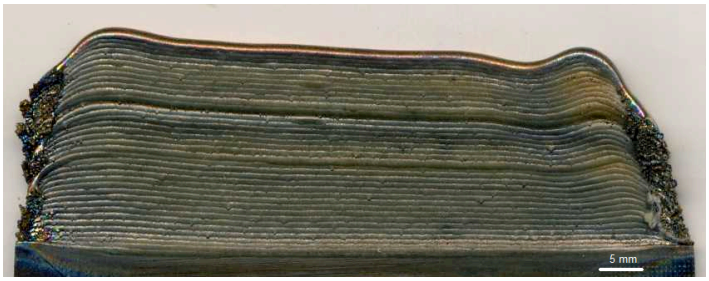

Ra=0,68 µm Rt= 43,48 µm Rp= 24,3 µm
Wa= 13,9 µm Wt= 127,39µm Wp= 78,69 µm

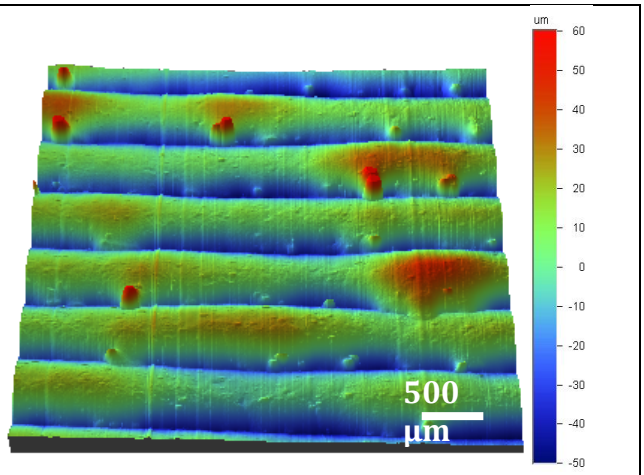

Tr_P_2 ; v= 400 mm/min

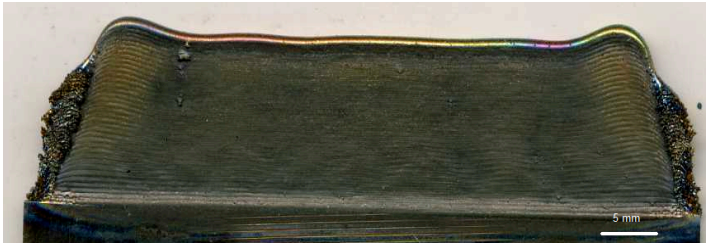

Ra= 0,43 µm Rt= 26,88 µm Rp= 9,18 µm
Wa= 8,3 µm Wt= 60,30 µm Wp= 27,92 µm

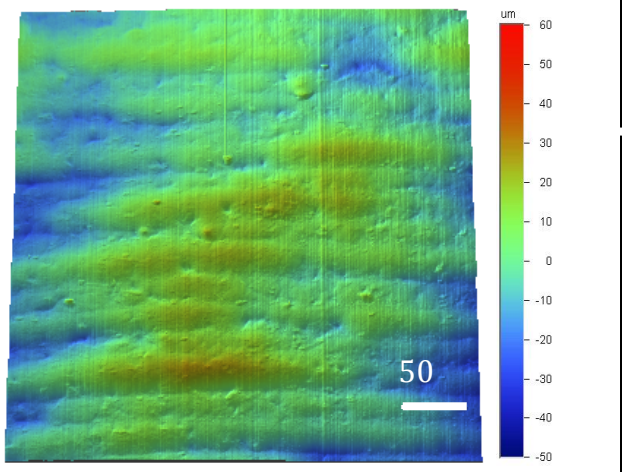

Figure 69: Roughness analysis of the fabricated samples for the tensile tests

From the so far analysis, it is understandable that there are a lot of different variables that affect the microstructure of the manufactured samples. The EBSD results showed that big dendrites are formed and are expanded through the Ti matrix. This is a usual explanation of what makes a material more brittle. Consequently, tensile tests are very important to predict how our material will react under other types of forces.

The results that were obtained can be summarized at the diagram below (Fig. 71 a) and Table 12). Fig. 71 b) illustrates the edited Stress-Strain diagram. The samples have very important differences in comparison with pure Ti6Al4V. The presence of TiC particles significantly decreases their plasticity and as a result the samples break just a few minutes after there are positioned at the tensile machine.

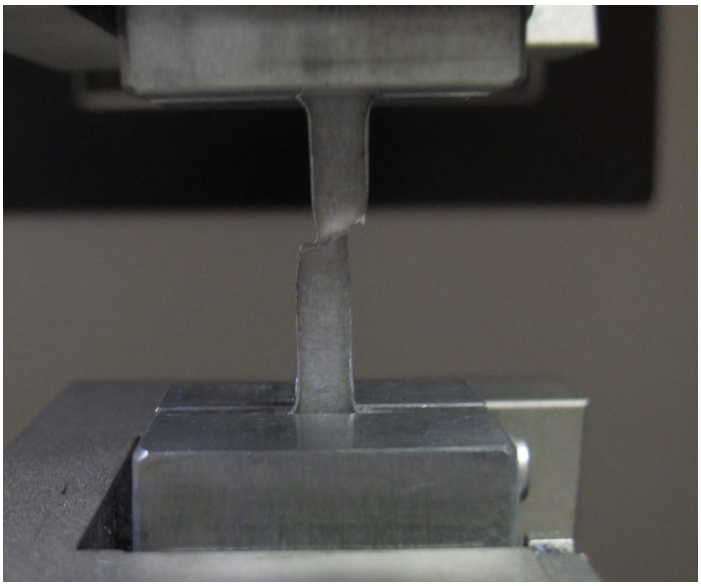

Figure 70: Sample after the tensile test was realized.

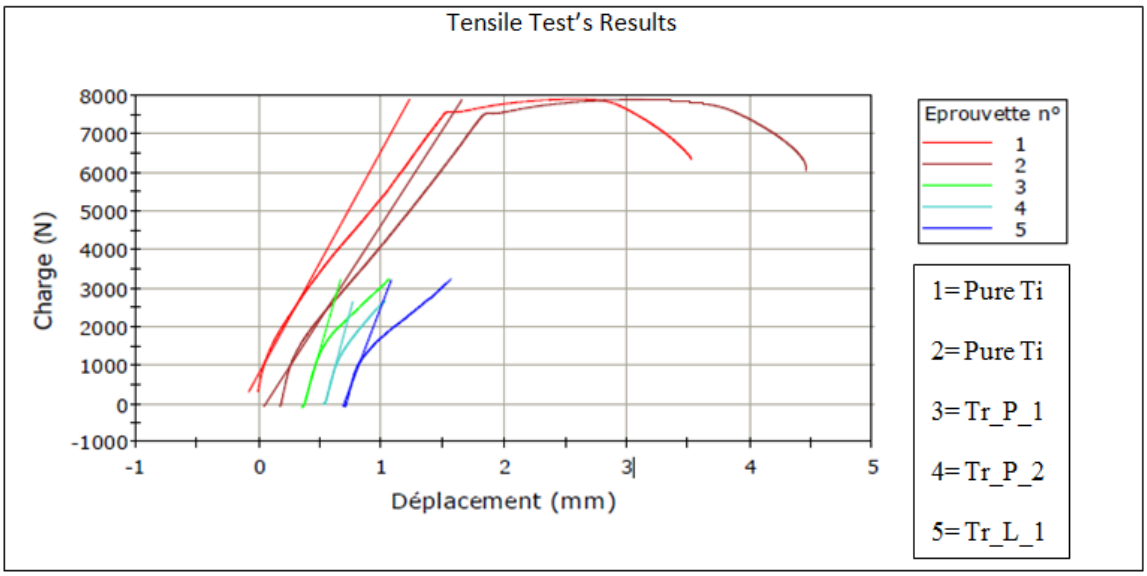

Figure 71: a) Tensile Tests results diagram-unedited.
*NOTE: sample described as "1" is not used for further analysis as it corresponds to a sample with different parameters from the others and for this reason it would not be of any use to compare it with the rest.

Sample name	Velocity for tensile test [mm/min]	Load until rupture [N]	Young's modulus E [N/mm^2]	Tensile strain at rupture [%]
Pure Ti6Al4V	0,2	6104,67	113.3333333	25,18
Tr_P_1	0,2	3243,40	89.47368421	4,19
Tr_P_2	0,2	2668,61	80.95238095	2,93
Tr_L_1	0,2	3225,39	70.83333333	5,05

Table 12: Rupture results of the tensile tests.

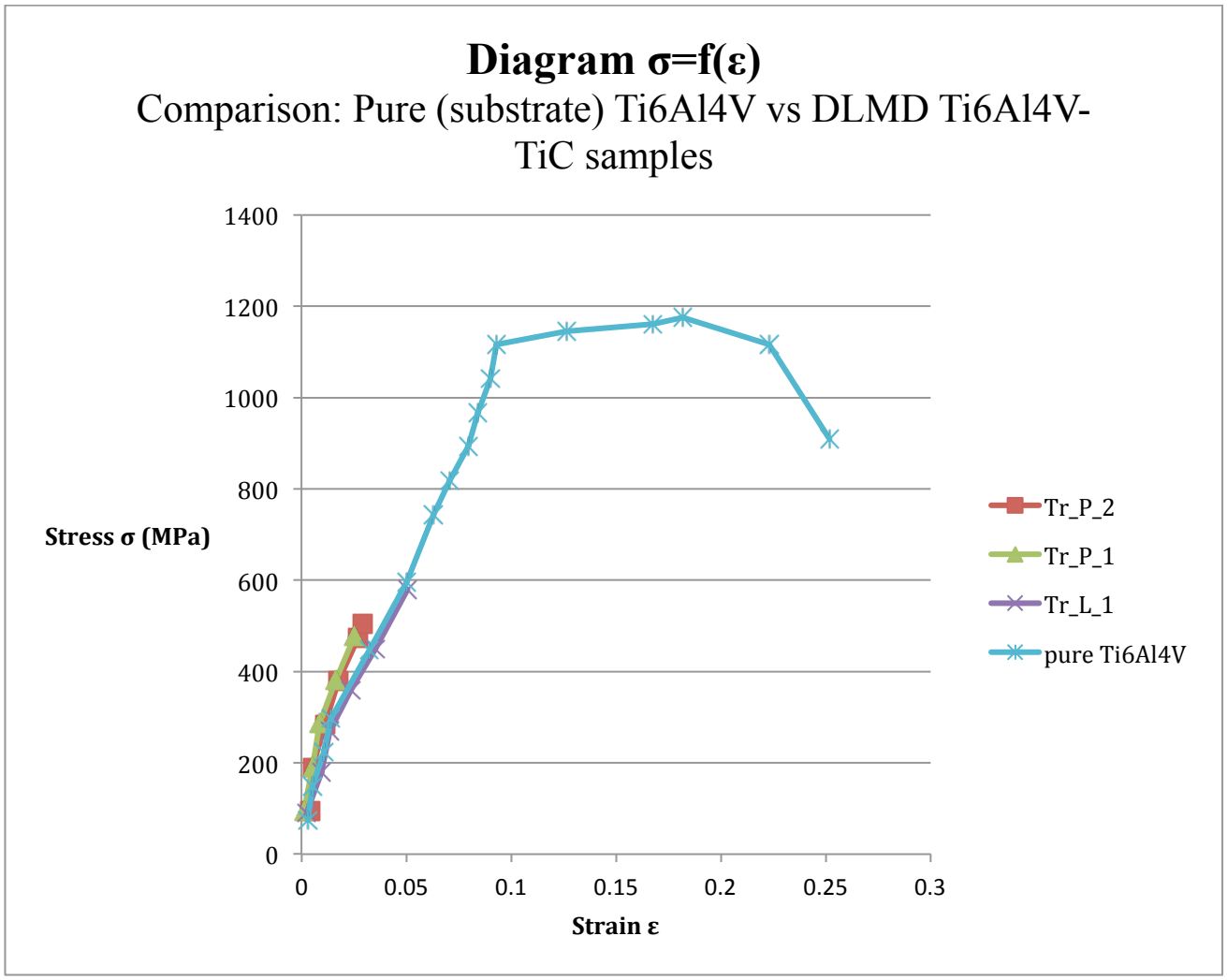

Figure 71: b) Tensile Tests results diagram: comparison between DLMD samples and Pure Ti substrate

According to the diagram in fig. 71b), it is evident that the DLMD samples that have TiC elements present a very decreased elasticity in comparison to the pure Ti6Al4V sample. This fact concerns also the samples that were remelted (represented here by Tr_L_1). Even if the re-melting of all the TiC primary partticles was succeeded with the introduction of the non powder re-melting passes, the final microstructure is not really satisfactory as TiC dendrites are much too large (up to several hundred of μm on the primary dendrite arm) which ultimately reduces the plasticity of the composite.

Fig. 72 illustrate SEM micrographs of the fracture surface where the microstructures are observed. Brittle fracture is obvious at the results displayed below.

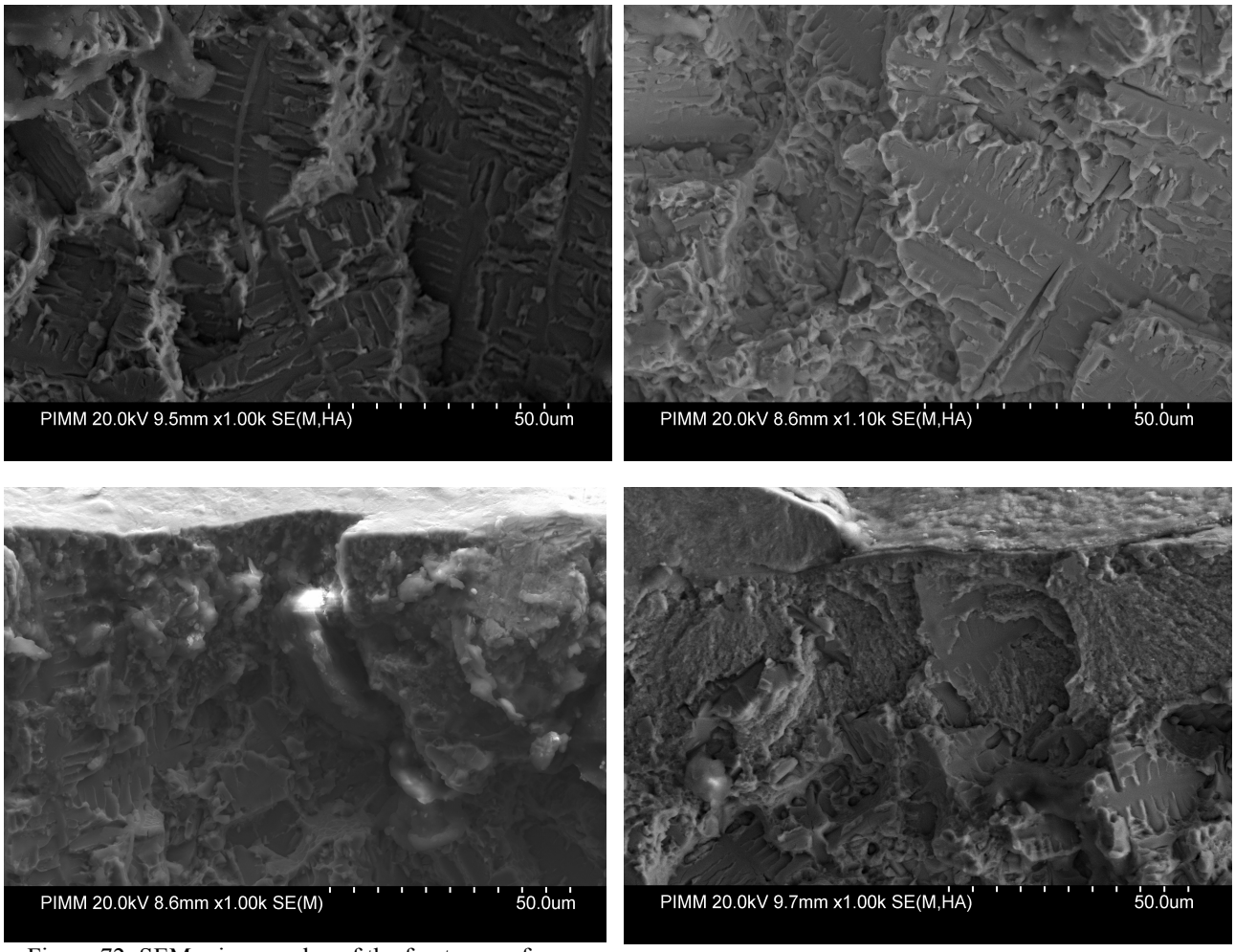

Figure 72: SEM micrographs o f the fracture surface.

IV. CONCLUSIONS

IV.1 Conclusions

After the analysis and examination of the connection between the DLMD parameters and the microstructures obtained the findings in this research work can be summarized below:

- Effect of the remelting factor:

  - ✓ The homogeneity regarding the dendrites distribution and the proportion of the unmelted particles was improved with the introduction of the remelting parameter.
  - ✓ The dendrites are well distributed with a relatively bigger concentration at the center of the samples.
  - ✓ The presence of TiC, although it significantly improved the hardness of the samples, it also significantly decreased their strength to tensile tests.
  - ✓ The remelting factor did not greatly affect the acquired results concerning the hardness.
  - ✓ Overall, the implementation of the novel remelting parameter improved the samples condition and properties.

- Effect of the velocity factor:

  - ✓ Regarding the hardness and the surface roughness, the samples that were fabricated with velocity 200 mm/min present slightly better results.
  - ✓ Regarding the homogeneity along the microstructures of the fabricated samples, the differences observed between the samples with different velocities are not very important.

In conclusion, taking into account the overall analysis that was realized in the context of the current diploma thesis project, the optimum conditions to achieve better homogeneity along the microstructure of a sample fabricated with the Direct Laser Metal Deposition process is:

⇨ velocity: 200 mm/min with remelting.

IV.2 Future Perspectives

For future research purposes and in order to further advance the current outcomes, the following suggestions are possible:

- Future researchers should focus on finding new modes to limit dendrite growth and also further cellular re-crystallization of TiC particles, which should guarantee much better plasticity. For instance, using smaller Ti particles (around 20 μm) with nearly similar Ti6Al4V particles (20-40 μm) could be a possibility.
- Another important point should be to make thermal treatments after DMD tests (at nearly 700-800°C) to relax stresses.
- EBSD analysis in bigger maps to investigate bigger areas of the examined sample and possibly identify any differences on the microstructure among the layers.
- Macro hardness testing to examine more globally the hardness of the samples.
- X-Ray Tomography to try to understand how the dendrites are developed in a three-dimensional sense.

V. REFERENCES

[1] Dimitrios I. Pantelis, Yiannis D. Xrysoulakis. Επιστήμη και Τεχνολογία των Μεταλλικών Υλικών. Papasotiriou. Athens, 2007

[2] Prototyping History and Prototype Development Information. Available: [http://www.prototypezone.com]. Generated: 27 March, 2012.

[3] William Palm. Rapid Prototyping Primer. In *PennState Learning Factory.* Available: [http://www.me.psu.edu/lamancusa/rapidpro/primer/chapter2.htm], May 1998, revised 30 July 2002.

[4] Pulak M. Pandey. Rapid prototyping technologies, applications and part deposition planning. Available:[http://web.iitd.ac.in/~pmpandey/MEL120_html/RP_document.pdf]

[5] I. J. Polmear. Light Alloys: metallurgy of the light metals. Third Edition, J. Wiley & Sons, 1995.

[6] Colin E. Webb, Julian D. C. Jones. Handbook of Laser Technology and Applications, Volume III: Applications. Institute of Physics, 2004.

[7] John F. Ready, Dave F. Farson. LIA Handbook of Laser Materials Processing. Springer, 2001.

[8] Antonio D. Ludovico, Andrea Angelastro and Sabina L. Campanelli. Experimental Analysis of the Direct Laser Metal Deposition Process. Polytechnic of Bari, Department of Management and Mechanical Engineering Italy. Available: [http://cdn.intechweb.org/pdfs/12286.pdf]

[9] Christoph Levens, Manfred Peters. Titanium and Titanium Alloys. John Wiley & Sons. 2006

[10] Fritz Appel, Jonathan David Heaton Paul, Michael Oehring. Gamma Titanium Aluminide Alloys: Science and Technology. John Wiley & Sons, 2011.

[11] Srikumar Banerjee, Pradio Mukhopadyay. Phase Transformations: Examples from Titanium and Zirconium Alloys. Elsevier, 2010.

[12] F. Wang, J. Mei, H. Jiang, and X. Wu. Laser Fabrication of Ti6Al4V/TiC composites using simultaneous powder and wire feed. In *Materials Science and Engineering,* volumes 445-446, pages 461-466, 2007.

[13] F. Wang, J. Mei, X. Wu. Microstructure study of direct laser fabricated Ti alloys using powder and wire. *Applied Surface Science* 253, pages 1424-1430, 2006.

[14] F. Wang, J. Mei, X. Wu. Compositionally graded Ti6Al4V + TiC made by direct laser fabrication using powder and wire. In *Materials and Design,* vol. 28, pages 2040-2046, 2007.

[15] W.U.H Syed, A. J. Pinkerton, L. Li. A comparative study of wire feeding and powder feeding in direct diode laser deposition for rapid prototyping. In *Applied Surface Science,* vol. 247, pages 268-276, 2005.

[16] C. Mitchell, X. Wu, J. Liang, J. Mei, P.S. Goodwin, W. Voice. Microstructures of laser-deposited Ti-6Al-4V. In *Materials and Design,* vol. 25, pages 137-144, 2004.

[17] X. Wang, P. Gai. Effect of carbon content on microstructures and property of TiC-Ti-6Al-4V composite. In *Transactions of Nonferrous Metals Society of China,* vol. 17, s546-550, 2007.

[18] J. Alcisto, A. Enriquez, H Garcia, s. Hinkson, T. Steelman, E. Silverman, P.Valdovino, H Gigernazer, J. Foyos, J. Orgen, J. Dorey, K. Karg, T. McDonald and S.Es-Said. Tensile Properties and Microstructures of Laser-Formed Ti-6Al-4V. In *Journal of Materials Engineering and Performance,* vol. 20, pages 203-212, 2011.

[19] D. Liu, S.Q. Zhang, A. Li, H.M Wang. Microstructure and tensile properties of laser deposited TiC/ TA15 titanium matrix composites. In *Journal of Alloys and Compounds,* vol. 485, pages 156-162, 2009.

[20] K. Frisk. A revised thermodynamic description of the Ti-C system. In *Computer Coupling of Phase Diagrams and Thermochemistry,* vol. 27, pages 367-373, 2003.

[21] M.J. Hamedi, M.J. Torkamany, J. Sabbaghzadeh. Effect of pulsed laser parameters on in-situ TiC synthesis in laser surface treatment. In *Optics and Lasers in Engineering,* vol. 49, pages 557–563, 2011.

[22] Y. Zhang, Z. Wei, M. Xi. Characterization of laser powder deposited Ti-TiC composites and functional gradient materials. In *Journal of Materials Processing Technology*, vol. 206, pages 438-444, 2008.

[23] D. Gu, Y. Shen, G, Meng. Growth morphologies and mechanisms of TiC grains during Selective Laser Melting of Ti-Al-C composite powder. In *Materials Letters*, vol. 63, pages 2536-2538, 2009.

[24] S.M. Kelly, S.L. Kampe. Microstructural Evolution in Laser-Deposited Multilayer Ti-6Al-4V Builds: Part 1. Microstructural Characterization. In *Metallurgical and Materials Transactions A,* vol. 35A, pages 1861-1867, 2004.

[25] S.M. Kelly, S.L. Kampe. Microstructural Evolution in Laser-Deposited Multilayer Ti-6Al-4V Builds: Part 2. Thermal Modeling. In *Metallurgical and Materials Transactions A,* vol. 35A, pages 1869-1879, 2004.

[26] E. Zhang, S. Zeng, Z. Zhu. Microstructures of XD^{TM} Ti-6Al/TiC composites. In *Journal of Materials Science,* vol. 35, pages 5989-5994, 2000.

[27] A. Mbaye. Modes d'élaboration (laser et autres techniques) et propriétés des composites a matrices métallique Ti-TiC. *Rapport de Stage de Master MAGIS (Materials Science and Engineering),* 2010- 2011.

[28] A. Racle. Fabrication additive par projection laser de composites à matrices métalliques Ti-TiC et microstructures associées. *Rapport de Stage du Master recherche MAGIS,* 2009-2010.

[29] T.Maitland, S. Sitzman. Electron Backscatter Diffraction (EBSD) Technique and Materials Characterization Examples. In "*Scanning Microscopy for Nanotechnology. Techniques and Applications" by W. Zhou, Z. L. Wang,* Chapter 2, pages 41-75, Springer, 2007.

[30] T. Baudin. Analyse EBSD. Principe et cartographies d'orientation. In *Les Techniques de l'Ingénieur,* M4138, 1-17, 2010.

[31] Oxford Instruments. EBSD Analysis. Available at : http://www.ebsd.com/

[32] J. Lorincz. Laser-Based Powder Metal Process Builds Up Rapid Prototypes. Available : [http://www.machinetoolsonline.com/doc.mvc/Laser-Based-Powder-Metal-Process-Builds-Up-Ra-0001], 2000.

[33] Y. Ya, S. Li, R. Zhang, F. Lin, R. Wu, Q. Lu, Z. Xiong, X. Wang. Rapid Prototyping and Manufacturing Technology: Principle, Representative Technics, Applications, and Development Trends. In *Tsinghua Science And Technology* pp1-12 vol. 14, Number S1, pages 1-12, June 2009.

[34] Rajeev Dwivedi, Srdja Zekovic,Radovan Kovacevic. A novel approach to fabricate uni-directional and branching slender structures using laser-based direct metal deposition. In *International Journal of Machine Tools and Manufacture,* vol. 47, issues 7-8, pages 1246-1256, June 2007.

[35] B. K. Kad, S. E. Schoenfeld, M. S. Burkins. Through thickness dynamic impact response in textured Ti–6Al–4V plates. In *Materials Science and Engineering : A,* vol. 322, issues 1-2, pages 241-251, January 2002.

[36] M. J. Donachie. Titanium: A Technical Guide. ASM Internation, 2nd Edition, 2000.

[37] Karl U. Kainer. Metal Matrix Composites: Custom-made Materials for Automotive and Aerospace Engineering. Chapter 1: Basic of Metal Matrix Composites, Wiley - Online Library, pages 1-54, 2006.

[38] J. C. Li. Microstructures and Properties of Materials. Word Scientific, 2000.

[39] Yaxin Bao. Mechanical properties and microstructure study for direct metal deposition of titanium alloy and tool steel. Thesis for the Master of Science in Manufacturing Engineering-University of Missouri-Rolla, 2007.